

I hereby declare that I am the sole author of this thesis. This is a true copy of the thesis, including any required final revisions, as accepted by my examiners.

I understand that my thesis may be made electronically available to the public.

John W.H. Molson

“You can’t tell if its the right model, only if its a good model”

... Stephen Hawking

Abstract

The behaviour of hydrocarbon fuels in contaminated groundwater systems is studied using a multicomponent reactive transport model. The simulated processes include residual NAPL dissolution, aerobic and anaerobic biodegradation with daughter-product transport, and transport of a reactive carrier with mixed equilibrium/kinetic sorption. The solution algorithm is based on a three-dimensional Galerkin finite element scheme with deformable brick elements and capacity for a free watertable search. Nonlinearities are handled through Picard iteration. Convergence is rapid for most applications and mass balance errors for all phases are minimal.

The model is first applied to simulate a pilot scale diesel fuel dissolution experiment in which humic acid is used as a natural organic carrier to enhance dissolution and to promote biodegradation of the aqueous components. The pilot scale experiment is described by Lesage et al. (1995) and Van Stempvoort et al. (2000). The conceptual model includes 8 unique components dissolving from 500 mL of residual diesel fuel within a 3D saturated domain. Oxygen-limiting competitive aerobic biodegradation with a dynamic microbial population is also included. A mixed 2-site equilibrium/kinetic model for describing sorption of the carrier to the aquifer solids was adopted to reproduce the observed breakthrough of the humic acid and organic components. Most model parameters were obtained independently with minimal calibration. Batch sorption data were found to fit well at the pilot scale, however biodegradation and dissolution rates were not well known and had to be fitted. Simulations confirmed the observed 10-fold increase in effective solubility of trimethylnaphthalene, and increases on the order of 2-5 for methyl- and dimethylnaphthalene. The simulated plumes showed almost complete attenuation after 5 years, in excellent agreement with observed data. A sensitivity analysis showed the importance of carrier concentrations, binding coefficients, dissolution and biodegradation rates. Compared to a dissolution scenario assuming no carrier, the humic acid-enhanced dissolution case decreased the remediation time by a factor of about 5.

The second application of the model involves simulating the effect of ethanol on the persistence of benzene in gasoline-impacted groundwater systems. The conceptual model includes a 4-component residual gasoline source which is dissolving at the watertable into a 3D aquifer. Comparisons are made between dissolved plumes from a gasoline spill and those from an otherwise equivalent gasohol spill. Simulations have shown that under some conditions, a 10% ethanol component in gasoline can extend the travel distance of a benzene plume by at least 150% relative to that

from an equivalent ethanol-free gasoline spill. The increase is due to preferred consumption of oxygen by ethanol and a corresponding reduction in the biodegradation rate of benzene while the two plumes overlap. Because of differences in retardation however, the ethanol and benzene plumes gradually separate. The impact therefore becomes limited because oxygen rapidly disperses behind the ethanol plume and benzene degradation eventually resumes. A sensitivity analysis for two common spill scenarios showed that background oxygen concentrations, and benzene retardation had the most significant influence on benzene persistence. A continuous gasohol spill over 10 years was found to increase the benzene travel distance by over 120% and a pure ethanol spill into an existing gasoline plume increased benzene travel distance by 150% after 40 years. The results are highly relevant in light of the forthcoming ban of MTBE in California and its likely replacement by ethanol by the end of 2002.

Acknowledgments

I would like to give special thanks to my supervisor, Dr. Emil Frind for his insight and guidance throughout our many years of collaboration at Waterloo. I would also like to thank my committee members Dr. Jim Barker, Dr. Suzanne Lesage and Dr. Edward Sudicky for their valuable contributions, and Dr. Dale Van Stempvoort of the National Water Research Institute for providing the lab data from the diesel fuel dissolution experiment and for engaging in many fruitful discussions on the behaviour of humic acid. Dr. Susan Powers of Clarkson University, Potsdam NY and Dr. Barb Butler generously offered their time as external readers.

I am grateful for the friendship of many colleagues during my time at Waterloo: especially Jos Beckers, Uli Mayer, Mario Schirmer, Jeff Bain, Steve Shikaze, Rob McLaren, Tony Radcliffe and Michelle Bester. Friendships and collaboration with many visiting students, including Adam Brun and Michael Petersen (Danish Technical University), Gudrun Franken (Hannover), Uli Maier (Tübingen), Florian Werner (Dresden) and Michael Mößner (Stuttgart) has been particularly valuable. I would especially like to thank my wife Jenny for her love and patience during those many working evenings & weekends, and my parents for their support and encouragement (and for finding my thesis in Montreal!).

A large component of the model development was completed during a 3-month stay at the Geological Institute, Tübingen, Germany. I would like to thank my hosts, Dr. Georg Teutsch and Dr. Peter Grathwohl for a most memorable visit.

Financial support was provided by the Natural Sciences and Engineering Research Council of Canada (NSERC) through operating grants to Dr. E.O. Frind, and by the Centre for Research in Earth and Space Technology (CRESTech). Financial support for the humic acid pilot experiment was provided by the Groundwater and Soil Remediation Program (GASReP) of Natural Resources Canada, the National Energy Board and Environment Canada to Dr. Suzanne Lesage of the National Water Research Institute, Burlington, Ontario. The study of ethanol impact on gasoline-contaminated groundwater was generously funded through a research contract with the California MTBE Research Partnership, and assisted by the (U.S.) National Water Research Institute. The support of all funding agencies is sincerely appreciated.

Dedication

This thesis is dedicated to my children, Christian, Sarah and Alexander, who seemed to grow up so fast during its completion.

Contents

Abstract	iv
Acknowledgements	vi
1 Introduction	1
1.1 Background	1
1.2 Objectives and Scope	2
1.3 Organization of Thesis	3
2 Theoretical Development	5
2.1 Introduction	5
2.2 Governing Equations	5
2.2.1 Groundwater Flow	5
2.2.2 Reactive Transport	7
2.2.3 First-Order Degradation Rates	9
2.3 Solution Approach	10
2.4 Verification Examples	12
2.4.1 Existing Model Applications	12
2.4.2 Illustrative Example 1: Enhanced Dissolution of a Chlorinated Solvent Source	14
2.4.3 Illustrative Example 2: Toluene Biodegradation with Multiple Electron-Acceptors	20

3	Numerical Simulation of Enhanced Diesel Fuel Dissolution	23
3.1	Introduction	25
3.2	Insight from Existing Numerical Models	26
3.3	Current Objectives	29
3.4	Theoretical Development	31
3.4.1	The Conceptual Model	31
3.4.2	Governing Equations for Carrier Transport	32
3.4.3	Governing Equations for Reactive Organic Transport	34
3.4.4	Numerical Solution Approach	37
3.5	Model Application to the Diesel Fuel Dissolution Experiment	37
3.5.1	Description of the Pilot Scale Experiment	37
3.5.2	Interpretation of Laboratory Batch Results	38
3.5.3	Pilot Scale Simulation Model	39
3.6	Sensitivity Analysis	67
3.6.1	Dissolution Rate	67
3.6.2	Biodegradation Rate	70
3.6.3	Substrate-Carrier Sorption	73
3.6.4	Binding Coefficient: TMN - HA	75
3.6.5	Long-Term Dissolution	76
3.7	Conclusions	77
4	Modelling the Impact of Ethanol on the Persistence of BTEX Compounds in Gasoline-Contaminated Groundwater	79
4.1	Introduction	80
4.1.1	Background	80
4.1.2	Review of Existing Modelling Approaches	81
4.1.3	Objectives	83
4.2	Theoretical Development	84

4.2.1	Modelling Approach	84
4.3	Conceptual Model	89
4.3.1	Flow System	89
4.3.2	Transport System	91
4.4	Simulation Results	97
4.4.1	Conceptual Model 1: A 10% ethanol gasoline spill into a pristine aquifer	97
4.4.2	Sensitivity Analysis	106
4.4.3	Conceptual Model 2: A Pure Ethanol Spill into an Existing Gasoline Plume	115
4.4.4	Conceptual Model 3: A Gasohol Spill Simulation with Ethanol Conversion to Methane	119
4.5	Summary	121
5	Summary and Conclusions	123
	Bibliography	126

List of Figures

2.1	Layout of the Borden emplaced source experiment.	16
2.2	Observed (symbols) vs. simulated (lines) data for the emplaced source experiment: (a) peak concentrations at the 1-m fence, and (b) mass remaining in the source.	17
2.3	Humic acid-enhanced PCE solubilization. BIONAPL/3D simulation vs. observed data from Johnson & John (1999).	18
2.4	Comparison of long-term dissolution of the Borden source: Field condition (natural gradient) vs. HA-enhanced dissolution of PCE. .	19
2.5	Simulated plumes, at 20 years, showing toluene and methane plumes, depletion of oxygen, nitrate and sulphate, and the growth of the oxygen-utilizing microbes. Electron acceptors are only plotted where they are depleted below their background levels. Vertical slice through a symmetric 3D system.	22
3.1	Conceptual model for development of a residual LNAPL source within the saturated zone.	30
3.2	Conceptual model for NAPL dissolution and sorption to the organic carrier and solids. Here, C_w^m represents the aqueous pseudo-phase including both the free and carrier-bound dissolved organic.	32
3.3	Plan view of the pilot scale tank showing location of the source, monitor wells and extraction well. Selected monitor wells are mentioned in the text.	38
3.4	Observed vs. fitted Langmuir isotherm for lab batch sorption test of humic acid to winter sand (after Van Stempvoort et al., 2000). . . .	39
3.5	Observed vs. simulated transient sorption profile showing early equilibrium and late kinetic behaviour.	40

3.6	Outline of the 3D finite element mesh for the pilot scale model. The residual diesel source is located at the intersection of the fine-mesh areas, 1.0 m from the inflow boundary.	42
3.7	Plan view of the pilot scale model showing source location and streamlines converging to the extraction well.	43
3.8	Simulated vs. observed breakthrough of the humic acid carrier in the pilot scale experiment at monitors T3B4 (top) and T7C4 (bottom).	45
3.9	Simulated vs. observed BTEX concentrations at monitor T4M4.	53
3.10	Observed total BTEX plumes, plan view through source centre. After Van Stempvoort et al. (2000).	54
3.11	Simulated total BTEX plumes at 3, 10, 46 and 95 days. Plan view through source centre.	55
3.12	Observed vs. simulated breakthrough of the naphthalene components at monitor well T3B4 (immediately downgradient from the source).	56
3.13	Observed vs. simulated breakthrough of the naphthalene components at monitor well T6B4 (1.2 m downgradient from the source).	57
3.14	Observed vs. simulated breakthrough of the naphthalene components at monitor well T7M4 (1.5 m downgradient from the source).	58
3.15	Observed total methylnaphthalene plumes from the pilot scale experiment (plan view through source centre). After Van Stempvoort et al. (2000).	61
3.16	Simulated total methylnaphthalene plumes corresponding to observed times. Plan view through the source centre.	62
3.17	Simulated total methylnaphthalene plumes at 50-65 days showing corresponding humic acid profiles. Contour plots are plan view, located through the source centre.	63
3.18	Simulated oxygen depletion plumes, caused by biodegradation of the diesel fuel components. The images represent a horizontal slice through the source centre. Contours are only flooded for depleted areas with less than the background concentration of 6 mg/L.	64
3.19	Simulated microbe concentrations within the pilot scale tank. Contour units are mg/L, plan view through source centre.	65

3.20	Simulated longitudinal profiles through the source centre showing diesel saturation, naphthalene concentrations and dissolved oxygen.	66
3.21	Sensitivity of naphthalene breakthrough to dissolution rate (Sherwood number), at monitor T3B4.	68
3.22	Observed vs. simulated breakthrough curves of the naphthalene components at T3B4 using single and dual-solubility equilibrium dissolution models.	69
3.23	Breakthrough curves at T3B4 (immediately downgradient from the source) showing effect of the maximum biodegradation rate for the naphthalenes.	71
3.24	Breakthrough curves at T7C4 (1.5 m downgradient) showing effect of the maximum biodegradation rate for the naphthalenes.	72
3.25	Breakthrough curves at T3B4 showing effect of humic acid concentration on enhanced dissolution of diesel fuel.	74
3.26	Breakthrough of trimethylnaphthalene at T3B4 showing sensitivity to the binding coefficient K_m .	75
3.27	Long-term dissolution of the diesel fuel source: comparison between the calibrated, humic acid-enhanced model, and an equivalent simulation without a carrier. Arrows indicate shift in component dissolution curves from the carrier-enhanced simulation to the no-enhancement simulation.	76
4.1	A vertical slice through the 3D steady state flow system assumed for the gasoline dissolution simulations. The residual source is located at the upper left.	89
4.2	Simulated aqueous concentrations from the dissolving residual gasoline and gasohol sources: conceptual model 1, base case scenario.	99
4.3	Simulated benzene, TEX and remaining component plumes from the base case gasoline source at 10 years (left) and 20 years (right). Contour intervals are 10, 100, 1000 and 10,000 ppb.	100
4.4	Simulated oxygen depletion plumes at 10 and 20 years.	101
4.5	Simulated benzene mass distribution showing source mass depletion, mass lost to biodegradation and sorption, and aqueous plume mass.	101

4.6	Simulated benzene plumes from the gasohol source at 10, 15 and 20 years. Also shown is the ethanol plume and dissolved oxygen depletion plume at 20 years. Benzene and ethanol concentration contours are 10, 100, 1000 ppb. Oxygen contours vary from a background of 3.8 mg/L to 0.0 mg/L within the gasoline and ethanol plumes. . . .	104
4.7	Comparison of mass profiles showing the effect of ethanol on benzene persistence.	105
4.8	Simulated evolution of the benzene plume from a gasoline (left) and gasohol (right) source, assuming a relatively higher benzene retardation of 1.5.	111
4.9	Simulated advance of the 10 ppb benzene contour from the gasoline and gasohol sources, comparing the effect of benzene retardation: base case (R=1.1) and high-retardation scenario (R=1.5).	112
4.10	Simulated benzene plumes assuming a relatively lower background oxygen concentration of 2.0 mg/L.	113
4.11	Multi-spill scenario: benzene plume evolution from gasoline (left) and gasohol (right) sources.	114
4.12	Simulated source concentrations for Conceptual Model 2: a pure ethanol spill at 5 years into an existing gasoline spill.	117
4.13	Benzene plumes from Conceptual Model 2: A pure ethanol spill into a 5-year gasoline plume. In this scenario, cosolvency effects are included.	118
4.14	Simulated ethanol, methane, oxygen and benzene plumes: Conceptual Model 3.	120

List of Tables

2.1	Summary of simulated redox reactions for example 2.	20
3.1	Flow system parameters used in simulating the pilot scale dissolution test.	46
3.2	Humic acid sorption parameters assumed in the pilot scale simulation model.	46
3.3	Physical properties of the diesel fuel components assumed in the pilot scale model.	51
3.4	Characterization of the simulated diesel fuel source.	51
3.5	Biodegradation parameters for the simulated diesel fuel components.	52
3.6	Reaction stoichiometries for the simulated diesel fuel components.	52
3.7	Summary of naphthalene dissolution times (at T3B4, to 10 ppb) using different humic acid concentrations. Bracketed values represent percent differences in dissolution times relative to those from the experimental humic acid concentration of 0.83 g/L.	73
4.1	Flow system properties for the gasoline/gasohol transport simulations.	90
4.2	Physical properties of the gasoline components assumed in the model.	95
4.3	Assumed characteristics of the residual gasoline source.	95
4.4	Assumed biodegradation parameters for the gasoline components, base case scenario.	96
4.5	Reaction stoichiometries for the simulated gasoline components. . .	96
4.6	Overview of simulation scenarios and influence of ethanol on the extent of the benzene plume, Conceptual Model 1.	107

Chapter 1

Introduction

1.1 Background

Non-aqueous phase liquids, or NAPL's, are a group of multicomponent fluids including such ubiquitous products as solvents, hydrocarbon fuels and oils. When spilled into the subsurface, they create a potentially serious threat to drinking water supplies because of their slow dissolution and high toxicity.

Groundwater contamination by hydrocarbon fuels is a particularly widespread and serious problem. Leaking underground storage tanks (LUST's), or accidental surface spills, for example, can leave a residual product trapped within the subsurface, often taking decades or longer to dissolve. Designing a successful remediation scheme often requires predicting the time scale for complete dissolution, assessing the potential for natural attenuation and understanding the influence of fuel additives, sorption processes and organic or surfactant carriers. Advanced numerical models can now provide unique insight into these issues by considering many non-linear processes in the context of multicomponent reactive transport in complex groundwater systems.

Over the past decade, research in this field has focussed on the dissolution behaviour of NAPL's in heterogeneous and fractured systems, reactive transport processes of the dissolved phase components and assessing efficiencies of active and passive remediation options. Most recently, there has been growing interest in understanding the processes of natural attenuation, as well as in the use of surfactants or natural carriers for enhancing NAPL dissolution and mobilization. Chapelle (1998) and Wiedemeier et al. (1999) provide excellent reviews of past and present remediation strategies for groundwater contaminated by petroleum hydrocarbons.

Chapelle (1998) notes, for example, that after two or three decades of testing various remediation alternatives and engineering designs, intrinsic bioremediation has emerged as the favoured approach under most conditions.

This thesis will present and apply a numerical simulation model to gain insight into two highly relevant topics concerning groundwater contamination from residual hydrocarbon fuels. The first topic involves assessing the remediation efficiency of a natural organic carrier (humic acid) to enhance the dissolution and biodegradation of a residual diesel fuel, and the second involves determining the impact of ethanol as a gasoline fuel additive on the persistence of BTEX in gasoline-contaminated groundwater. These applications are related in that they both involve dissolving residual hydrocarbon fuels under the influence of natural or enhanced dissolution and biodegradation. The recently developed BIONAPL/3D model, developed by the author, will be used for both applications. The model couples nonlinear groundwater flow with advective-dispersive reactive transport of dissolved-phase species from a multi-component residual NAPL.

This research is unique in several respects. To the author's knowledge, this is the first fully 3D multicomponent model of enhanced NAPL dissolution coupled with carrier sorption and electron acceptor-limited biodegradation. It is the first 3D numerical validation to a pilot scale experiment using humic acid as an organic carrier, and is the most comprehensive numerical approach to date for simulating the effect of ethanol on BTEX persistence in groundwater.

1.2 Objectives and Scope

The specific objectives of this research are:

1. To develop and validate a 3D numerical model for simulating residual NAPL dissolution and multicomponent reactive transport. The model will also include nonlinear flow, nonlinear kinetic sorption, multiple electron acceptors and coupled reactive carrier transport.
2. To apply the model to a well-documented pilot scale experiment involving the use of humic acid to enhance the dissolution of a residual diesel fuel source. This objective will not only validate the numerical approach and conceptual model, but will also test the suitability of applying batch scale sorption parameters to the pilot scale, quantify dissolution and biodegradation

rates, and test the sensitivity of various system parameters. The simulations will help verify the effectiveness of humic acids as a remediation option, and the model can serve as a tool for predictive assessment at the field scale.

3. To assess the impact of ethanol as a fuel additive on the persistence of BTEX in gasoline-contaminated groundwater. The model will be applied to simulate three conceptual spill scenarios involving dissolving residual gasoline and gasohol sources within a 3D aquifer system.

Under the general theme of groundwater contamination by dissolving residual hydrocarbon fuels, the model will be applied to help gain insight into two unique problems of hydrocarbon fuel contamination:

1. Can humic acid, a natural organic carrier, be effective in enhancing the dissolution of a residual diesel fuel?, and
2. How will the addition of ethanol to gasoline affect the persistence of BTEX compounds in gasoline-contaminated groundwater?

Through meeting these objectives, the accuracy, efficiency, and versatility of the numerical model will also be evaluated.

1.3 Organization of Thesis

Following the introductory chapter, this thesis is divided into three main sections: a chapter on model development and previous applications, a chapter on the application of the model to a diesel fuel dissolution experiment, and a chapter on use of the model for predicting impact of ethanol on gasoline contamination in groundwater.

Chapter 2 reviews the theoretical development of the model, outlines the solution approach and includes a review of previous applications. Examples are provided showing enhanced dissolution of a chlorinated solvent spill, and toluene biodegradation in the presence of multiple electron acceptors.

Chapter 3 presents the model development and application to the pilot scale humic acid - diesel dissolution experiment. The conceptual model is developed

and the governing equations for organic and carrier transport are provided. Model comparisons to the observed experiment are given both as breakthrough curves and as plan-view concentration distributions for the dissolved organics, oxygen and microbe population. A sensitivity analysis highlights the influence of several key parameters including dissolution and biodegradation rates, binding coefficients and carrier concentrations.

Chapter 4 presents an application of the model to study the influence of ethanol on benzene persistence in gasoline-contaminated aquifers. The conceptual model is defined and simulations are presented for two common spill scenarios. Impact is assessed based on the relative increase in travel distance of the benzene plumes.

Finally, Chapter 5 provides some concluding remarks.

A general abstract, introduction and summary is provided for the entire thesis. Because Chapters 3 and 4 were originally developed as separate, stand-alone sections, they each contain their own abstract, introduction and conclusions. Detailed literature reviews are included in each of these two chapters.

Chapter 2

Theoretical Development

2.1 Introduction

In this chapter, the governing equations and solution method for NAPL dissolution and transport are presented, and some existing model applications are reviewed. In Chapter 3, the equations will be extended to include co-transport of a reactive carrier, including nonlinear and kinetic sorption processes. Because the model has already been thoroughly tested and successfully applied to a number of lab and field-scale systems, an extensive verification section is not provided here. Rather, the focus will be on highlighting model capabilities with applications to a few multi-component systems. A review of past model applications is provided in section 2.4.

To simulate a dissolving residual NAPL, we must consider the equations governing groundwater flow, NAPL dissolution, advective-dispersive transport and biodegradation. The current approach is restricted to a saturated porous medium under isothermal conditions. Since the NAPL phase is assumed immobile, the approach is only valid for relatively low NAPL saturations on the order of less than 0.2.

2.2 Governing Equations

2.2.1 Groundwater Flow

The governing equation for density-dependant saturated groundwater flow in the presence of a dissolving residual NAPL (Frind et al. 1999; Huyakorn and Pinder,

1983) can be expressed as

$$\frac{\partial}{\partial x_i} \left(K_{ij} k_{rw} \frac{\partial h}{\partial x_j} + \gamma C_w^m n_j \right) + \sum_{k=1}^n Q_k(t) \cdot \delta(x_k, y_k, z_k) = S_w S_s \frac{\partial h}{\partial t} + \theta \frac{\partial S_w}{\partial t} \quad (2.1)$$

where h (m) is the hydraulic head, C_w^m (kg/m^3) is the aqueous (water) phase concentration of organic contaminant m , K_{ij} (m/day) is the hydraulic conductivity tensor, k_{rw} is the relative permeability with respect to water, θ is the porosity, S_w (m^3/m^3_{voids}) is the water saturation, S_s (day^{-1}) is the specific storage, γ is a relative density term, $Q_k(t)$ (m^3/day) is a source/sink term for well k , δ is the Dirac delta function, t is the time ($days$), $x_i = (x, y, z)$ are the spatial coordinates (m) and $n_j = (0, 0, -1)$.

The density term γ in equation 2.1 is defined as

$$\gamma = \frac{\rho_{\max}}{\rho_o} - 1 \quad (2.2)$$

where ρ_{\max} is the maximum fluid density and ρ_o is the reference density of water. Further insight into the approach for simulating density-dependent flow is provided by Frind (1982a) and Molson and Frind (1994). In the model applications considered here, the dissolved phase components are assumed dilute and the density term is not used. Oswald (1999) and Ghassemi et al. (1999) provide examples where the model is applied to density-dependent systems.

As the NAPL dissolves, the water saturation S_w and relative permeability k_{rw} will increase. The relationship can be expressed (Corey, 1986) in the form

$$k_{rw} = \left(\frac{S_w - S_{rw}}{1 - S_{rw}} \right)^4 \quad (2.3)$$

where S_{rw} is the irreducible degree of water saturation. The saturations are constrained by

$$S_w + S_n = 1 \quad (2.4)$$

where S_n (m^3_{NAPL}/m^3_{voids}) is the NAPL saturation.

Groundwater velocities v_i (m/day) are obtained from Darcy's Law according to

$$v_i = \frac{q_i}{\theta S_w} = \frac{-K_{ij} k_{rw}}{\theta S_w} \left(\frac{\partial h}{\partial x_j} + \rho_r n_j \right) \quad (2.5)$$

where q_i is the Darcy flux and ρ_r is the relative density defined as $\rho_r = \rho/\rho_o - 1$.

2.2.2 Reactive Transport

The governing equation for advective-dispersive transport of a NAPL component m undergoing rate-limited biodegradation and kinetic dissolution from a residual source can be written as

$$\theta S_w D_{i,j}^m \frac{\partial^2 C_w^m}{\partial x_i^2} - q_i \frac{\partial C_w^m}{\partial x_i} - \theta S_w [\lambda_{BIO}^m C_w^m + \lambda_{DIS}^m (C_s^m - C_w^m)] = \theta S_w R_w \frac{\partial C_w^m}{\partial t} \quad (2.6)$$

where C_w^m (kg/m^3) is the aqueous (water) phase concentration of organic contaminant m , $D_{i,j}^m$ (m^2/day) is the hydrodynamic dispersion tensor (as defined by Burnett & Frind, 1987), q_i (m/day) is the Darcy flux, λ_{BIO}^m (day^{-1}) is the biodegradation rate, λ_{DIS}^m (day^{-1}) is the NAPL dissolution rate coefficient, R_w is the retardation, t is time ($days$) and x (m) represents the spatial dimensions ($x_i = x, y, z$).

In equation 2.6, C_s^m is the effective saturation of the NAPL component defined, assuming validity of Raoult's Law (Mackay et al. 1991), as

$$C_s^m = X^m C_o^m \quad (2.7)$$

where X^m is the mole fraction and C_o^m (kg/m^3) is the pure phase aqueous solubility of component m . Assuming linear equilibrium partitioning to the aquifer solids, the retardation R_w (equation 2.6) can be expressed by $R_w = 1 + \rho_b K_d / \theta$ where ρ_b (kg/m^3) is the bulk density and K_d (m^3/kg) is the distribution coefficient.

The biodegradation rate λ_{BIO}^m for organic component m in equation 2.6 can be expressed in terms of N_A parallel degradation reactions as

$$\lambda_{BIO}^m = \sum_{n=1}^{N_A} \left[k^{m,n} M^n \left(\frac{1}{K_C^{m,n} + C_w^m} \right) \left(\frac{A^n}{K_A^{m,n} + A^n} \right) \cdot I^n \right] \quad (2.8)$$

where $k^{m,n}$ ($kg_{organic}/kg_{microbes}/day$) is the maximum utilization rate of component m with electron acceptor n , M^n ($kg_{microbes}/m_w^3$) is the concentration of the microbes associated with electron acceptor n , A^n is the concentration of electron acceptor n , $K_C^{m,n}$ and $K_A^{m,n}$ are the half-utilization rate concentrations for the organic and electron acceptor, respectively, and I^n is the electron acceptor inhibition function. Equation 2.8 represents the net organic biodegradation rate of component m due to N_A electron acceptors.

In the case of multiple electron acceptors, the inhibition function (I^n) allows either a gradual or abrupt change between preferred electron acceptors. The function takes the form of

$$I^{n=1} = 1; \quad I^{n>1} = \prod_{i=2}^n \frac{1}{1 + \frac{A^{i-1}}{K_I^{i-1}}} \quad (2.9)$$

where K_I^n represents the inhibition coefficient for electron acceptor n . In the case of two electron acceptors, oxygen and nitrate for example, if $K_I^{O_2} = \epsilon[O_2]_{max}$, then nitrate can be utilized, at its maximum rate reduced by a factor of ϵ , in the presence of oxygen at high concentrations. Setting $\epsilon = 1/100$ for example, will prevent utilization of nitrate until oxygen is nearly completely depleted. The approach follows that developed by Widdowson et al. (1988) and applied by Schäfer et al. (1998).

The dissolution rate coefficient in equation 2.6 is expressed as (Frind et al., 1999)

$$\lambda_{DIS}^m = \frac{ShD^m}{(d_{50})^2} \left(\frac{f^m S_n}{S_{n_0}} \right)^{\beta^m} \quad (2.10)$$

where Sh is the Sherwood number, D^m (m^2/s) is the aqueous diffusion coefficient, d_{50} is the median grain diameter (m), S_n is the degree of NAPL saturation, with S_{n_0} the initial saturation, f^m is the local NAPL volume fraction of component m and β^m is a nonlinear coefficient.

The electron acceptor concentration (A^n) in equation 2.8 is assumed to be dissolved in the aqueous phase therefore transport is also assumed governed by advection and dispersion according to

$$\theta S_w D_{i,j} \frac{\partial^2 A^n}{\partial x_i^2} - q_i \frac{\partial A^n}{\partial x_i} - \theta S_w \lambda_{BIO}^n \cdot A^n = \theta S_w \frac{\partial A^n}{\partial t} \quad (2.11)$$

where the electron acceptor rate term λ_{BIO}^n represents the net reaction rate due to biodegradation of all N_m organic components according to

$$\lambda_{BIO}^n = \sum_{m=1}^{N_m} \left[k^{m,n} M^n \mathbf{X}^{m,n} \left(\frac{C_w^m}{K_C^{m,n} + C_w^m} \right) \left(\frac{1}{K_A^{m,n} + A^n} \right) \cdot I^n \right] \quad (2.12)$$

where $\mathbf{X}^{m,n}$ represents the stoichiometric ratio of electron acceptor mass to organic mass.

After extending the approach of Frind et al. (1989) to account for multiple populations, microbial growth is calculated according to

$$\sum_{m=1}^{N_m} \left[Y^{m,n} M^n k^{m,n} \left(\frac{C_w^m}{K_C^{m,n} + C_w^m} \right) \left(\frac{A^n}{K_A^{m,n} + A^n} \right) \cdot I^n \right] - bM^n = \frac{\partial M^n}{\partial t} \quad (2.13)$$

where $Y^{m,n}$ is the yield coefficient ($\text{kg}_{mic}/\text{kg}_{org.}$) and b is a microbial decay rate (day^{-1}). The microbes are assumed immobile.

2.2.3 First-Order Degradation Rates

First-order (linear) degradation rates can be simulated in the model by manipulating the rate expression terms in equation 2.8. First, the following parameters are set for the specific component and electron acceptor:

- $\mathbf{X}^{m,n} = 0$
- $Y^{m,n} = 0$
- $K_A^{m,n} \ll A^n$
- $K_C^{m,n} \gg C_w^m$

The first order rate is then specified by

$$\lambda_{BIO}^m = \frac{k^{m,n} M^n}{K_C^{m,n}} \quad (2.14)$$

2.3 Solution Approach

Equations 2.1 and 2.6 are coupled through the velocity term in equation 2.5 and are in general, nonlinear. A Galerkin finite element solution approach is adopted using deformable brick elements and a conjugate gradient solver (Schmid & Braess, 1988). The nonlinear dissolution and decay terms are handled using a Picard iterative scheme with central time-weighting. An automatic watertable search is available for unconfined systems. Similar numerical approaches have been used in reactive transport modeling by Frind et al. (1999, 1990) and Molson et al. (1992).

The nonlinear terms arise from:

- the unknown watertable position within unconfined aquifers,
- the relative density term $\gamma C_w^m n_j$, which is a function of the concentration,
- the relative permeability k_{rw} , which is dependent on the NAPL saturation,
- the NAPL dissolution rate λ_{DIS}^m , which depends on the NAPL saturation, and
- the biodegradation rates λ_{BIO}^m , which depend on the concentrations of the organic contaminant, the electron acceptor and the microbe population.

Within each time step, the iterative routine follows the order given below:

1. Solve equation 2.1 assuming a given aquifer geometry and initial concentration and NAPL saturation distribution. For the case of an unconfined aquifer, iterate and deform the mesh until the watertable heads match the watertable elevation.
2. Solve equation 2.6 independently for each organic component, assuming identical electron acceptor concentrations for the organic Monod term in equation 2.8.
3. Solve equation 2.11 for each electron acceptor, using the Monod decay term 2.12 and the new organic concentrations from step 2. The decay term of 2.12 represents the net electron acceptor consumption rate due to each of the organics, assuming parallel reactions.

4. Update the remaining NAPL source mass, mole fractions and effective solubilities based on the mass dissolved into the aqueous phase.
5. Return to step 2, update the new organic and electron acceptor concentrations at the $(t+\Delta t)$ time-level, and repeat until convergence is achieved. The microbe concentrations are updated at each iteration using equation 2.13, and again following convergence.
6. In the case of density-dependent flow, return to step 1 and re-solve for flow with the new concentration distribution.
7. Following convergence, update all concentrations for the next time level and begin the next time level solution at step 1.

The iterative scheme allows simultaneous degradation of multiple compounds provided the electron acceptor concentrations are sufficient. If two compounds co-exist, for example, they will both deplete the available electron acceptor(s) but at different rates depending on their reaction parameters and nodal substrate and electron acceptor concentrations. Substrate inhibition, in which the existence of one compound inhibits the degradation of another (in addition to competition for the electron acceptor), is also supported but was not employed in the current applications.

Groundwater flow velocities are provided through coupling with a transient, saturated flow algorithm (Molson et al., 1992). Deformable brick elements are used with an iterative watertable search, and both flow and transport matrices are solved using an efficient conjugate gradient solver (Schmid & Braess, 1988; Braess & König, 1995).

Daughter-product transport is also included using the given degradation rates and option switches. First, second and third-type boundary conditions can be assigned to any boundary and the material properties can be heterogeneous and anisotropic. Source/sink wells can be located anywhere within the domain and 1D line elements are included to represent the vertical well bore, following the approach of Sudicky et al. (1995) and Lacombe et al. (1995). Stability and convergence is controlled through the grid Peclet and Courant criteria (Daus et al., 1985) and mass balance has been excellent. Further details of the numerical approach are provided in Frind et al. (1999) and Molson et al. (1992, 2000b).

2.4 Verification Examples

The BIONAPL/3D model has evolved over the past several years beginning from a single component, aerobic biodegradation transport model (Frind et al. 1989). The model was later extended to include density-dependent heat transport (Molson et al., 1992) and a version was also adapted for dense salt transport (Molson & Frind, 1994) and temperature-dependent reactive mass transport (Molson et al., 1994). BIONAPL/3D currently includes multiple component kinetic NAPL dissolution and nonlinear reactive transport (Frind et al., 1999; Molson, 2000). Verification examples and practical applications at both the lab and field scale are extensive; a brief review is provided here.

2.4.1 Existing Model Applications

The first applications of the model focussed on the behaviour of single organic contaminants under oxygen-limiting biodegradation. Frind et al. (1989), for example, used the model to show the importance of a three-dimensional approach for reactive transport. They showed the first examples of dimensionality effects for biodegrading organics. In another application, Molson & Frind (1990) simulated a field-scale benzene plume in order to highlight the problem of non-uniqueness between source concentration and biodegradation rates. They showed that high source concentrations combined with active degradation could reproduce observed rates of mass loss as accurately as a non-reactive approach using lower source concentrations.

Comparisons of the model to linear analytical solutions of biodegradation, and between 1D, 2D and 3D systems were presented by Schirmer et al. (1995). In all cases, the model produced excellent fits to analytical solutions and to independent numerical models. Schirmer (1998) and Schirmer et al. (2000a,b) applied the model to simulate transport and natural attenuation of a field-scale 3D multi-component gasoline plume as well as to study the effects of flow transients on the rate of biodegradation. The model helped show that laboratory-derived biodegradation parameters can be accurately applied to simulate field-scale behaviour of BTEX plumes. Also, transient flow fields were shown to significantly increase the degree of mixing with background oxygen.

Frind et al. (1999) applied the BIONAPL/3D model to simulate the Borden emplaced source experiment in which a mixture of pure-phase residual TCM, TCE and PCE was emplaced below the watertable. The dissolution behaviour was monitored at the 1-m fence over a period of 3 years. The model included nonlinear flow which was coupled with the dissolving NAPL, however biodegradation was

not considered because of the proximity of the monitoring fence to the source. The three-dimensional simulations compared well with the observed 1-m peak fence concentrations and integrated mass flux data, and conclusively showed that the NAPL mixture was indeed dissolving at equilibrium or at near-equilibrium conditions. Predictive simulations suggested that complete source dissolution under natural flow gradients would require on the order of 30 years. The work also included testing the model against a lab column experiment presented by Powers et al. (1994) involving styrene dissolution. An excellent match to the observed data was obtained assuming values of β (in equation 2.10) of 0.80 to 0.90.

Knaus (1999) used the model to study dissolution processes of a NAPL pool and compared numerical simulations with observed data and with analytical solutions for vertical diffusion profiles above the pool. He found excellent agreement between the observed and simulated profiles, but required a discretization on the order of millimetres across the NAPL/water interface to reproduce the high vertical concentration gradients. Similarly, Grathwohl et al. (2000) used BIONAPL/3D to simulate transport and oxidation of ammonium. Under conditions of low transverse vertical dispersivity, they showed the development of a steady state plume and associated microbial growth at the plume interfaces.

Forsey (2000) applied BIONAPL/3D to simulate *in situ* dissolution and oxidation of residual creosote in laboratory columns. He transported 13 creosote compounds simultaneously and studied their reactive dissolution behaviour with a permanganate oxidizing agent. Biodegradation was not considered because permanganate is toxic to microbes. Chemical oxidation was simulated using two different approaches. First, calibrated oxidation factors were applied to reduce the aqueous component concentrations and increase the NAPL dissolution rate. This approach assumes instantaneous oxidation. The second approach used measured first-order oxidation rate constants for each component. The rates were applied in BIONAPL/3D by linearizing the Monod biodegradation terms (equation 2.14). While the first method provided reasonable fits to the data, the second approach is more physically realistic. Good agreement was obtained with the measured rates of mass loss for the various components which varied between 10% and 80% over 5 days.

Further model applications include those by King (1997) and Durrant (2000) who applied the model to simulate an emplaced creosote source at Borden. These applications were less insightful, however, because of uncertainties in the source characterization and lack of consistent data.

2.4.2 Illustrative Example 1: Enhanced Dissolution of a Chlorinated Solvent Source

The Borden emplaced source contained a mixture of 22.8 kg of residual TCM, TCE and PCE, dissolving under natural gradient conditions 2 m below the watertable (Figure 2.1). Aqueous concentrations were monitored for over 40 months at a fence located 1 m downgradient from the source. Further details are provided by Rivett et al. (1992).

The experiment was initially conducted under natural gradient conditions with no dissolution enhancement. Since the complete source dissolution time is controlled by the most abundant and least soluble component (PCE), increasing the dissolution rate of PCE would be the most efficient means of enhanced remediation. In Chapter 3, an experiment is simulated in which humic acid is used to enhance the dissolution rate of a residual diesel source. Here, humic acid is applied in a similar fashion to enhance the dissolution of PCE in the Borden source. A comparison is made between the dissolution behaviour of the three chlorinated solvents (TCM, TCE and PCE) with and without humic acid as an organic carrier for PCE. The example serves to further test the model against independent source data, and highlights its versatility for simulating a variety of NAPL-contamination problems. The results show that applying humic acid to the source would decrease the time required for complete source dissolution from 23 years to 10 years.

Dissolution of the source was first simulated by Frind et al. (1999) assuming dissolution coefficients (β^m) ranging from 0.0 to 0.96 which showed progressively increasing tailing with increasing β . The base case calibration with $\beta = 0$ is reproduced here over the range 0-1000 days (Figure 2.2). The results confirm that the source was dissolving at near-equilibrium conditions.

To provide enhanced remediation, the simulation is now repeated with partitioning to a humic acid carrier. The PCE partition coefficient is obtained by calibrating the model to data provided by Johnson & John (1999) who describe an experiment in which Aldrich humic acid was flushed through a column of Ottawa sand containing residual PCE. The column was 15 cm long, and 2.5 cm in diameter. The sand porosity was 0.35, the residual PCE saturation 0.1, and the flushing velocity was reported as 0.07 cm/min. After 2 hours of flushing with water, humic acid was introduced at 1.23 g/L, then increased sequentially to 6.15 g/L at 11.5 hrs. and 12.3 g/L at 21.5 hrs. The effluent aqueous concentration of PCE was monitored for about 1.5 days.

To obtain the PCE-HA partition coefficient, the column experiment was simulated using BIONAPL/3D with the given data, and assuming identical properties of

PCE as used in the original model ($\rho = 1630 \text{ kg/m}^3$, $MW = 0.166 \text{ kg/mol}$, $C_o = 0.242 \text{ kg/m}^3$, $D = 6.0 \times 10^{-10} \text{ m/s}$). The column was discretized with 40 elements and a time step of 0.004 days (5.8 min) was assumed. Biodegradation was inactive and sorption of the PCE and humic acid were considered negligible.

The simulated breakthrough concentrations of both the humic acid carrier (dissolved humic substances, or DHS) and aqueous PCE are shown in Figure 2.3. The primary calibration parameters were the partitioning coefficient K_m (m^3/kg), and the dispersivity α_L . The partitioning coefficient describes the sorption of an organic component to the HA carrier and is used to define the enhancement factor, given by Ji & Brusseau (1998) as

$$E^m = \frac{C^*}{C_s^m} = 1 + K_m^m C_c \quad (2.15)$$

where E^m is the enhancement factor of organic component m , C^* is the enhanced solubility in the carrier-water mixture and C_c is the concentration of the mobile humic acid carrier. Further details are provided in Chapter 3.

Although an excellent match to the four equilibrium plateaus was quickly obtained, a reasonable match in the time domain (i.e. a match to the three transient periods) was not possible with the given HA- increment times, provided by Wynn John (pers. communication, 2000), and given flushing velocity (Johnson & John 1999). Assuming some preferential flow could have occurred within the column, the flushing velocity was increased to 0.087 cm/min while maintaining the total volumetric flux of 0.018 mL/min. This small change produced a much better match to the observed data as shown in Figure 2.3. The calibration yielded final values of $K_m = 0.09 \text{ m}^3/\text{kg}$, and $\alpha_L = 0.002 \text{ m}$.

The scattered PCE data observed after the initial HA increment to 1.2 g/L was attributed to partial PCE mobilization (Johnson & John, 1999) which is not considered by the model. The simulated results correlate well with the observed data which show that humic acid at 12.3 g/L can increase the effective solubility of PCE by a factor of about $2\times$.

The Borden emplaced source dissolution model was next redesigned to accommodate the hypothetical scenario of flushing the source with humic acid. The calibrated HA-PCE partition coefficient of $K_m = 0.09 \text{ m}^3/\text{kg}$ was adopted, with all other parameters remaining identical. No enhancement for TCM or TCE was assumed since the focus here was on the least soluble component. Since TCM and TCE are relatively more soluble, the partition coefficient for these components

would likely be even less. The flushing of humic acid through the system was simulated by assigning a fixed inflow boundary concentration of 10 g/L after 100 days of natural gradient flushing by water.

The HA-enhanced simulated dissolution profiles are provided in Figure 2.4 which compares the field-condition natural-gradient dissolution profiles with the HA-enhanced profiles. Although only PCE was assumed directly affected by the humic acid, TCE also showed a small reduction in dissolution time from 5700 days (15.6 years) to 5234 days (14.3 years). This effect is due to the relative increase in mole fraction for TCE as PCE dissolves more rapidly. Because of its high solubility and low initial mole fraction, there was no effect on the TCM dissolution profile. The simulation shows that enhanced dissolution using a solution of 10 g/L humic acid would decrease the total remediation time of the 22.8 kg source from approximately 27 years to 16 years, a 41% decrease. The significance of this decrease would depend on other factors such as costs relative to alternative remediation options.

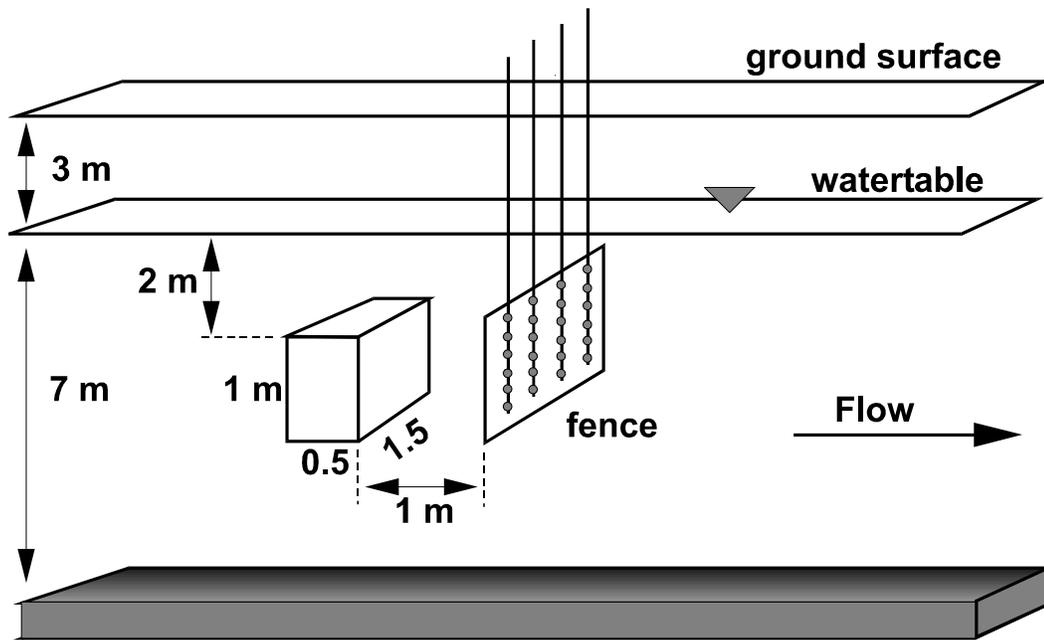


Figure 2.1: Layout of the Borden emplaced source experiment.

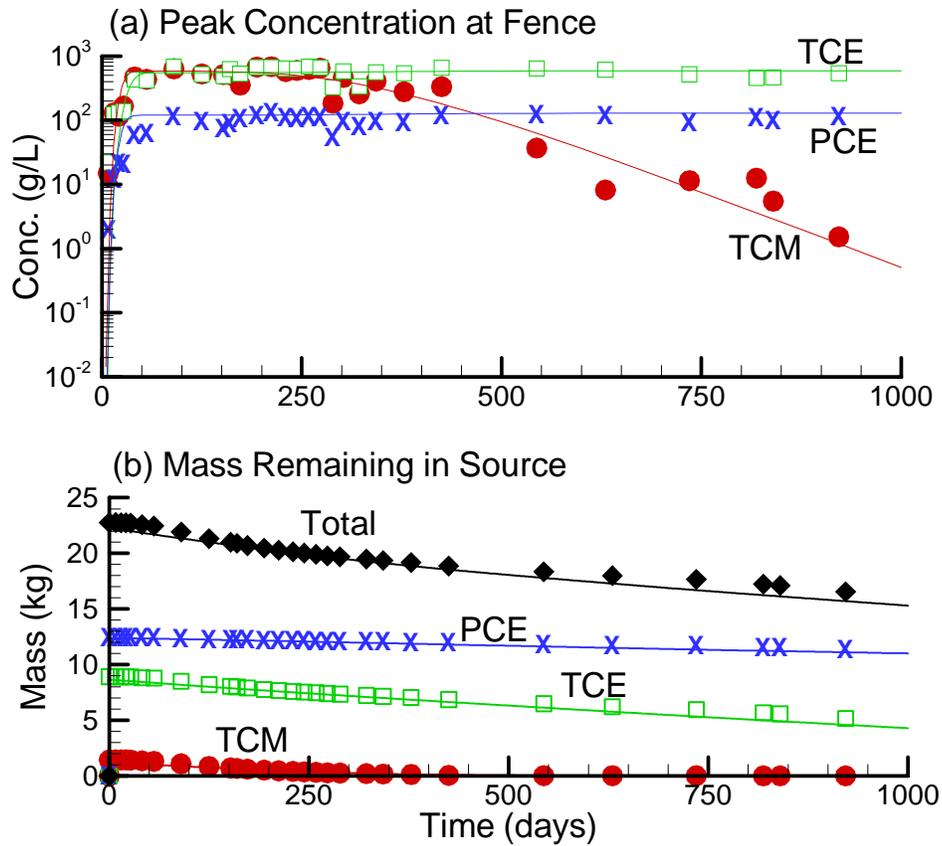


Figure 2.2: Observed (symbols) vs. simulated (lines) data for the emplaced source experiment: (a) peak concentrations at the 1-m fence, and (b) mass remaining in the source.

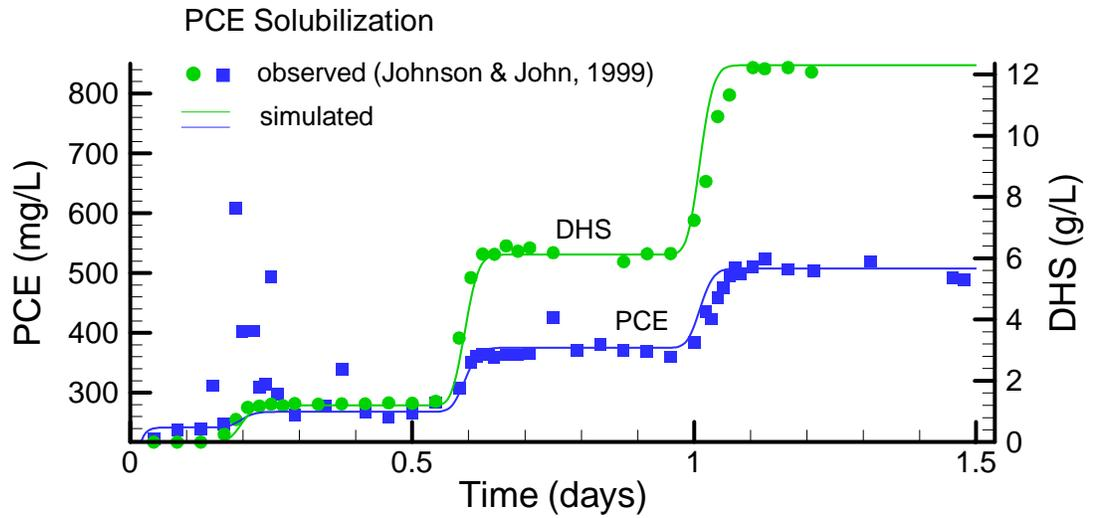


Figure 2.3: Humic acid-enhanced PCE solubilization. BIONAPL/3D simulation vs. observed data from Johnson & John (1999).

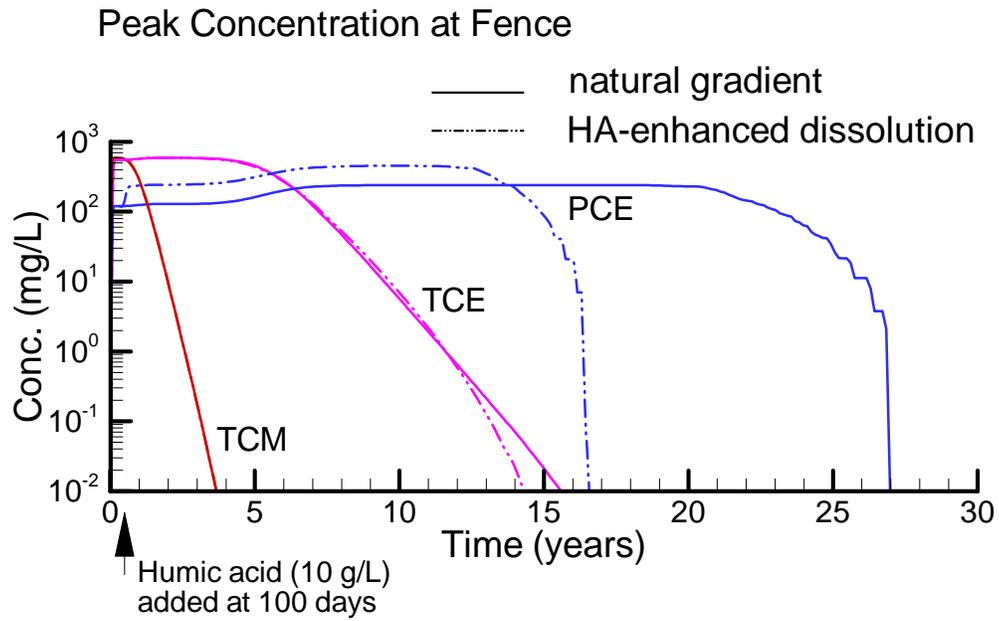


Figure 2.4: Comparison of long-term dissolution of the Borden source: Field condition (natural gradient) vs. HA-enhanced dissolution of PCE.

2.4.3 Illustrative Example 2: Toluene Biodegradation with Multiple Electron-Acceptors

In this example, BIONAPL/3D is applied to simulate dissolution, transport and biodegradation of toluene within a shallow aquifer system. Toluene is a major component of gasoline and although there are exceptions, it has been shown to degrade under a variety of aerobic and anaerobic conditions (Wiedemeier et al. 1999). Evidence for anaerobic toluene degradation, for example, has been provided by Ball & Reinhard (1996) (denitrification), Thierrin et al. (1993) (sulphate-reducing) and Acton & Barker (1992) (methanogenesis). Cozzarelli et al. (2000) describe a gasoline-contaminated field site in which these anaerobic processes, in addition to Fe(III) reduction, were considered important.

The conceptual model includes a dissolving source of toluene and a standard sequence of electron acceptors, or redox processes, beginning with aerobic respiration, followed by denitrification and sulphate reduction and finally, methanogenesis (Table 2.1). The 3D aquifer, measuring $400\text{ m} \times 6\text{ m} \times 10\text{ m}$, is discretized using $106 \times 14 \times 30$ ($= 44,520$) elements in the x, y and z directions, respectively. Longitudinal, transverse horizontal and transverse vertical dispersivities are assumed to be 1.0 m, 0.1 m and 0.01 m, respectively. The aquifer is assumed low in iron and nutrient limitations are not considered. Similar conceptual models for BTEX degradation have been proposed by Bouwer and McCarty (1984) and Wiedemeier et al. (1999), and corresponding redox zones have been identified at contaminated field sites by Lyngkilde & Christensen (1992) (Vejen Site, Denmark) and Ludvigsen et al. (1998) (Grindsted Site, Denmark). Similar 2D simulations have been presented by Brun et al. (1994).

Table 2.1: Summary of simulated redox reactions for example 2.

Reaction Type	Reaction Stoichiometry	$\frac{Mass\ EA}{Mass\ Toluene}$
Aerobic Respiration	$C_7H_8 + 9O_2 \implies 4H_2O + 7CO_2$	3.13
Denitrification	$C_7H_8 + 6NO_3 \implies 4H_2O + 3N_2 + 7CO_2$	4.04
Sulphate-reducing	$C_7H_8 + 4SO_4 \implies 2H_2O + 4HS + 7CO_2$	4.2
Methanogenesis	$C_7H_8 + 5H_2O \implies \frac{9}{2}CH_4 + \frac{5}{2}CO_2$	0.78

Toluene is dissolving from the source at a concentration of 50 mg/L into a clean aquifer. The initial condition for the electron acceptors was fixed at 5 mg/L, 10 mg/L and 20 mg/L for oxygen, nitrate and sulphate, respectively. Maximum degradation rates were fixed at $k = 0.02\text{ mg}_{org}/\text{mg}_{mic}/\text{day}$, while a half-life of 50

days was assumed for methanogenesis, which was simulated by allowing methane to form as a first-order daughter-product of toluene degradation. A retardation factor of $R = 2$ was assigned for toluene. A steady state flow system is assumed with recharge across the top and left boundaries.

In this example, a fully 3D system is assumed, with uniform inhibition coefficients (K_I^n , see equation 2.9) equal to 10^{-6} , essentially restricting use of each electron acceptor to only those areas in which the previous electron acceptor has been totally consumed. The results at 20 years are provided in Figure 2.5. Oxygen, the initial preferred electron acceptor, shows the largest depletion zone, extending from the source to about 350 m downgradient. Although oxygen is only being depleted where toluene exists, the dissolved oxygen plume is more extensive because toluene is retarded and the oxygen depletion plume continues to advance at approximately the rate of groundwater flow. Nitrate becomes depleted in the core of the oxygen depletion plume, decreasing from a background of 10 mg/L to essentially 0 mg/L , and sulphate becomes depleted within the core of the nitrate depletion plume, decreasing from 20 mg/L to about 15 mg/L . Once sulphate concentrations are reduced, methane is produced at a first-order rate from toluene degradation. In this example, however, oxygen and nitrate are the primary electron acceptors and sulphate is not significantly depleted. Dissolved methane concentrations therefore remain relatively low.

The nitrate and sulphate depletion zones do not extend up into the source area, as is often observed, because of the assumption that these components are entering the aquifer at background concentrations. In reality, they would likely be consumed within the source area itself, assuming no microbial inhibition. This could easily be simulated in the model by including the source within the aquifer domain (instead of at the boundary), or by lowering the source input concentration of the electron acceptors. The microbe populations grow only where the concentrations of toluene and the respective electron acceptor are sufficiently high. The oxygen-utilizers (Figure 2.5), for example, show growth only within the source area and around the periphery of the oxygen depletion plume.

The simulated system is conceptually valid, although highly idealized. In heterogeneous systems, for example, the redox zones would tend to overlap because of dispersive mixing, spatially variable microbial growth and nutrient limitations.

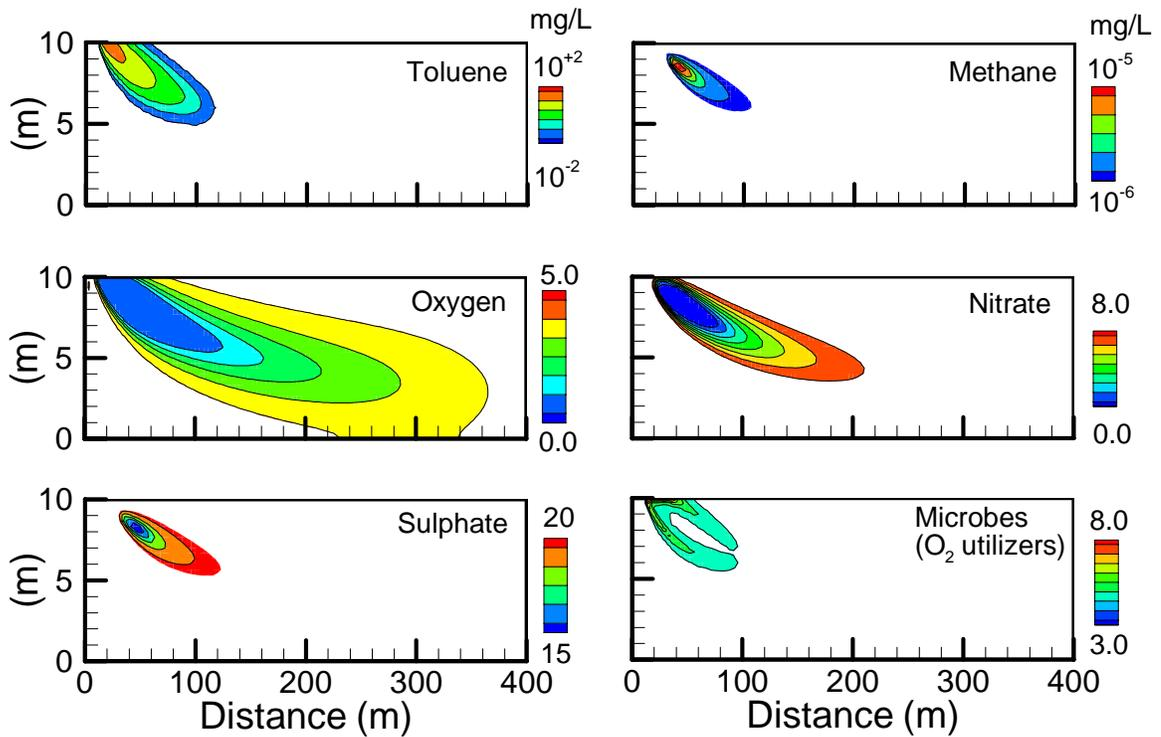


Figure 2.5: Simulated plumes, at 20 years, showing toluene and methane plumes, depletion of oxygen, nitrate and sulphate, and the growth of the oxygen-utilizing microbes. Electron acceptors are only plotted where they are depleted below their background levels. Vertical slice through a symmetric 3D system.

Chapter 3

Numerical Simulation of Enhanced Diesel Fuel Dissolution

Abstract

A pilot scale experiment involving humic acid-enhanced diesel fuel dissolution is numerically simulated in three dimensions. The simulation approach considers the nonlinear coupled processes of multicomponent enhanced NAPL dissolution, reactive mass transport of the dissolved organics and humic acid carrier and aerobic biodegradation. Calibration is achieved by comparing observed and simulated concentrations of seven diesel fuel components (BTEX and methyl-, dimethyl- and trimethylnaphthalene) over a 1500-day monitoring period. Dissolution and biodegradation rates were calibrated, however most physical parameters required by the model were obtained from independent data including partition coefficients for the organics to the humic acid carrier and sorption to aquifer solids. The observed asymmetric breakthrough of the humic acid was reproduced assuming a kinetically-limited Langmuir sorption model. The model showed an excellent fit to the observed data, and accurately reproduced the humic acid-induced 10-fold increase in apparent solubility of trimethylnaphthalene. Solubility increases on the order of 2-5 were simulated for methylnaphthalene and dimethylnaphthalene respectively. A sensitivity analysis showed that the time required for complete source depletion was most dependent on the organic/humic acid partitioning coefficients, on the humic acid concentration and on the rate of NAPL dissolution. The simulations suggest that biodegradation was most active for BTEX and the remaining, unmonitored fraction of diesel fuel (including the n-alkanes), and that dissolution of the diesel source was occurring at near-equilibrium throughout the experiment. Under the experimental conditions, the residual 500 mL diesel source was almost completely dissolved and degraded within 5 years. Without humic acid flushing, complete remediation to drinking water limits would take about 5 times longer.

3.1 Introduction

Under natural conditions, multicomponent nonaqueous phase liquids (NAPL's) trapped within an aquifer typically dissolve very slowly, taking several decades or longer to completely dissolve. Conventional pump-and-treat technology is often not a practical option under these conditions. Much of the current NAPL remediation research is therefore focussing on enhanced dissolution processes in which the effective source dissolution rate is increased by introducing a flushing agent to which aqueous hydrophobic organic contaminants (HOC's) can partition. Possible approaches, for example, include flushing a residual NAPL source with surfactants, cosolvents or dissolved organic carbon (DOC).

Surfactants have shown excellent promise as a NAPL remediation option due to their high solubilization potential (EPA, 1995; Sabatini et al. 1995; Danzer & Grathwohl, 1998; Brusseau et al. 1999), however they can be relatively expensive and are often toxic to the indigenous microbes (Lewis, 1991; Laha & Luthy 1991, 1992; Rouse et al., 1994). Surfactants can act as preferred carbon sources over organic contaminants (Tiehm, 1994), and can reduce organic bioavailability (Guha & Jaffe, 1996; Zhang et al., 1997). Surfactants and cosolvents also tend to reduce the NAPL-water interfacial tension (IFT). While this is often used to advantage (Martel et al. 1998; Grubb & Sitar 1999), reducing the IFT may be detrimental to remediation efforts if downward mobilization is undesired, for example to an underlying aquifer. At contaminated sites requiring NAPL solubilization but not mobilization, surfactants and cosolvents may not be the best choice.

Dissolved organic carbon is now receiving increased attention as an alternative to surfactants and cosolvents for NAPL remediation. DOC is a naturally occurring product of organic matter decay which is relatively inexpensive, non-toxic to microbes and has shown strong sorbing potential for HOC's (McCarthy & Jiminez, 1985; Chiou et al. 1986a,b; Johnson & John 1999). In contrast to surfactants, humic acid concentrations do not have to reach a critical micelle concentration for enhanced dissolution (Lesage et al. 1997; Guetzloff & Rice, 1994). Furthermore, in cases where NAPL mobilization would risk further contamination, DOC may be preferred because it tends to decrease the interfacial tension to a lesser extent than surfactants or alcohol cosolvents (Johnson & John, 1999). DOC is also of interest for its effects on mobilizing metals (Bryan et al. 1997) and radionuclides (McCarthy et al. 1998; Warwick et al. 2000).

A significant fraction of DOC is often composed of dissolved humic substances (DHS), or humic acid (HA), a mixture of complex macromolecular compounds to which dissolved organic contaminants are readily bound (McCarthy & Zachara,

1989). Humic substances have been studied in great detail over the past decades, both with respect to their behaviour in the natural environment (Visser 1964; McCarthy et al. 1993; Gu et al. 1994) and with respect to their potential use as a carrier for contaminant remediation (Abdul et al. 1990; Magee et al., 1991; Gauthier et al., 1987; Johnson & John 1999). Gron et al. (2000) study the origin of aquifer humic substances in relation to their importance in water quality and aquifer vulnerability.

Sorption processes play critical roles in determining whether the carrier will enhance or reduce contaminant mobilization. Sorption of mobile organics to the mobile humic acid, for example, will enhance mobilization, however sorption of organic-laden humic acid to aquifer solids will tend to reduce mobilization. Furthermore, these sorption processes often show nonlinear behaviour (Carter & Weber, 1994; Roy & Dzombak, 1998) .

Johnson and John (1999) suggest that HA can be superior to surfactants in many cases because HA-enhanced solubilization does not depend on the formation of a micellar (aggregate) phase. They highlight the need to more accurately define the sorption behaviour of both HA and surfactants before choosing the most suitable option. In a comparison of enhanced TCE solubility using six flushing agents, including surfactants, complexing agents and alcohol, Boving & Brusseau (2000) found humic acid to be most efficient on a molar-efficiency basis, and found no residual mobilization.

In this Chapter, an advanced 3D numerical model is developed to help interpret a pilot-scale experiment involving humic acid flushing of a residual diesel fuel source. Details of the experiment are provided by Van Stempvoort et al. (2000). The model is calibrated with respect to dissolution and biodegradation rates, however most simulation parameters were obtained from independent sources. The results show that laboratory-derived sorption parameters can be applied at larger scales and that nonlinear and kinetic sorption behaviour of the humic acid must be considered to reproduce the observed trends. A sensitivity analysis highlights the relative importance of the sorption, biodegradation and dissolution processes and predictive simulations are made to assess remediation efficiency under different conditions.

3.2 Insight from Existing Numerical Models

The interactions between multiple component phases involved in enhanced solubilization are complex and often difficult to interpret. Advanced numerical models can now help provide much insight into system behaviour by validating conceptual

models, assessing parameter sensitivity and predicting remediation efficiency. For example, simulations can help identify the limitations of a proposed remediation approach including availability of electron acceptors and rate-limited dissolution and sorption.

Processes which are fundamental to the current simulation problem include ambient groundwater flow, dissolution of the residual NAPL, sorption to the mobile HA carrier, sorption to aquifer solids and biodegradation of the mobile organics. The NAPL may have multiple components and the dissolution, sorption and biodegradation processes may be rate-limited. Ideally, the processes should be considered within a fully 3D dynamic system.

Several models have been developed in the past which address some, but not all of these processes together. Simulation models for DOC-facilitated transport have been developed, for example, by Corapcioglu & Jiang (1993), Liu & Amy (1993), Johnson et al. (1995), Knabner et al. (1996), Rebhun et al. (1996), Totsche et al. (1997) and Johnson (2000). A review of some earlier models for DOC transport in aquifer columns is provided by Jardine et al. (1992).

Various conceptual models and numerical solution approaches have been used and most models can be applied to a variety of carriers. Ibaraki & Sudicky (1995), for example, present a 2D finite element model for single-contaminant, colloid-facilitated transport in discretely fractured porous media. Their approach includes a two-site sorption model and first-order decay of the contaminant. McCarthy et al. (1996) apply a 3D numerical model to simulate a field injection test of natural organic matter (NOM) in a sand aquifer. Deviations between some observed and simulated NOM-breakthrough curves were thought to result from the complex mixture of different NOM subcomponents. Sorptive behaviour of the NOM was derived indirectly by comparing travel times of NOM with those from a simulated conservative tracer. Their study focussed on the behaviour of NOM in a natural field environment and did not consider contaminant interactions.

There is a general consensus among the simulation approaches that DOC can be considered as an aqueous phase colloid or carrier and that nonlinear and non-equilibrium sorption or mass transfer of both the carrier and organic contaminant should be considered. Haggerty & Gorelick (1995) present an overview of standard first-order mass transfer models as well as a more general multi-rate model. Although they do not consider multi-component carrier transport, their approach and insights are directly applicable to the sorption processes considered herein. Warwick et al. (2000) compare equilibrium and mixed equilibrium/kinetic models for sorption of europium in the presence of humic substances. They found a significantly improved fit with their mixed kinetic approach.

A versatile simulation approach is presented by Ji & Brusseau (1998) which is applicable to a variety of surfactants, cosolvents and natural organic matter. They transport the free aqueous phase organic contaminant and carrier-sorbed pseudo-phase as a single component and include two-rate (equilibrium/kinetic) sorption and kinetic NAPL dissolution. Biodegradation is not considered. The model is verified against two 1D experiments assuming a Freundlich isotherm for the flushing agents. A sensitivity analysis highlights system behaviour for various sorption parameters and dissolution rates.

Numerical models have also been widely used to help interpret the processes of residual NAPL dissolution (Sleep & Sykes, 1989; Powers et al. 1994b; Chrysikopoulos & Lee, 1998; Frind et al. 1999) and electron acceptor-limited biodegradation (MacQuarrie et al. 1990; Essaid et al. 1995; Bekins et al. 1998). Additional models incorporating various combinations of enhanced NAPL dissolution, contaminant degradation and sorption have been presented by Corapcioglu & Kim (1995), Guha & Jaffe (1996), Grimberg et al. (1996), Zhang et al. (1997) and Ramaswami & Luthy (1997), however all are limited to various degrees in the number of processes or components included. Grimberg et al. (1996) and Zhang et al. (1997), for example, develop models for simulating surfactant-enhanced dissolution, partitioning and biodegradation, but only consider a single component (phenanthrene) in simplified batch systems.

Two well-known existing models, BIOMOC (Essaid & Bekins, 1997) and BIOPLUME III (Rifai et al., 1997) include several relevant processes but are also limited in scope. Both models, for example, are based on a finite-difference flow solution and are limited to two dimensions. Neither model includes NAPL dissolution or carrier transport. BIOPLUME III cannot simulate multi-species competitive biodegradation and multiple organics must be treated as a single lumped component.

Hunter et al. (1998) present a comprehensive model for simulating multi-component transport and microbially-driven redox processes in groundwater but do not include NAPL dissolution. Most recently, Mayer (1999) has developed one of the most advanced multicomponent reactive transport models to date, including unsaturated flow and kinetic geochemical reactions. This model is currently being updated to include NAPL dissolution and active microbial populations; carrier transport is not included.

Despite the recent advances in numerical models for carrier-enhanced NAPL dissolution and reactive transport, fully three-dimensional simulation approaches remain scarce. Since model verification and applications have also been primarily restricted to 1D single-component column experiments, there is a definite need for multi-component DOC-enhanced dissolution experiments as well as model applica-

tions at larger scales. Furthermore, kinetic electron acceptor-limited biodegradation of aqueous contaminants has not yet been simulated in a multi-component, DOC-enhanced NAPL dissolution system, even though one of the primary functions of using DOC for NAPL remediation is to promote natural attenuation. Indeed, there appears as yet no existing model for simulating such a system.

3.3 Current Objectives

Most applied research on the potential of humic acids for groundwater remediation has focussed on laboratory batch or column experiments (e.g. Dunnivant et al. 1992; Johnson & Amy, 1995) which do not account for larger scale flow system dynamics or transport processes. To be a practical remediation option, the behaviour of humic acid as an organic carrier must be well understood at larger scales. A pilot-scale experiment was therefore designed at the National Water Research Institute (NWRI, Burlington, ON), in which humic acid was used to enhance the dissolution of residual diesel fuel within a controlled environment (Lesage et al., 1997; Van Stempvoort et al., 2000). The pilot scale experiment was completed in conjunction with detailed batch experiments in which sorption behaviour of the carrier and aqueous diesel components was well defined. The primary objective of the experiment was to assess the efficiency of humic acids for enhancing the dissolution of some relatively less-soluble components of diesel fuel.

The dissolution experiment was performed under water-saturated conditions where natural volatilization and aerobic biodegradation losses would normally be less than in the vadose zone and where enhanced remediation methods would more likely be considered. Although diesel fuel is a light non-aqueous liquid (LNAPL), it may be found below the watertable for example, after leaking from a deep underground storage tank or from a remnant watertable pool becoming trapped as the watertable rises (Figure 3.1).

As part of the data analysis, and to help demonstrate this remediation technology, a comprehensive 3D numerical model of the pilot scale experiment has been developed. The model can simulate the coupled processes of kinetic multi-component NAPL dissolution and organic biodegradation within a saturated system and includes the processes of humic-acid enhanced dissolution and kinetic nonlinear sorption. The model is first calibrated to laboratory batch experiments to define sorption behaviour of the HA carrier, then applied to the full pilot scale experiment including verification against breakthrough data for seven diesel fuel components. Most model parameters were obtained from the literature or from laboratory tests

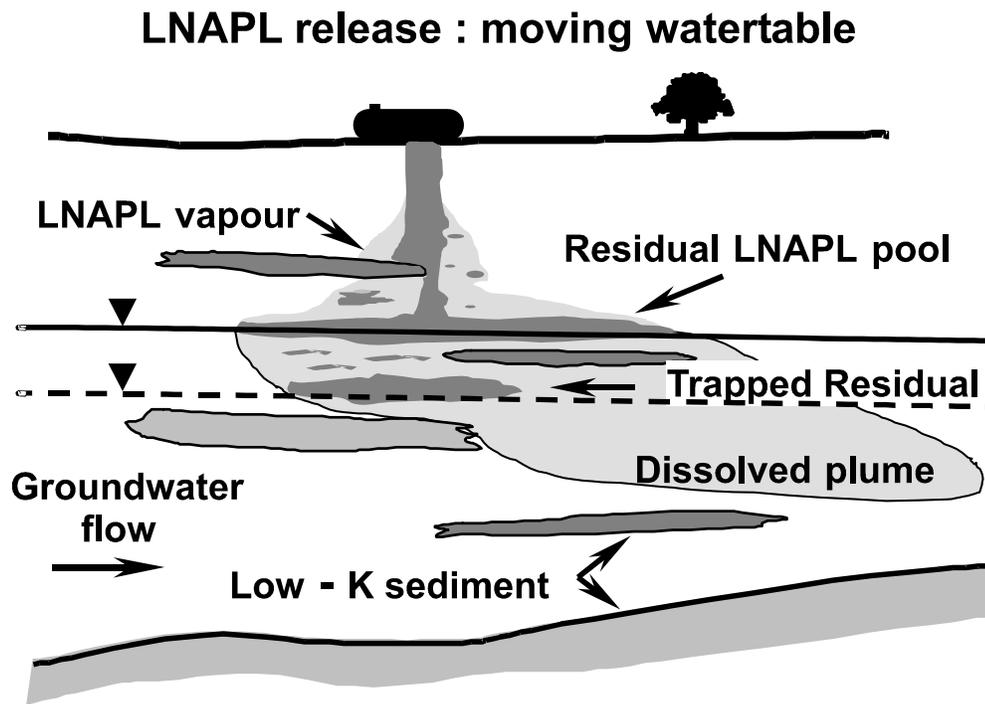


Figure 3.1: Conceptual model for development of a residual LNAPL source within the saturated zone.

described by Van Stempvoort et al. (2000). Minimal calibration was required although some degree of non-uniqueness remains in the biodegradation and dissolution rates. The simulations provide the first fully 3D results of a pilot scale enhanced dissolution experiment. Further details of the numerical simulations are provided by Molson & Frind (2000), and Molson et al. (2000b,c).

The numerical simulations have confirmed that humic acid carriers at high concentration can increase the solubility of relatively low-soluble diesel fuel compounds. Solubility enhancement factors of 2-10 were observed and simulated for the naphthalene components under the pilot scale conditions. Additional work is required to obtain unique biodegradation rates, and to further identify kinetic limitations of the sorption processes.

3.4 Theoretical Development

3.4.1 The Conceptual Model

The conceptual model for the diesel fuel simulations assumes a three-dimensional (3D), three-phase system (Figure 3.2) consisting of a non-aqueous phase (the residual multicomponent diesel source), an aqueous phase (containing the dissolved diesel components and mobile carrier), and a sorbed phase (including the sorbed diesel components and sorbed carrier). The humic acid carrier (Aldrich HA) is assumed here to behave as a single compound, although in reality it is a mixture of various components with similar structure but different molecular weights (Stevenson & Goh, 1971). The results will show that this approach is reasonable.

Sorption of the carrier to the aquifer solids is represented by a mixed equilibrium/kinetic two-site conceptual model using Freundlich or Langmuir isotherms for the equilibrium component. In this approach, a fraction of the solid sorption sites for the carrier is assumed to be in equilibrium with the carrier while sorption to the remaining fraction is kinetically limited. The approach combines the 2-site sorption model used by Haggerty & Gorelick (1995) (extended here to include Langmuir isotherms) with the dissolution enhancement approach as presented by Ji & Brusseau (1998).

In order to simulate the pilot scale test, several coupled processes must be considered in the model. These processes include dissolution of the residual diesel source, transport and sorption of the aqueous diesel components, transport and sorption of the humic acid carrier, and electron acceptor-limited organic biodegradation. The simulation approach for the processes of dissolution, transport and

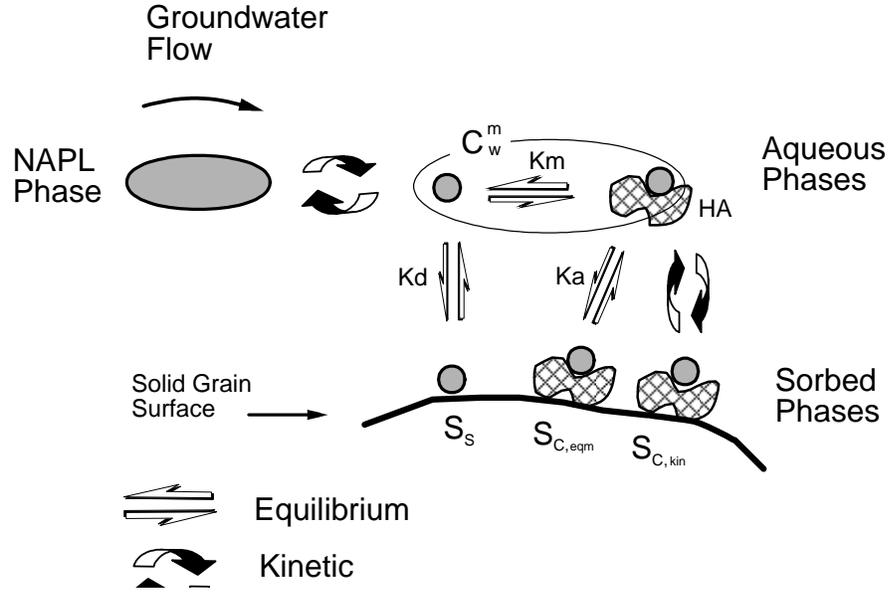


Figure 3.2: Conceptual model for NAPL dissolution and sorption to the organic carrier and solids. Here, C_w^m represents the aqueous pseudo-phase including both the free and carrier-bound dissolved organic.

biodegradation was outlined in Chapter 2. In this chapter, the focus will be on the sorption processes and interaction between the diesel compounds and the organic carrier.

3.4.2 Governing Equations for Carrier Transport

Adapting equation 2.6 from Chapter 2, the general equation for reactive transport of an organic carrier can be expressed as:

$$L(\theta S_w C_c) = \frac{\partial(\theta S_w C_c)}{\partial t} + f \rho_b \frac{\partial(S_c)}{\partial t} + (1 - f) \rho_b \frac{\partial(S_{c,kin})}{\partial t} \quad (3.1)$$

where $L(\theta S_w C_c)$ is an operator for advective-dispersive transport (see equation 2.6), $C_c(kg/m_w^3)$ is the aqueous carrier concentration, f is the mass fraction of sorption

sites available for equilibrium sorption, t is time, S_w is the water saturation, and θ is the porosity. The sorbed phase carrier concentrations S_c ($kg_{carrier}/kg_{eqm_solids}$) and $S_{c,kin}$ ($kg_{carrier}/kg_{kin_solids}$) represent the equilibrium and kinetic sorbed fractions, respectively. In this approach, transport behaviour of the humic acid is assumed unaffected by the presence of sorbed aqueous contaminants.

In general, S_c can be a linear or non-linear function of the carrier concentration C_c . Assuming a Freundlich isotherm for example, the sorbed carrier concentration can be written as

$$S_c = K_a(C_c)^n \quad (3.2)$$

where K_a (m_w^3/kg_{solids}) is the sorption coefficient and n is a fitting parameter. If we assume a Langmuir-type isotherm for the equilibrium sorbed phase of the carrier, we can write:

$$S_c = QK_a C_c / (1 + K_a C_c) \quad (3.3)$$

where Q ($kg_{carrier}/kg_{solids}$) is the maximum sorbed concentration for the equilibrium phase. The total sorbed phase carrier concentration (S_T) is therefore

$$S_T = f \cdot S_c + (1 - f) \cdot S_{c,kin} \quad (3.4)$$

Substituting either equations 3.2 or 3.3 into 3.1, and letting $\partial S_c / \partial t = \partial S_c / \partial C_c \cdot \partial C_c / \partial t$, we obtain

$$L(\theta S_w C_c) = \frac{\partial(\theta S_w C_c)}{\partial t} R_1 + (1 - f) \rho_b \frac{\partial(S_{c,kin})}{\partial t} \quad (3.5)$$

where, assuming a Freundlich isotherm:

$$R_1 = 1 + \frac{f \rho_b}{\theta S_w} K_a n (C_c)^{(n-1)} \quad (3.6)$$

or, assuming a Langmuir isotherm:

$$R_1 = 1 + \frac{f\rho_b}{\theta S_w} \cdot \frac{QK_a}{(1 + K_a C_c)^2} \quad (3.7)$$

Following the approach of Haggerty & Gorelick (1995), we express the kinetic sink term in equation 3.5 using

$$(1 - f)\rho_b \frac{\partial(S_{c,kin})}{\partial t} = \rho_b \alpha (S_c - S_{c,kin}) \quad (3.8)$$

where $\alpha(day^{-1})$ represents a first-order mass transfer coefficient between the equilibrium and kinetic carrier concentrations. The transport equation for the reactive carrier then becomes

$$L(\theta S_w C_c) = \frac{\partial(\theta S_w C_c)}{\partial t} R_1 + \rho_b \alpha (S_c - S_{c,kin}) \quad (3.9)$$

During the solution of equation 3.9, the kinetic sorbed carrier concentration $S_{c,kin}$ is updated using 3.8 according to

$$S_{c,kin}^{t+\Delta t} = \frac{\alpha \Delta t}{(1 - f)} (S_c - S_{c,kin}) + S_{c,kin}^t \quad (3.10)$$

For one-site sorption, we assign $\alpha = 0$.

3.4.3 Governing Equations for Reactive Organic Transport

The equation governing reactive transport of the dissolved phase diesel fuel components in the presence of an organic carrier can be expressed, following the convention of equation 2.6 (Chapter 2), as:

$$L(\theta S_w C_w^m) + \theta S_w \lambda_{DIS}^m (C_s^m - \frac{C_w^m}{E}) = \theta S_w \frac{\partial(C_w^m)}{\partial t} + \rho_b \frac{\partial(S_{s-s}^m)}{\partial t} + \rho_b \frac{\partial(S_{s-c}^m)}{\partial t} \quad (3.11)$$

where C_w^m (kg/m^3) represents the *total* aqueous concentration of substrate component m (aqueous + "pseudophase" sorbed to the mobile carrier), λ_{DIS}^m (day^{-1}) is the NAPL dissolution rate coefficient, E is the solubility enhancement factor and S_{s-s}^m and S_{s-c}^m (kg/kg_{solid}) represent the concentrations of the substrate sorbed to aquifer solids and substrate sorbed to sorbed carrier, respectively (for simplicity, the biodegradation term is omitted here - see Chapter 2 for details). Following the terminology of Frind et al. (1999), the NAPL dissolution rate is expressed as

$$\lambda_{DIS}^m = Sh^m \cdot \frac{D^m}{(d_{50})^2} \quad (3.12)$$

where Sh^m is the Sherwood number, D^m is the diffusion coefficient (m^2/s) and d_{50} is the mean grain size diameter (m). Although BIONAPL/3D includes a nonlinear rate coefficient, a linear coefficient is assumed here which will be shown to fit the data very well (i.e. $\beta = 0$ in Chapter 2, equation 2.10).

By transporting only the total aqueous organic concentration, it is assumed that transport of the carrier is governed by the same velocity field as the aqueous contaminants. Filtration, in which the large HA molecules may become trapped in narrow or dead-end pores, is therefore not included. This approach is not a serious limitation since the use of DOC as an organic carrier is usually limited to medium or coarse-grained porous media where filtration effects are considered not significant.

In equation 3.11, C_s^m is the effective saturation of the NAPL component, assuming validity of Raoult's Law (modified to account for component activity), given as:

$$C_s^m = C_o^m X^m a^m \quad (3.13)$$

where C_o^m is the pure phase solubility (kg/m^3), X^m is the mole fraction and a^m is the activity coefficient. Raoult's Law has been shown valid for predicting aqueous phase concentrations of diesel fuel components by Lee et al. (1992).

Following the approach of Ji & Brusseau (1998), the influence of a carrier on kinetic NAPL dissolution can be expressed in terms of an "enhancement factor" E which can be expressed as

$$E^m = 1 + K_m^m C_c \quad (3.14)$$

where K_m^m is the linear partition coefficient for the substrate to aqueous mobile carrier, and C_c is the mobile carrier concentration. The free, unbound organic concentration, which controls the dissolution gradient, is then defined as $C_w^{free} = C_w^m/E$.

Assuming a Freundlich isotherm for sorption of the substrate to the aquifer solids, we can express the concentration of the substrate which is sorbed to the aquifer solids as

$$S_{s-s}^m = K_d^m (C_w^m/E^m)^n \quad (3.15)$$

where K_d^m is the linear distribution coefficient (m^3/kg_{solids}). Assuming linear partitioning between the substrate and carrier, the concentration of the organic substrate which is sorbed to the sorbed carrier can be expressed as

$$S_{s-c}^m = \frac{K_m^m S_T C_w^m}{E^m} \quad (3.16)$$

where S_T is the total sorbed carrier concentration defined by equation 3.4.

Substituting equation 3.15 and 3.16 into equation 3.11, we obtain the general reactive transport equation:

$$L(\theta S_w C_w^m) + \theta S_w \lambda_{DIS}^m (C_s^m - \frac{C_w^m}{E}) = \theta S_w \frac{\partial(C_w^m)}{\partial t} R_{eff}^m \quad (3.17)$$

where R_{eff} is the effective retardation coefficient which depends on the assumed sorption model. Assuming a Freundlich equilibrium model for sorption of substrate to solids, and a two-site equilibrium/kinetic model for sorption of carrier to solids, we have

$$R_{eff}^m = 1 + \frac{\rho_b K_d^m n (C_w^m)^{n-1}}{\theta S_w E^n} + \frac{\rho_b K_m^m}{\theta S_w E} \cdot [f \cdot (S_c^m) + (1-f) (S_{c,kin}^m)] \quad (3.18)$$

For one-site models in which only equilibrium carrier sorption is considered, we let $S_{c,kin}^m = 0$.

3.4.4 Numerical Solution Approach

Equations 3.9 and 3.10 for the HA carrier, and equation 3.17 for the organic substrate are solved using a Galerkin finite element scheme using deformable brick elements. The equations are coupled using Picard iteration, within the general nonlinear context of a dissolving NAPL and multiple organic transport and biodegradation. All nonlinear terms are centred in time and updated at each iteration.

Standard first, second and third-type (Cauchy) boundary conditions are available and convergence traps can be specified for the hydraulic head, HA carrier and organics. The matrices are solved using a preconditioned conjugate gradient solver (Braess & König, 1995). The full numerical solution approach is provided in Chapter 2 and a user guide is provided by Molson (2000).

3.5 Model Application to the Diesel Fuel Dissolution Experiment

3.5.1 Description of the Pilot Scale Experiment

The pilot scale experiment was performed at the National Water Research Institute (NWRI), Burlington, Ontario (Lesage et al., 1997; Van Stempvoort et al., 2000). A model sand aquifer, shown in Figure 3.3, was constructed within a stainless steel tank measuring $5.5 \times 1.2 \times 2$ metres in the longitudinal, transverse horizontal and vertical directions respectively and was filled with winter sand of porosity 0.30 and bulk density 1860 kg/m^3 . Approximately 500 mL of diesel fuel was mixed with 25 kg of water-wet sand, creating an initial residual source with a NAPL saturation (V_{NAPL}/V_{VOIDS}) of approximately 0.09. Water and the humic acid solution enters from the left face of the domain (corresponding to the head tank) while effluent is withdrawn from a fully-screened well located just inside the right boundary near the end of the tank. The extracted humic acid is recirculated through the head tank.

Initial flow velocities were maintained at approximately 2 cm/hr but may have decreased later in time due to bacterial pore clogging. The source was allowed to dissolve for 50 days under ambient conditions after which humic acid at a continuous concentration of 0.83 g/L was added at the head tank and recirculated using the extraction well. Throughout the 5-year experiment, the dense 3D multilevel sampling array was monitored for humic acid and several diesel components, including BTEX, methyl, dimethyl and trimethylnaphthalene.

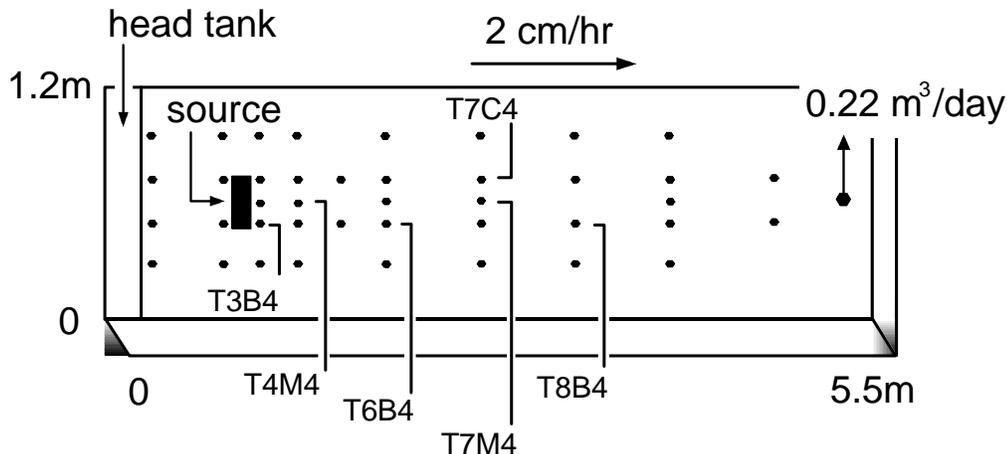


Figure 3.3: Plan view of the pilot scale tank showing location of the source, monitor wells and extraction well. Selected monitor wells are mentioned in the text.

3.5.2 Interpretation of Laboratory Batch Results

Prior to developing the pilot-scale model, sorption behaviour of the organics and humic acid was quantified at the laboratory batch scale. The relevant processes here include sorption of the organic substrates and humic acid to the aquifer solids, and binding of the organic substrates to the humic acid (Van Stempvoort & Lesage, 2000; Van Stempvoort, 2000).

Long-term batch equilibrium sorption of humic acid to aquifer solids clearly shows a Langmuir-type isotherm from which best-fit parameters of $K_a = 39.1 \text{ m}^3/\text{kg}$ and $Q = 0.00042 \text{ kg}/\text{m}^3$ were obtained (equation 3.3 & Figure 3.4). The fit is excellent, and reflects that most sorption to the aquifer solids occurs at low aqueous HA concentrations from 0 - $0.2 \text{ kg}/\text{m}^3$ while at aqueous HA concentrations above $0.2 \text{ kg}/\text{m}^3$, there is relatively minor additional sorption. This behaviour is significant since at the high aqueous HA concentrations used here (approx. $0.83 \text{ kg}/\text{m}^3$), a greater proportion of the aqueous HA is available for binding with the aqueous organics. At lower aqueous HA concentrations, much of the HA is sorbed to the solids and may, in fact, lead to *reduced* mobility of the organic contaminants as observed, for example, by Totsche et al. (1997).

A significant kinetic component of HA sorption to aquifer solids was also observed in which an initial fast equilibrium sorption component is followed by a slow

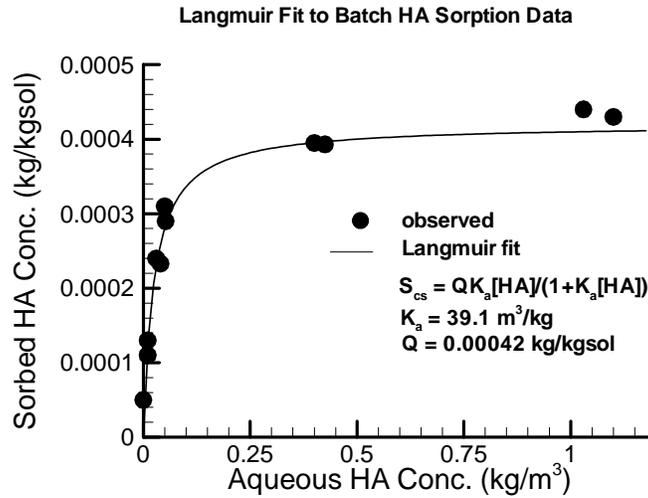


Figure 3.4: Observed vs. fitted Langmuir isotherm for lab batch sorption test of humic acid to winter sand (after Van Stempvoort et al., 2000).

kinetically-limited component (Figure 3.5). This behaviour was reproduced with the two-site sorption model using $\alpha=0.005 \text{ day}^{-1}$ and $f = 0.47$. Approximately one-half of the solid sorption sites are therefore interpreted as being "fast" sites while the remainder are kinetically "slow". Kinetic sorption limitations can be due to several factors including development of boundary interference layers and charge variations along the grain surfaces.

3.5.3 Pilot Scale Simulation Model

Following the fitting of the batch sorption data, the 3D model was applied to simulate the enhanced dissolution of the residual diesel fuel source at the pilot scale. The domain consisted of a three-dimensional grid measuring $5.5 \text{ m} \times 1.2 \text{ m} \times 1.25 \text{ m}$, resolved using $57 \times 20 \times 15 (= 17,100)$ elements in the longitudinal, transverse horizontal and vertical dimensions, respectively (Figure 3.6). Grid spacing varied

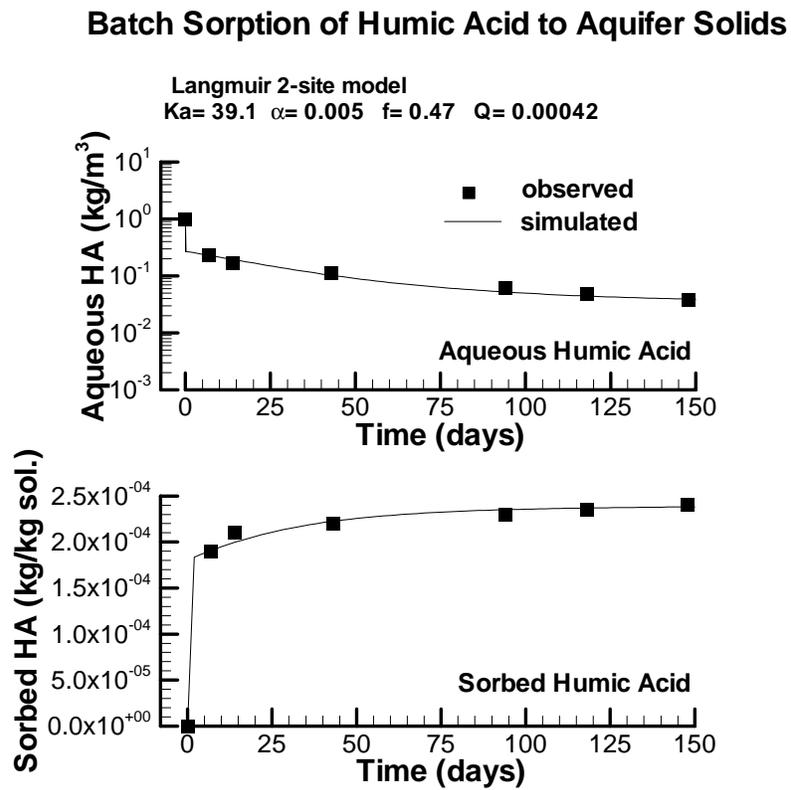


Figure 3.5: Observed vs. simulated transient sorption profile showing early equilibrium and late kinetic behaviour.

along the flow direction from 0.016 m within the source to 0.2 m towards the downgradient boundary.

Spatial resolution was constrained by the grid Peclet criteria (Daus et al., 1985) and by reaction stability and convergence constraints. The small source-element dimensions were used to resolve the dissolution profile and to prevent mass balance errors as the components become completely dissolved. In a 3D simulation of an emplaced solvent at the Borden field site, Frind et al. (1999) found that a slightly larger 0.05 m grid spacing worked well. Somewhat finer dimensions were used for the diesel model because of the relatively higher flow velocities and dissolution rates.

Material properties and flow gradients were obtained from the experimental data (Table 3.1). A fixed head was assigned at the left inflow face (corresponding to the head tank) while all remaining boundaries were impermeable. The withdrawal well was assigned a total flux of $0.216 \text{ m}^3/\text{day}$. Dispersivities of 0.025, 0.005 and 0.005 m were assigned for the respective x , y and z dimensions based on model calibration to a conservative bromide tracer. Simulation time steps varied from 0.2 days at early time and during initial HA flushing, to 1.0 days at later times.

The source consisted of 500 mL of diesel fuel at a residual saturation of approximately 0.09. Groundwater was flushed through the tank at 2 cm/hr over 5 years. Seven unique diesel fuel components were considered in the model: benzene, toluene, ethylbenzene and the xylene isomers (BTEX), as well as methyl-naphthalene, dimethylnaphthalene and trimethylnaphthalene. An eighth "pseudo-component" was used to represent the remaining, relatively less soluble, diesel fuel fraction (referred to here as "other" components). Organic properties, including aqueous solubilities and partition coefficients were obtained from laboratory batch tests or published data. Oxygen was considered as the single electron acceptor with a single microbial population.

Including the humic acid carrier, the concentration of 11 "species" are therefore simulated at each time step over the 19,488-node grid. The computational effort decreases over time as the more soluble components dissolve and are removed from the model.

Calibration of the pilot scale model proceeded in the following sequence:

1. The flow velocity and longitudinal dispersivity were calibrated using breakthrough of a Bromide tracer (not shown)
2. The mass transfer rate of HA to solids was calibrated using breakthrough of the HA.

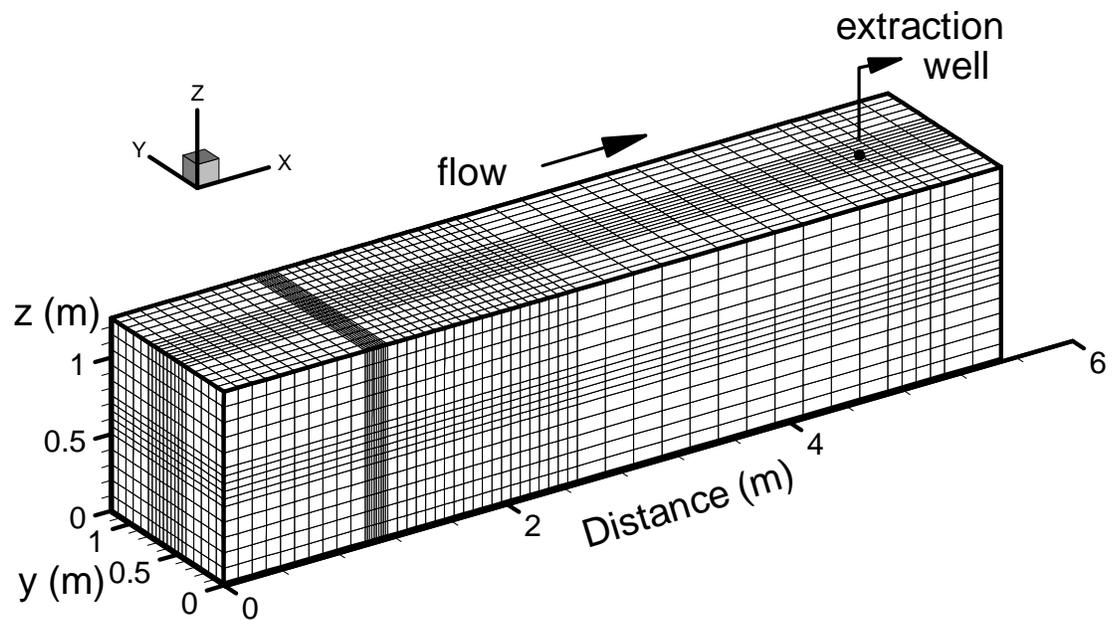


Figure 3.6: Outline of the 3D finite element mesh for the pilot scale model. The residual diesel source is located at the intersection of the fine-mesh areas, 1.0 m from the inflow boundary.

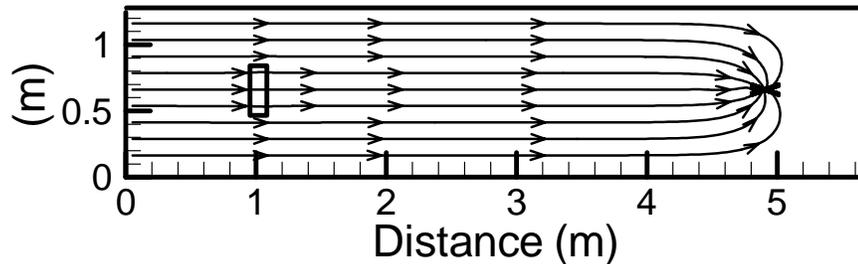


Figure 3.7: Plan view of the pilot scale model showing source location and streamlines converging to the extraction well.

3. Activity coefficients, dissolution rates and degradation rates were calibrated using breakthrough of the organic components.

Physical data for the pilot scale model are provided in Table 3.3. These parameters are considered accurate and unique because they are either based on independent measurements or are calibrated using a conservative Bromide tracer. The flow velocity of 2 cm/hr represents an average across the tank. The initial velocity within the source during the dissolution experiment is approximately 15 % lower because the NAPL is occupying pore space which reduces the relative permeability. The effect is relatively minor, however, and flow lines pass relatively unperturbed through the source, converging downgradient at the withdrawal well (Figure 3.7). As the NAPL dissolves, the relative permeability increases and velocities within the source gradually recover to background levels. The deviation of flow around the source is less than that simulated by Frind et al. (1999) since their source was also characterized by an intrinsically lower permeability. Microbial pore clogging is not considered.

The first test of the model to the pilot scale experiment was with respect to the breakthrough of the humic acid carrier which was added to the tank 51 days after source emplacement at a concentration of 0.83 g/L . The observed vs. simulated breakthrough of the humic acid at monitor wells T3B4 and T7C4 is provided in Figure 3.8 which shows a good model fit to the observed data and verifies that the sorption processes have been accurately reproduced.

The carrier arrives at the two respective monitor wells approximately 5 and 10 days following addition to the head tank. The arrival curves are steep until the

concentration reaches about 0.5 g/L after which nonlinear sorption of the carrier to aquifer solids induces significant tailing. For this simulation, only the kinetic sorption rate coefficient had to be calibrated ($\alpha = 0.05 \text{ day}^{-1}$), all other parameters were obtained independently from batch experiments (Table 3.2). Simulations assuming the lower batch-calibrated rate of 0.005 day^{-1} (not shown) induced a steep arrival curve with almost no tailing and clearly did not match the observed behaviour.

The reason for the discrepancy between the sorption rate coefficient for the batch experiment (0.005 day^{-1}) and that fitted at the pilot scale (0.05 day^{-1}) is not clear. The dynamic nature of the pilot scale experiment and the effect of mixing over the discrete elements may be important.

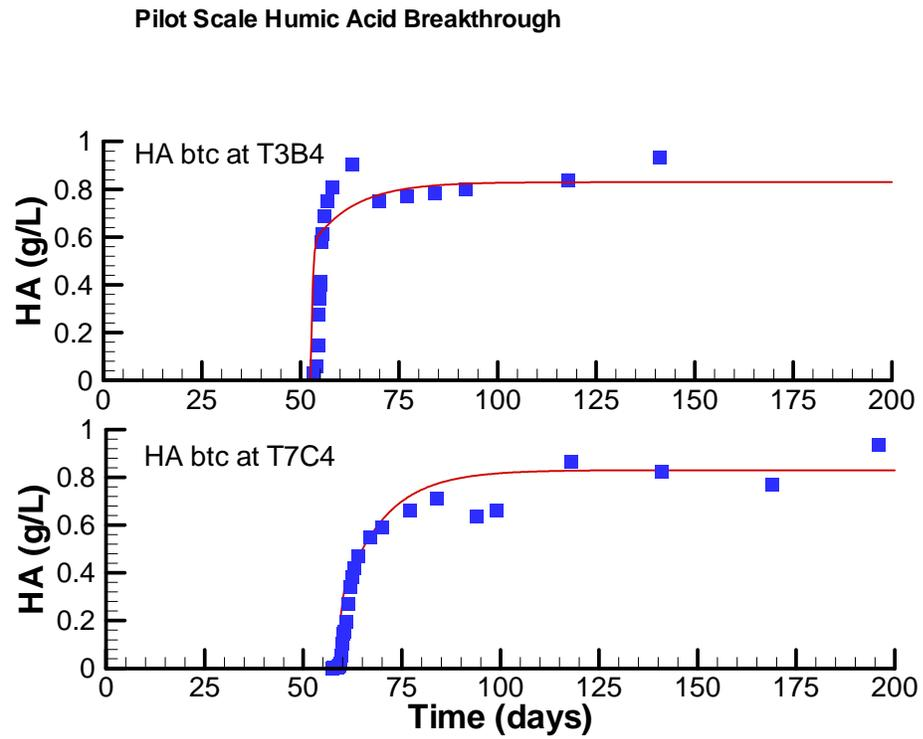


Figure 3.8: Simulated vs. observed breakthrough of the humic acid carrier in the pilot scale experiment at monitors T3B4 (top) and T7C4 (bottom).

Table 3.1: Flow system parameters used in simulating the pilot scale dissolution test.

Parameter	Value	Source
dispersivity:		
longitudinal (α_L)	0.025 <i>m</i>	Br tracer calibration
transverse horizontal (α_{TH})	0.005 <i>m</i>	Frind et al. (1999)
transverse vertical (α_{TV})	0.005 <i>m</i>	Frind et al. (1999)
conductivity (K_x)	1.0×10^{-4} <i>m/s</i>	adjusted to fit initial velocity
gradient (∇h)	0.0167	measured
porosity (θ)	0.30	measured
velocity (<i>v</i>)	≈ 2.0 <i>cm/hr</i> *	Br tracer calibration
bulk density (ρ_b)	1860. <i>kg/m³</i>	measured
median grain size (d_{50})	1.0 <i>mm</i>	measured
extraction rate	0.216 <i>m³/day</i>	measured

* represents the average velocity across the tank.
(measured data from Van Stempvoort et al., 2000)

Table 3.2: Humic acid sorption parameters assumed in the pilot scale simulation model.

Parameter	Value	Source
binding coefficient:		
HA-solids (K_a)	39.1 <i>m³/kg</i>	Langmuir fit to batch data
max. sorbed conc.:		
HA-solids (Q)	0.00042 <i>kg/kg_{sol}</i>	Langmuir fit to batch data
sorption mass transfer coefficient (α)	0.05 <i>day⁻¹</i>	calibrated to pilot scale HA breakthrough
fraction of equilibrium sites (f)	0.47	calibrated from kinetic batch data

Physical properties assumed for the diesel fuel components are provided in Table 3.3. Densities, molecular weights, pure phase aqueous solubilities and diffusion coefficients were obtained or estimated from independent literature sources. The binding coefficients K_c (HOC-solids) and K_m (HOC-HA) were also obtained independently from batch test data (Van Stempvoort et al., 2000).

Additional parameters pertaining to the diesel fuel source are provided in Table 3.4. Mass estimates were obtained from laboratory data and from cumulative flux calculations based on the observed breakthrough data (Van Stempvoort et al., 2000). The mass of the remaining, unknown components is then computed based on assuming an average molecular weight for diesel fuel of 0.230 kg/mole, an average density of 1000 kg/m^3 , and a source volume of 500 mL.

The Sherwood number, which affects the NAPL dissolution rate, (equation 3.12) was unknown and had to be calibrated using the observed breakthrough data of each component. Frind et al. (1999) compare their calibrated Sherwood number (for the Borden emplaced source model) with the Reynolds number for the field experiment and found good agreement with previously published trends. In the current study, the Reynolds number is on the order of 4×10^{-3} and the range of calibrated Sherwood numbers (0.9 -2.2) lies very close to the trend observed by Powers et al. (1994b). Other data (reproduced in Frind et al. 1999, Figure 8) predict somewhat lower Sherwood numbers. It will later be shown that the diesel source was dissolving at or near equilibrium, and therefore the Sherwood number only needed to be high enough to ensure equilibrium dissolution. Activity coefficients for the naphthalenes were also calibrated using the observed breakthrough data, and agree well with published data based on synthetic jet fuel mixtures (Burris & MacIntyre, 1987).

Biodegradation parameters are provided in Table 3.5. Maximum utilization rates (k^m) are consistent with observed data from Schirmer (1998) for the BTEX components, and were calibrated for the naphthalenes. The half-saturation constants (K_C and K_A , the concentrations at which the rate is half-maximum) were fixed at 2.0 mg/L to be consistent with previous estimates (e.g. Schirmer, 1998, Bekins et al., 1998) and to ensure rapid convergence. The microbial yield coefficient (Y) was also based on results from Schirmer (1998) and are applied under the assumption that the biomass carbon is not a significant fraction of the mineralized carbon. The oxygen:substrate mass stoichiometry ratios are calculated assuming complete mineralization (Table 3.6). Boundary input and initial background oxygen concentrations were assumed to be 6.0 mg/L, correlating with tank measurements. The initial microbe concentration was fixed at 5.0 mg/L and a constant microbial decay coefficient of $10^{-10} s^{-1}$ was assumed.

Out of the eight diesel fuel components included in the model, the four BTEX components are the most soluble and rapidly dissolve from the source. Because of their high solubility, it was assumed that humic acid would have minimal direct effect on the BTEX components (therefore $K_m = 0$). Observed and simulated breakthrough curves at monitor T4M4 show essentially complete dissolution within

100 days (Figure 3.9), and while the observed BTEX data are somewhat scattered, the simulated concentrations and general behaviour agree reasonably well with those observed. The observed and simulated total BTEX plumes are shown in plan view in Figures 3.10 and 3.11 respectively. Both the observed and simulated plumes are characterized by high source concentrations which rapidly decline towards the extraction well. The simulated source concentrations are slightly overestimated which can be accounted for by the uncertainty in the BTEX source mole fractions. The simulated plumes are also somewhat shorter than those observed, suggesting that the biodegradation rates for the simulated BTEX components may be high, perhaps a result of neglecting the initial lag period required for microbial growth.

The simulated breakthrough curves of the naphthalene components at a point immediately downgradient from the source (monitor T3B4) are compared to the observed data in Figure 3.12. Three distinct trends characterize both the simulated and observed concentration profiles: an early-time plateau, a sharp increase, and a slow decline.

During the initial 50-day period before humic acid was added, the diesel components dissolve from the source and reach their effective equilibrium saturations according to their aqueous solubilities, mole fractions and activities. Although the observed data show a steady concentration or slightly increasing trend, there is a slight decreasing trend in the simulated breakthrough, in particular for methyl and dimethylnaphthalene. Nevertheless, the fit over this early time period is very good.

At 51 days, humic acid (0.83 g/L) was added to the head tank which reached the diesel source within two days. Partitioning of the organics onto the humic acid rapidly increases the effective solubilities of the naphthalene components with the steepest rise occurring within 5 days of the humic acid arrival. Peak enhanced solubilities are not reached until somewhat later. For methylnaphthalene, the peak occurs 15 days after arrival of the humic acid, 30 days later for dimethylnaphthalene, and 45 days later for trimethylnaphthalene. The delay is due to the initial period of enhanced sorption during which aqueous organic mass is sorbing to the sorbed humic acid which reduces the aqueous organic concentrations. As the humic acid front passes the source, the humic acid concentrations reach the plateau of the Langmuir isotherm and the maximum enhanced solubility is reached.

The solubilities increased by up to a factor of 10 for the trimethylnaphthalenes, and by factors of 5 and 2 for dimethylnaphthalene and methylnaphthalene respectively. Afterwards, concentrations slowly decline due to source mass depletion, dispersion and biodegradation. The simulations suggest that the source was dissolving at equilibrium or near-equilibrium conditions throughout the experiment. The predicted dissolution times to reduce aqueous concentrations to $10 \mu\text{g/L}$ were

500, 1200 and 1700 days for the methyl-, dimethyl- and trimethylnaphthalenes, respectively. The excellent match to the observed data is particularly significant because many parameters were obtained from independent lab data.

The monitor wells immediately downgradient from the source (row T3) provided the best data for calibrating the enhanced source dissolution since they are least affected by flow transients and dispersion, and also seem less affected by biodegradation. As an independent verification, the simulated breakthrough curves at wells further downgradient were also compared to the observed data. For example, at monitors T6B4 (1.2 m downgradient from the source) and T7M4 (1.5 m downgradient), the model again provides a generally good match after addition of the humic acid, although there is somewhat increased scatter in the observed data (Figure 3.13 and 3.14).

The observed early-time trends (≤ 51 days) at T6B4 and T7M4, however, are not as well reproduced as those at T3B4. Whereas the observed trend from 0-50 days shows a gradual concentration increase without a distinct saturation plateau, the simulated concentrations show a rapid rise followed by a clearly decreasing trend. The observed trend may be due to nonlinear sorption of the naphthalenes to the aquifer solids whereas in the model this process is assumed to be linear. The discrepancy may also originate from changes in the flow field due to microbial clogging. Beyond 51 days, following addition of the humic acid, the observed trends are well reproduced at these two monitors. The concentrations are at all times reduced relative to T3B4 because of dispersion and biodegradation within their respective separation distances.

Several downgradient monitor wells showed a relatively consistent double-peak trend in the breakthrough profiles for the naphthalenes (Van Stempvoort, 2000). At T6B4 and T7M4, for example, there is a distinct drop in the breakthrough concentrations at about 200 days (Figure 3.13 and 3.14). This behaviour was thought to result from either slight lateral shifting of the plume, which in plan view contains a distinct low concentration zone down the centreline, or from spatial and temporal variations in the biodegradation rate. Due to the uncertainty in origin, no attempt was made to reproduce these secondary trends which appear relatively insignificant relative to the several orders-of-magnitude range in breakthrough concentrations.

The sharp decrease in the simulated component concentrations at the immediate arrival time of the humic acid (51 days) is due to a loss of mass to the sorbed humic acid ("enhanced sorption"). As the carrier advances through the initially carrier-free tank, sorption to the solids removes a significant quantity from the aqueous phase. As the humic acid front reaches the diesel source, the organic components become sorbed to the sorbed carrier which causes a temporary but distinct drop

in the aqueous concentrations. Although the effect is short-lived, a corresponding drop in some observed concentrations from 52-55 days suggests that this behaviour was indeed occurring in the tank. This trend in the observed data is most apparent at monitors T3B4 and T6B4.

Table 3.3: Physical properties of the diesel fuel components assumed in the pilot scale model.

Diesel Component	$\rho^{(1)}$ <i>kg/m³</i>	MW ⁽¹⁾ <i>(kg/mol)</i>	$C_o^{(2)}$ <i>(kg/m³)</i>	$K_d^{(3)}$ <i>(m³/kg)</i> $\times 10^{-3}$	$K_m^{(4)}$ <i>(m³/kg)</i>	D^* ⁽⁵⁾ <i>(m²/s)</i> $\times 10^{-10}$
Benzene	876.6	0.078	1.78	.0806	0.0	7.7
Toluene	870.	0.092	0.515	.161	0.0	6.6
Ethylbenzene	870.	0.106	0.152	.161	0.0	6.0
Xylenes	870.	0.106	0.198	.161	0.0	5.6
Methylnap.	1000.	0.142	0.035	.20	2.1	6.6
Dimethylnap.	1000.	0.156	0.008	.40	3.7	6.6
Trimethylnap.	1000.	0.170	0.0021	1.3	10.0	6.6
Other cpds.	862.	0.230	0.001	1.3	10.0 ⁽⁶⁾	5.0

^{(1),(2)} Wiedemeier et al. (1999); CRC Handbook, (1980).

^{(3),(4)} Derived from laboratory data: Van Stempvoort et al. (2000). Note: K_m is defined here as m^3/kg_{HA} ($= L/g_{HA}$); to compare with Van Stempvoort (2000), (L/g_{Carbon}) apply a correction assuming 38.2% organic C in HA.

⁽⁵⁾ Wiedemeier et al. (1999) Appdx. B, assuming a tortuosity of 0.7.

⁽⁶⁾ Assumed at least equal to K_m for trimethylnaphthalene; no data available.

Table 3.4: Characterization of the simulated diesel fuel source.

Diesel Component	Source Mass ⁽¹⁾ (kg)	Moles	Mole Fraction	Sh ⁽²⁾	Activity Coeff. ⁽³⁾
Benzene	4.7e-6	6.e-5	0.000028	1.0	1.0
Toluene	1.8e-4	0.002	0.000095	2.0	1.0
Ethylbenzene	5.3e-4	0.005	0.00237	1.0	1.0
Xylenes	1.1e-3	.01	0.00475	1.0	1.0
Methylnap.	0.001	0.007	0.00332	0.9	1.5
Dimethylnap.	0.005	0.032	0.0152	0.9	2.1
Trimethylnap.	0.005	0.029	0.0138	2.2	2.1
Other cpds.	0.465	2.022	0.9596	2.2	2.0
Total:	0.478	2.107	1.0		-

⁽¹⁾ Van Stempvoort et al. (2000), Table 3.

⁽²⁾ calibrated Sherwood number (see equation 3.12)

⁽³⁾ calibrated

Table 3.5: Biodegradation parameters for the simulated diesel fuel components.

Diesel Component	max. rate k ($\text{kg}_{org}/\text{kg}_{mic}/\text{day}$)	\mathbf{K}_C kg/m^3	\mathbf{K}_A kg/m^3	\mathbf{Y} $\text{kg}_{mic}/\text{kg}_{org}$
Benzene	0.5	0.002	0.002	0.5
Toluene	0.5	0.002	0.002	0.5
Ethylbenzene	0.5	0.002	0.002	0.5
Xylenes	0.5	0.002	0.002	0.5
Methylnap.	0.02	0.002	0.002	0.5
Dimethylnap.	0.02	0.002	0.002	0.5
Trimethylnap.	0.02	0.002	0.002	0.5
Other cpds.	0.20	0.002	0.002	0.5

Table 3.6: Reaction stoichiometries for the simulated diesel fuel components.

Diesel Component	Reaction Stoichiometry	Mass ratio X $\text{kg}_{O_2}/\text{kg}_{org.}$
Benzene	$C_6H_6 + \frac{15}{2}O_2 \Rightarrow 6CO_2 + 3H_2O$	3.08
Toluene	$C_7H_8 + 9O_2 \Rightarrow 7CO_2 + 4H_2O$	3.13
Ethylbenzene	$C_8H_{10} + \frac{21}{2}O_2 \Rightarrow 8CO_2 + 5H_2O$	3.17
Xylenes	$C_8H_{10} + \frac{21}{2}O_2 \Rightarrow 8CO_2 + 5H_2O$	3.17
Methylnap.	$C_{11}H_{10} + \frac{27}{2}O_2 \Rightarrow 11CO_2 + 5H_2O$	3.04
Dimethylnap.	$C_{12}H_{12} + 15O_2 \Rightarrow 12CO_2 + 6H_2O$	3.08
Trimethylnap.	$C_{13}H_{14} + \frac{33}{2}O_2 \Rightarrow 13CO_2 + 7H_2O$	3.11
Other cpds.	$C_pH_q + (p + q/4)O_2 \Rightarrow pCO_2 + (q/2)H_2O$	3.20

The (total) naphthalene plumes are shown in plan view (through the source centre) at 41, 70, 385, 958 and 1380 days in Figures 3.15 and 3.16 for the observed and simulated systems, respectively. At 41 days (10 days before adding humic acid), the simulated plume has attained a steady state configuration with source concentrations of about $400 \mu\text{g}/\text{L}$. Also, the outermost $50 \mu\text{g}/\text{L}$ contour has just reached the extraction well which is in good agreement with the observed plume. Although the observed plume appears somewhat wider than the simulated plume, this is possibly an artifact due to the monitor well spacing and contour interpolation between the monitors. The relatively narrow simulated plume is a result of using a low transverse horizontal dispersivity of 0.005 m, which is consistent with the

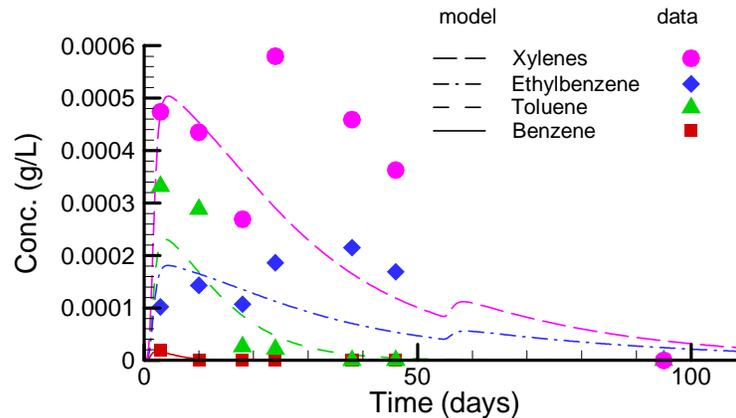


Figure 3.9: Simulated vs. observed BTEX concentrations at monitor T4M4.

scale of the system and previous estimates for systems of similar scale (Frind et al. 1999).

At 70 days (19 days after adding humic acid), the source concentration has increased to $1700 \mu\text{g}/\text{L}$ due to humic acid-enhanced dissolution of the residual diesel. The simulated $50 \mu\text{g}/\text{L}$ contour, however, has somewhat receded relative to its location at 41 days. The apparent shortening of the plume is caused by sorption of the aqueous organics to the sorbed carrier (enhanced sorption), immediately after humic acid flushing. This effect is not apparent in the contoured observed data, suggesting the effect of enhanced sorption may have been somewhat overpredicted. A narrow gap down the centreline of the observed plume at 70 days may have contributed to an extension the contoured observed plume. The origin of this gap is uncertain but may be related to microbial growth. The simulated plumes clearly do not match the observed small scale irregularities, however the general pattern and concentration levels are maintained.

Once the carrier reaches higher concentrations along the plateau of the Langmuir isotherm, the sorption sites become saturated and the organics, which are sorbed to the carrier, become fully mobilized. The plume then begins to re-advance. The effect is highlighted in Figure 3.17 which shows the total naphthalene plumes and corresponding humic acid profiles from 50-65 days. At 55 days, for example, the

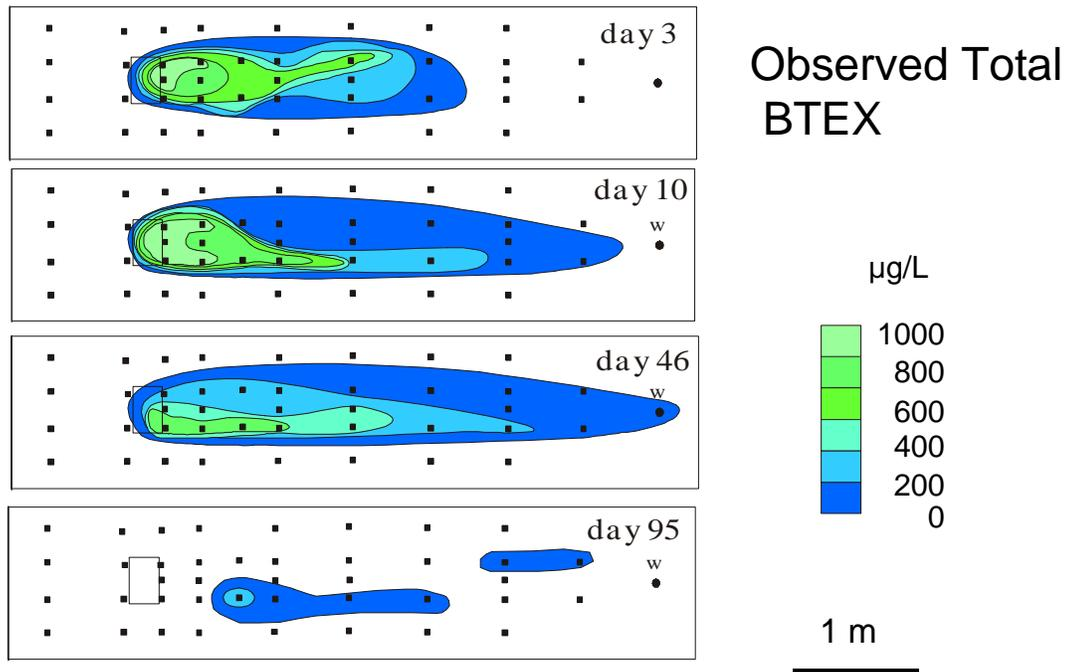


Figure 3.10: Observed total BTEX plumes, plan view through source centre. After Van Stempvoort et al. (2000).

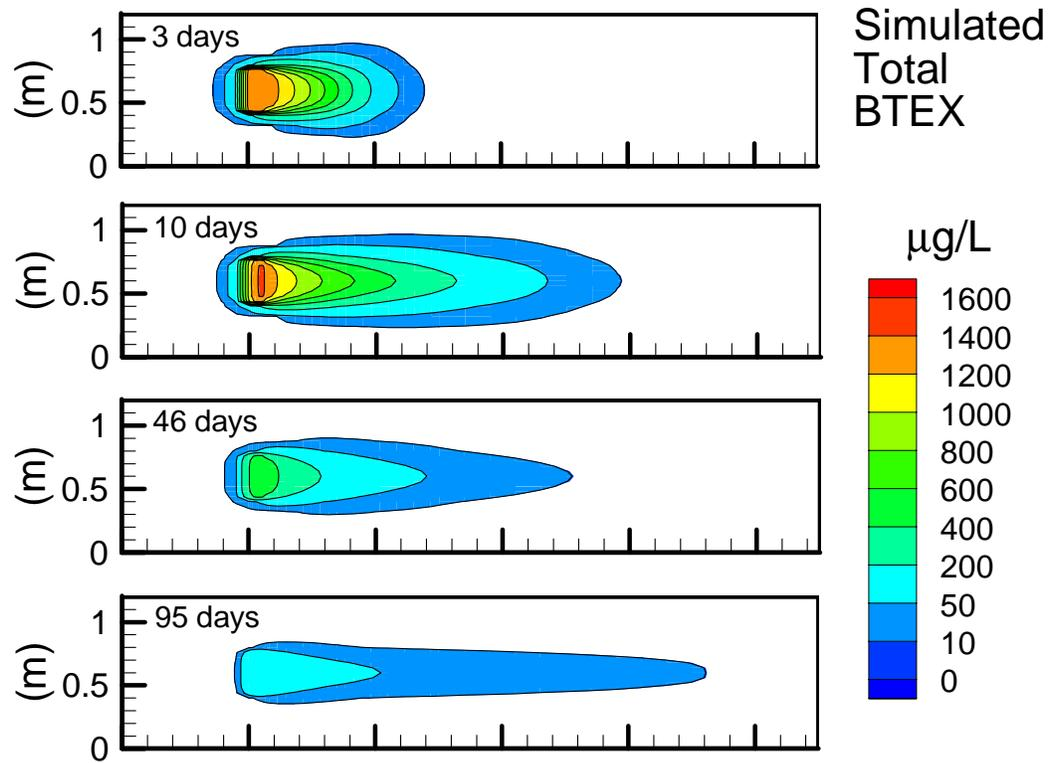


Figure 3.11: Simulated total BTEX plumes at 3, 10, 46 and 95 days. Plan view through source centre.

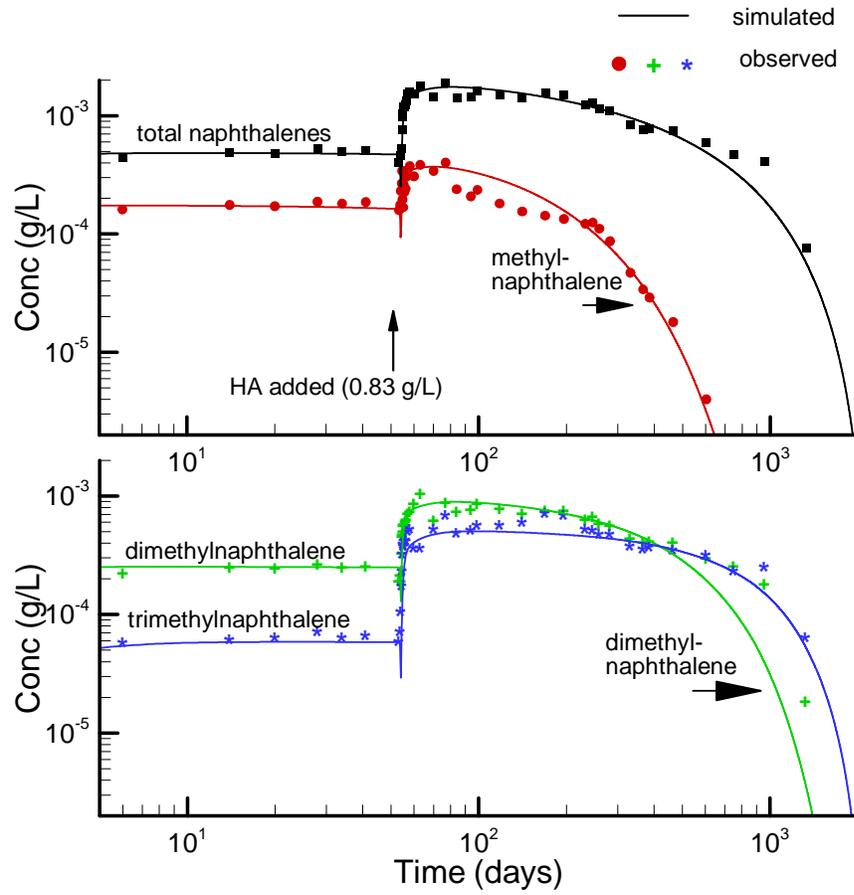


Figure 3.12: Observed vs. simulated breakthrough of the naphthalene components at monitor well T3B4 (immediately downgradient from the source).

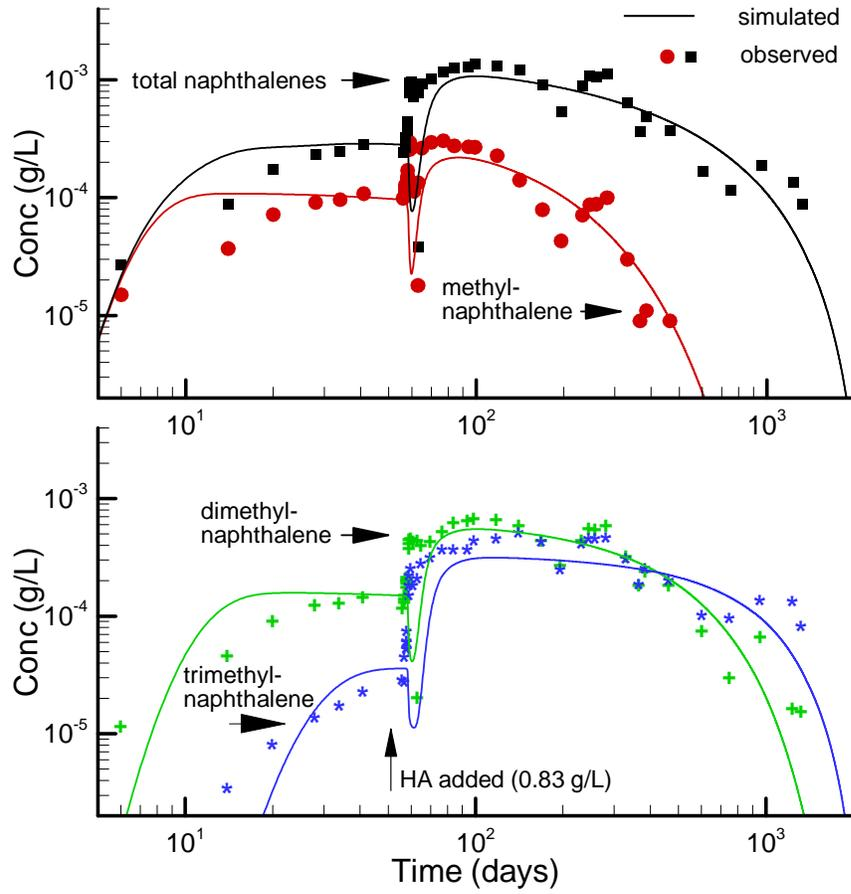


Figure 3.13: Observed vs. simulated breakthrough of the naphthalene components at monitor well T6B4 (1.2 m downgradient from the source).

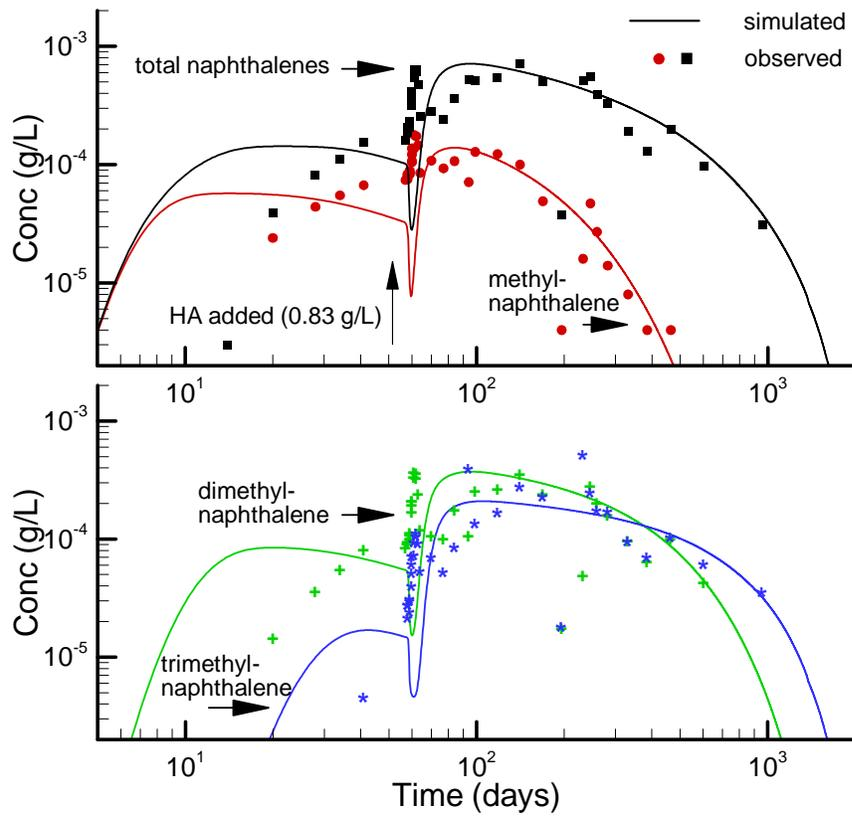


Figure 3.14: Observed vs. simulated breakthrough of the naphthalene components at monitor well T7M4 (1.5 m downgradient from the source).

humic acid front is located approximately 1.5 m from the head tank. The profile is asymmetric because of the nonlinear Langmuir isotherm and kinetic limitation of the HA sorption model.

The HA front correlates with the low-concentration break in the naphthalene plume where enhanced sorption has removed aqueous phase organic mass. From 55-65 days, the HA front advances, causing the depression to widen and by 65 days, the 50 $\mu\text{g}/\text{L}$ contour of the main plume has separated completely from the advanced lobe. No attempt was made to correlate this behaviour with the observed distribution, however it was observed in some of the breakthrough data as a distinct concentration drop after arrival of the humic acid (see Figures 3.12-3.14).

By 385 days, the total naphthalene plume has re-advanced although concentrations have already begun to decrease due to source depletion and biodegradation (Figure 3.16). By 958 days, the plume has receded to the extent that the 50 $\mu\text{g}/\text{L}$ contour no longer reaches the extraction well. After 1380 days, the source concentration has decreased to approximately 200 $\mu\text{g}/\text{L}$ and the plume extends less than a metre from the source.

Throughout the experiment, biodegradation of the source and dissolved organics was considered active. Supporting evidence came from measured background oxygen concentrations on the order of 6.5 to 8.5 mg/L , while oxygen data within the dissolved plume ranged from 0.03 to 2.98 mg/L , with most concentrations less than 0.5 mg/L (Van Stempvoort et al., 2000). Oxygen was clearly being depleted, however the spatial and temporal variation was unknown. The simulated oxygen depletion plumes are provided in Figure 3.18 which show oxygen concentrations ranging from a background of 6 mg/L to essentially zero within the plume-impacted zone of the tank. The oxygen depletion plumes grow in size from 41 to 385 days after which they essentially reach a steady state configuration, maintained by biodegradation of the remaining diesel fraction. Because of rapid upgradient replenishment, the lowest oxygen concentrations are not found within the source, but are located downgradient, close to the extraction well where biodegradation rates are high due to rapid mixing.

The depleted oxygen concentrations are accompanied by higher microbe concentrations, especially within the mixing zones where organic and oxygen concentrations are both sufficiently high to sustain growth (Figure 3.19). A minimum microbe concentration of 5 mg/L , and a maximum concentration of 14 mg/L was maintained throughout the simulation. At early time, the microbes grow rapidly within the source where organic concentrations remain high and oxygen-rich water arrives from upgradient. By 385 days, the microbes have formed a shell of elevated concentrations which correlates with the mixing zone surrounding the or-

ganic plumes. Somewhat higher concentrations are also found at the extraction well where enhanced mixing favours microbial growth. Microbe concentrations within the centre of the organic plumes remain at minimum levels because of almost complete oxygen depletion and natural microbial decay. Unfortunately, microbial mass was not monitored during the experiment and comparisons cannot be made.

The simulated microbial growth pattern suggests some interesting possibilities for explaining observed trends in the naphthalene concentrations that were not reproduced in the model. The observed low naphthalene concentrations down the plume centreline, for example, could be a result of the flow field partially bypassing the source due to microbial clogging. The decrease in relative permeability due to the presence of residual diesel is not sufficient to account for this trend. Also, the observed drop in the naphthalene breakthrough concentrations at several monitor wells could be due to small transients in the flow field, again caused by microbial growth and decay. Because of the high concentration gradients, a small lateral shift in the plume, on the order of a few centimetres, would be sufficient to cause the observed trend. To simulate these effects, the model could be modified to include coupling between the microbial mass and the relative permeability term.

The relationships between the dissolving source, the aqueous phase organics and the dissolved oxygen are shown along a central longitudinal profile in Figure 3.20. Source dissolution, as shown by the transient saturation profiles, proceeds from the upgradient face and by 1380 days, about one-half of the source has dissolved. The aqueous concentrations rise rapidly across the source and gradually decline toward the extraction well due to dispersion and biodegradation. The initial increase from 40 to 70 days is due to the humic acid enhancement, and after 70 days, the profiles gradually decline. The corresponding oxygen depletion profiles show a gradual decrease beginning at the residual source and rising again at the extraction well due to mixing with background flushing water. A steady state depletion profile is evident beginning at 385 days.

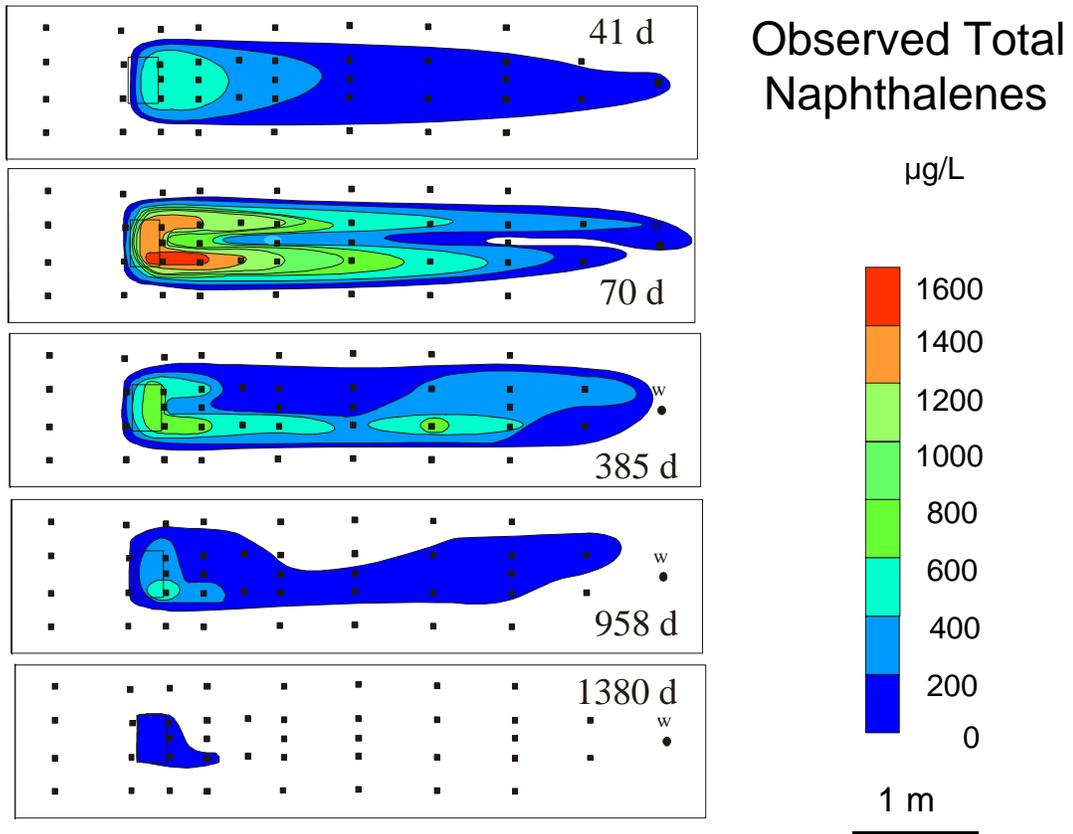


Figure 3.15: Observed total methyl-naphthalene plumes from the pilot scale experiment (plan view through source centre). After Van Stempvoort et al. (2000).

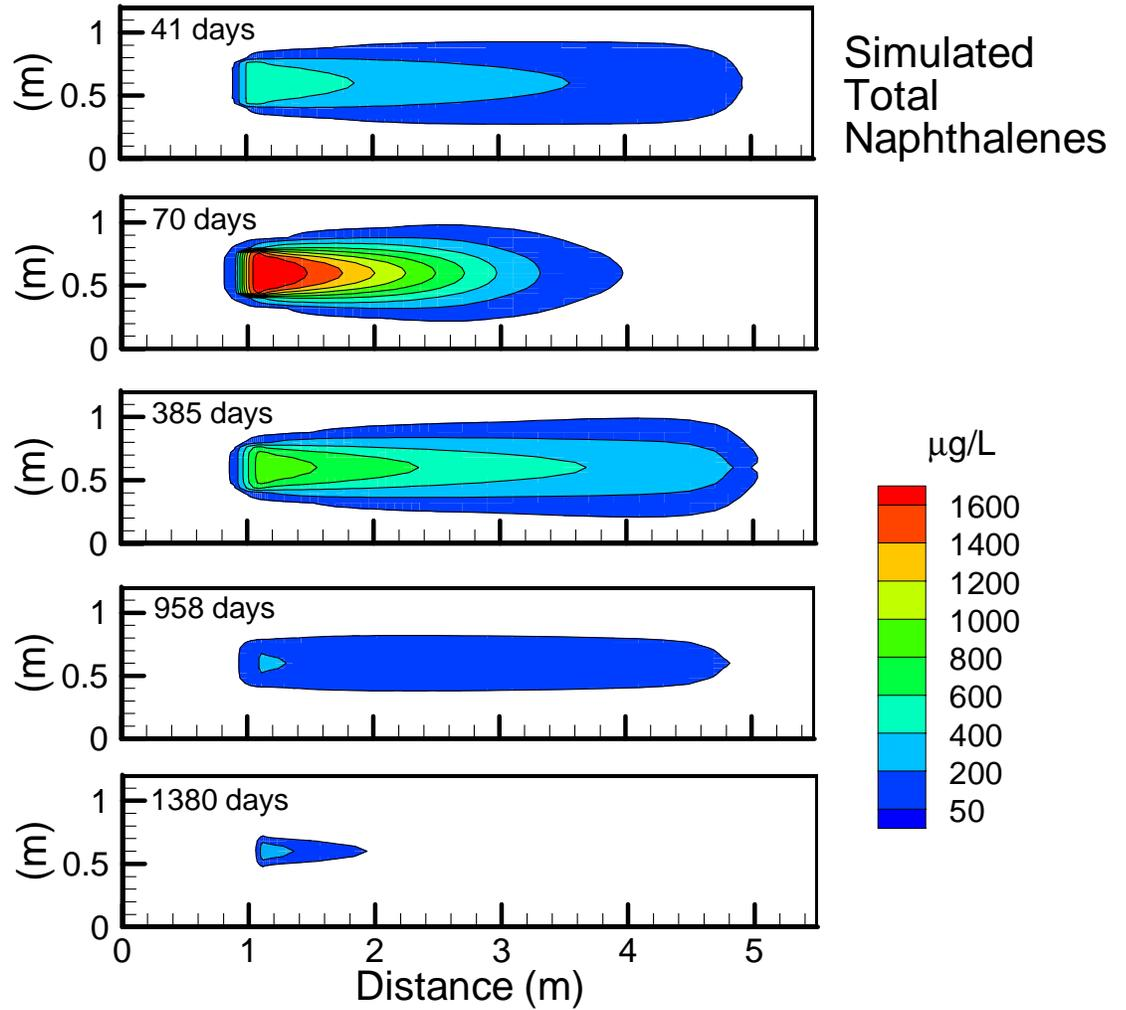


Figure 3.16: Simulated total methylnaphthalene plumes corresponding to observed times. Plan view through the source centre.

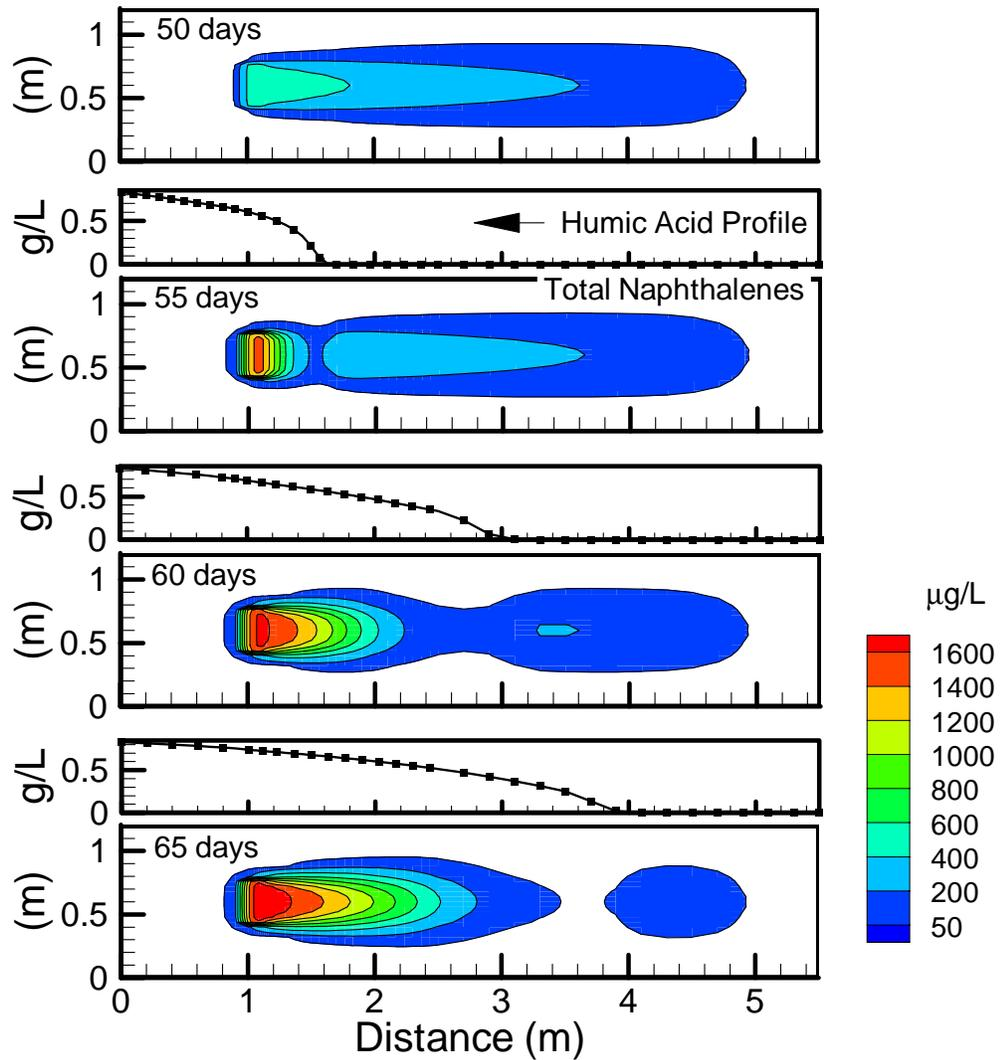


Figure 3.17: Simulated total methylnaphthalene plumes at 50-65 days showing corresponding humic acid profiles. Contour plots are plan view, located through the source centre.

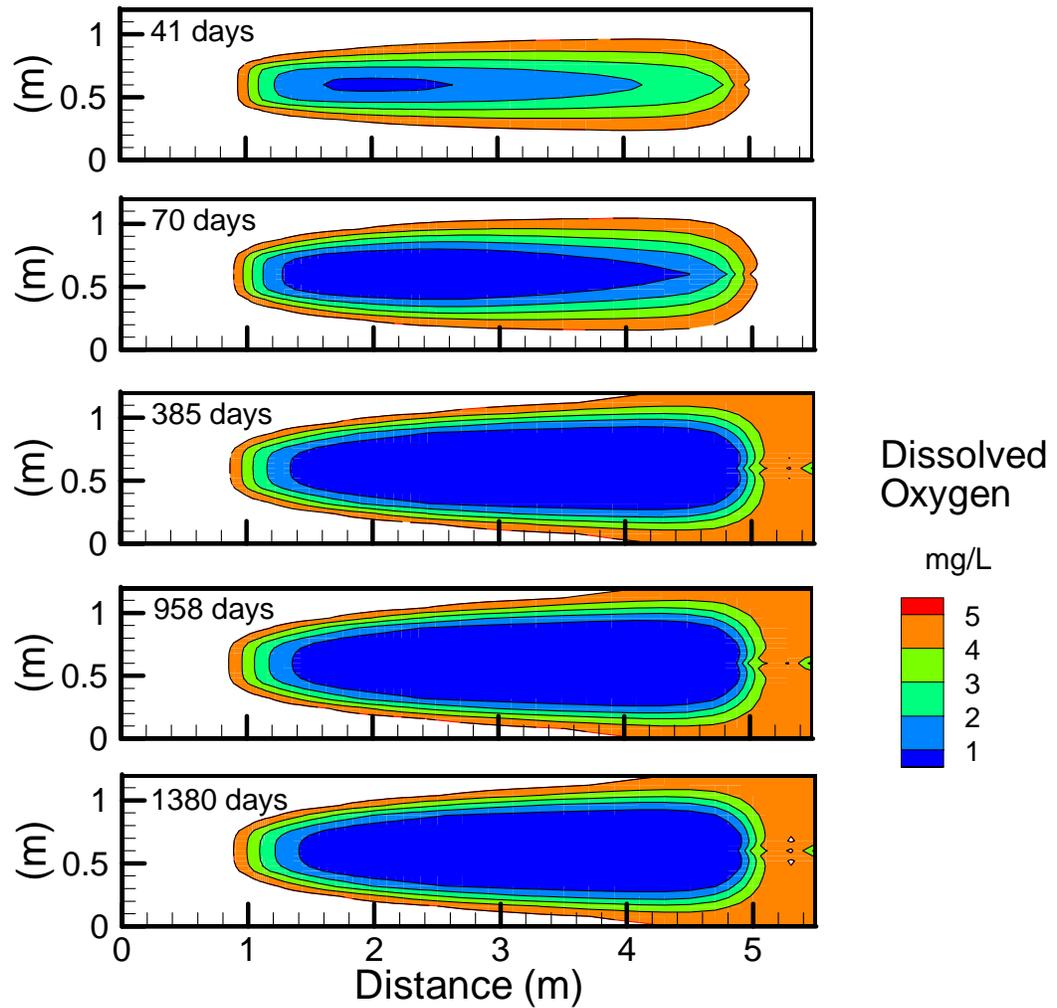


Figure 3.18: Simulated oxygen depletion plumes, caused by biodegradation of the diesel fuel components. The images represent a horizontal slice through the source centre. Contours are only flooded for depleted areas with less than the background concentration of 6 mg/L.

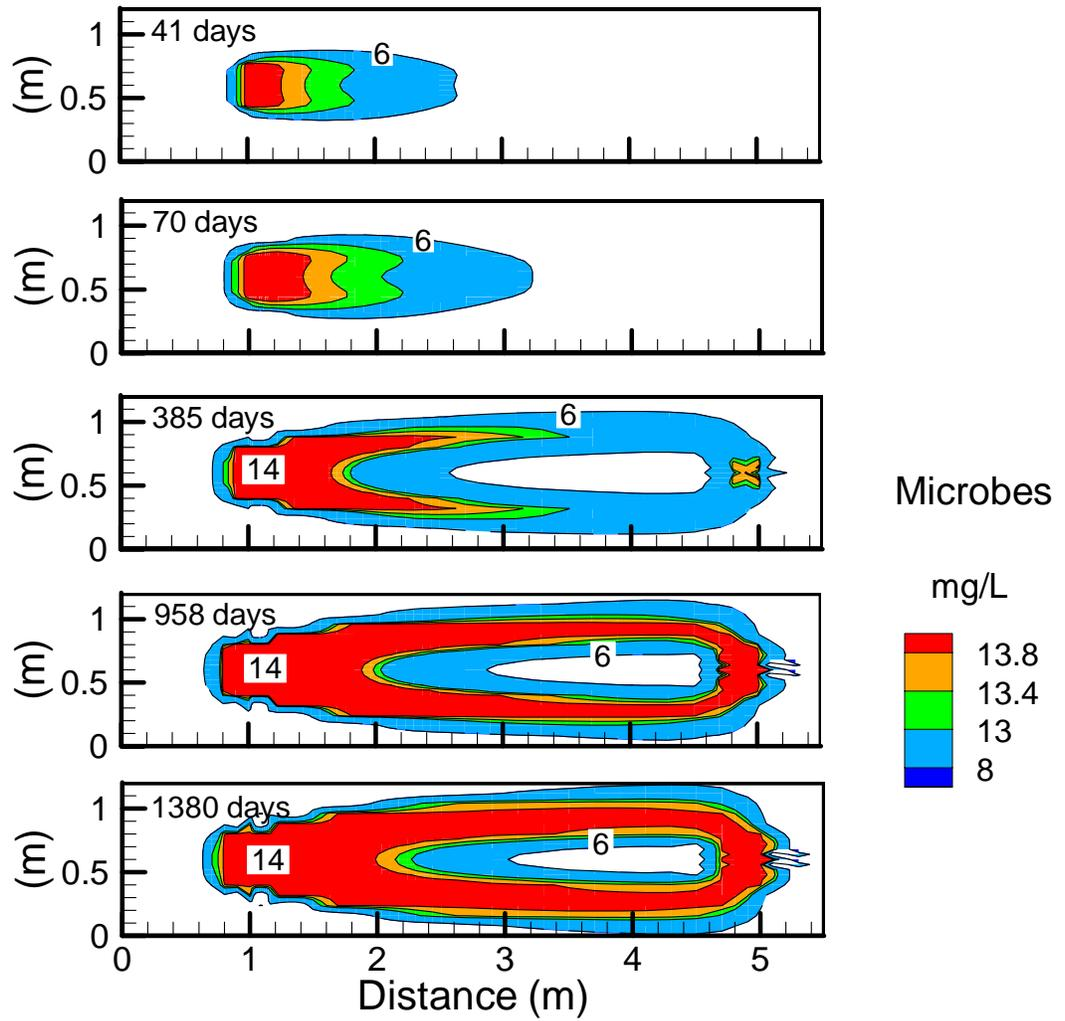


Figure 3.19: Simulated microbe concentrations within the pilot scale tank. Contour units are mg/L, plan view through source centre.

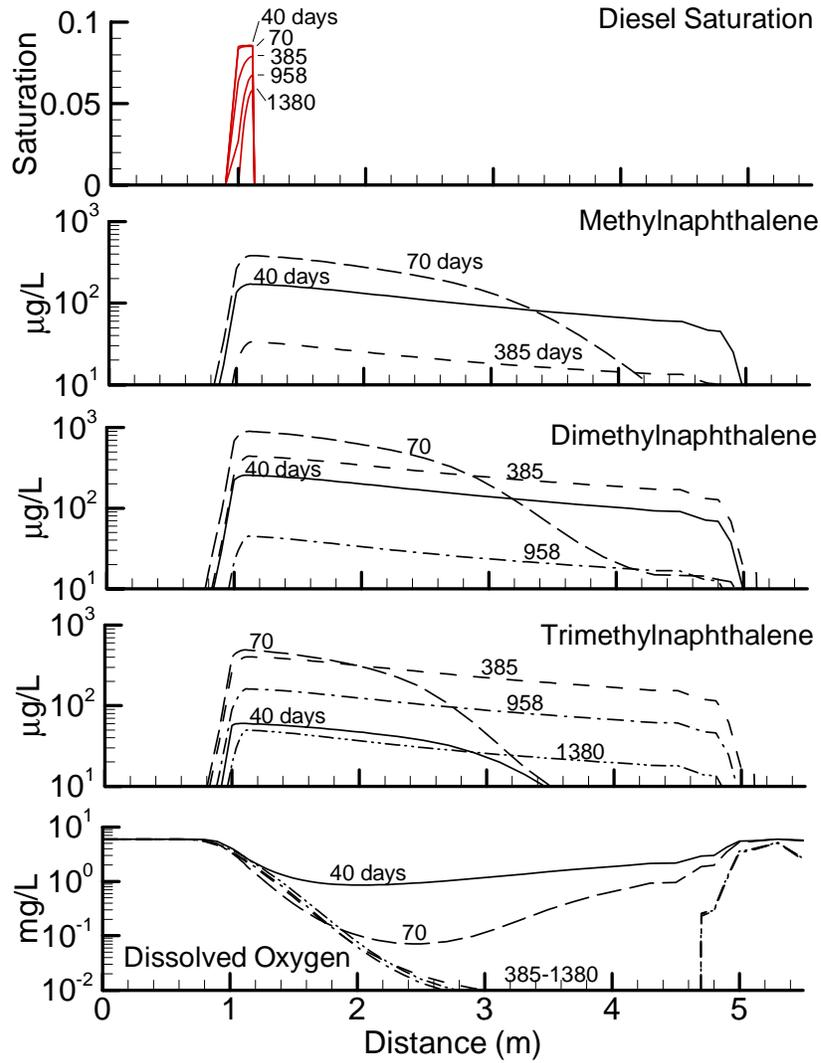


Figure 3.20: Simulated longitudinal profiles through the source centre showing diesel saturation, naphthalene concentrations and dissolved oxygen.

3.6 Sensitivity Analysis

3.6.1 Dissolution Rate

The dissolution rate coefficient (λ_{DIS}^m) in equation (3.12), and the Sherwood number (Sh) in particular, control the effective dissolution rate of the residual diesel. To investigate the influence of the dissolution rate in the pilot scale experiment, the model was run using Sherwood numbers of one-tenth and $10\times$ those calibrated (Table 3.4). The results are compared to the calibration run in Figure 3.21 which illustrates that the lower dissolution rate significantly reduces the breakthrough concentrations, even after the humic acid carrier arrives. The early-time (0-50 days) observed concentration plateaus are now underestimated and there is significantly more tailing in the breakthrough profiles resulting in much longer dissolution times. Increasing the dissolution rates by a factor of 10, however, has very little influence on the breakthrough concentrations which suggests that the diesel fuel is dissolving under equilibrium or near-equilibrium conditions. Some degree of non-uniqueness must be acknowledged here, since a lower dissolution rate would have a similar effect on the breakthrough curves as a lower HA binding coefficient (see section 3.6.4).

Observing the initial concentration plateaus from 0-50 days, it seems likely that the naphthalene components are dissolving at near-equilibrium conditions, at least over the early-time period, and perhaps throughout the experiment. This was confirmed by running a 1D equilibrium mixing cell model using identical parameters from the pilot scale model. Two conceptual equilibrium models were tested: a single solubility model in which the activity-corrected (non-enhanced) saturations ($C_o \cdot a_i$) are constant throughout the monitoring period, and a dual solubility model where the solubilities are instantaneously increased at 51 days to reproduce the enhanced dissolution after addition of humic acid. The approach is simplified in that it accounts for the humic acid only by increasing the effective component solubilities. Non-linear effects and biodegradation are not considered. Results are again compared at monitor T3B4, just downgradient from the source.

The dual-equilibrium model (Figure 3.22) provides a surprisingly good match to the observed data which lie neatly between the tails of the simulated breakthrough curves. The dual solubility model dissolves the naphthalenes more rapidly while the single model takes slightly longer, relative to the field data. Although the equilibrium model does not consider reactive mass loss, the fit is quite reasonable since biodegradation of the naphthalenes is likely quite low near the source where more readily degradable components have depleted the oxygen. The solution is very

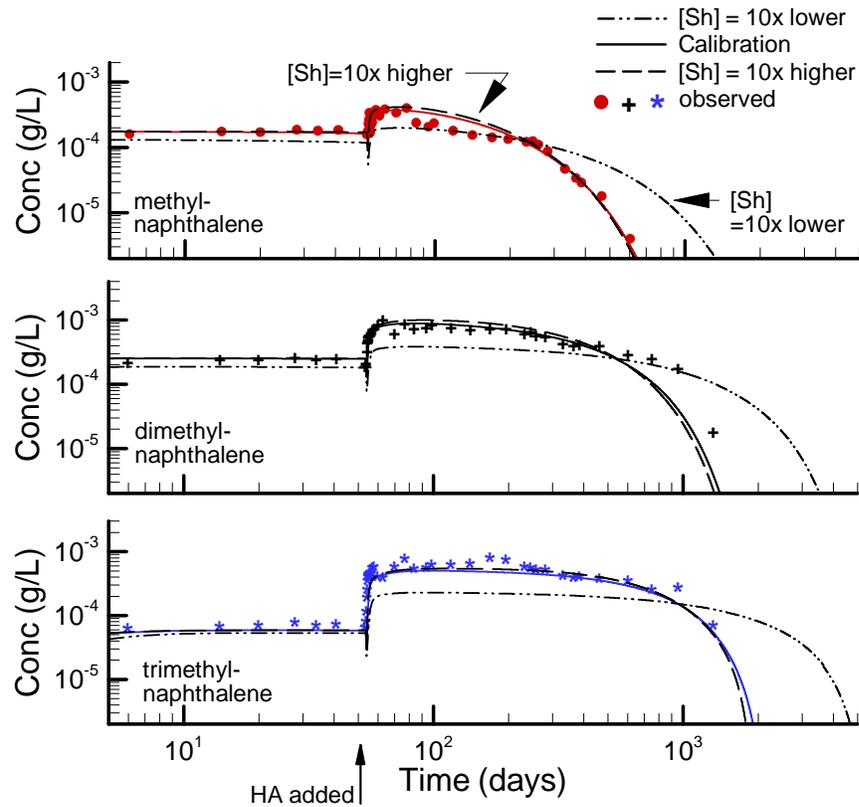


Figure 3.21: Sensitivity of naphthalene breakthrough to dissolution rate (Sherwood number), at monitor T3B4.

sensitive to the assumed enhanced solubility which may account for the apparent poor fit at later times. An equilibrium approach may therefore yield a reasonable first approximation of the dissolution behaviour; however the full reactive model clearly reproduces a better fit.

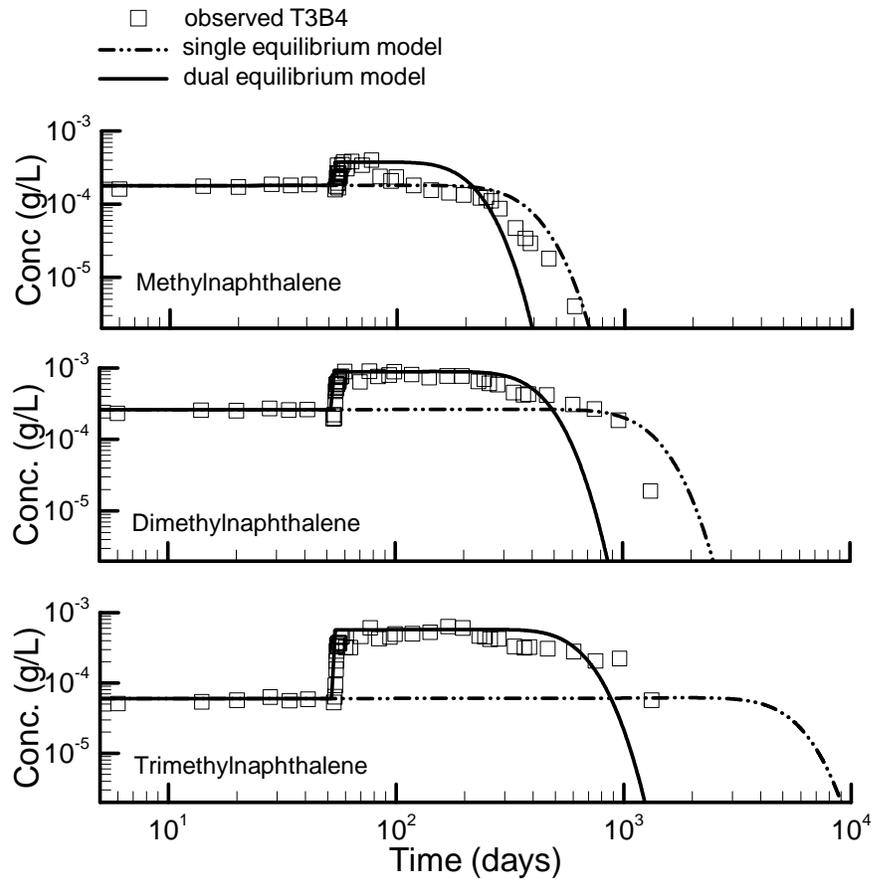


Figure 3.22: Observed vs. simulated breakthrough curves of the naphthalene components at T3B4 using single and dual-solubility equilibrium dissolution models.

3.6.2 Biodegradation Rate

The maximum biodegradation rate (k^m in equation 2.8 and Table 3.5) was not independently known for the pilot scale experiment and had to be calibrated based on the observed breakthrough curves. Calibration to the biodegradation rate was difficult because oxygen limitations made the solution generally less sensitive to changes in this otherwise critical parameter. Fortunately, the effect of the biodegradation rate was clearly distinguishable from that of the dissolution rate. Increasing the biodegradation rate, for example, reduces the concentrations throughout the observation period whereas decreasing the dissolution rate only reduces the early-time concentrations, and causes significant tailing (relatively higher concentrations) at longer times. In this section, the maximum biodegradation rate of the naphthalenes is changed while leaving the rates for BTEX and the remaining components unchanged.

The sensitivity of the component concentrations to k^m is provided in Figures 3.23 and 3.24 which show the breakthrough curves for the methyl-naphthalenes at monitors T3B4 (immediately downgradient from the source) and T7C4 (1.5 m downgradient), respectively. Increasing the maximum rate by a factor of 10 reduces the concentrations and produces a somewhat poorer fit to the observed data, particularly near the source; further from the source the observed data become more scattered and the best fit value is difficult to determine. Decreasing the rate by a factor of 10 has relatively less effect which may be due to oxygen limitations. The results also show a somewhat greater sensitivity further from the source area since more mass can biodegrade during the longer travel time.

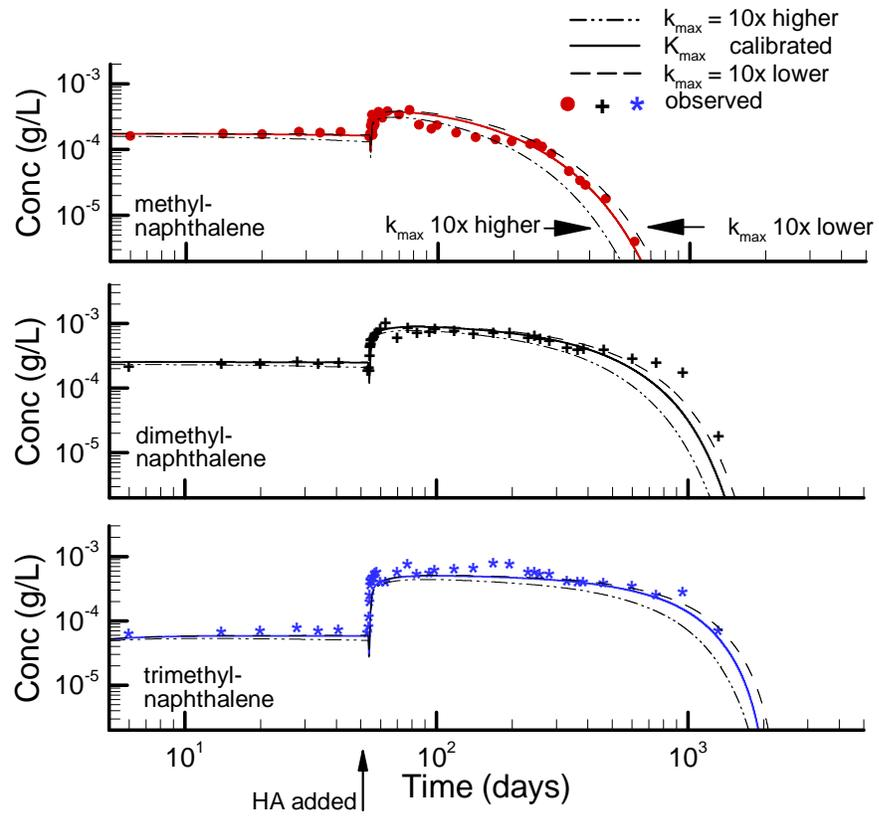


Figure 3.23: Breakthrough curves at T3B4 (immediately downgradient from the source) showing effect of the maximum biodegradation rate for the naphthalenes.

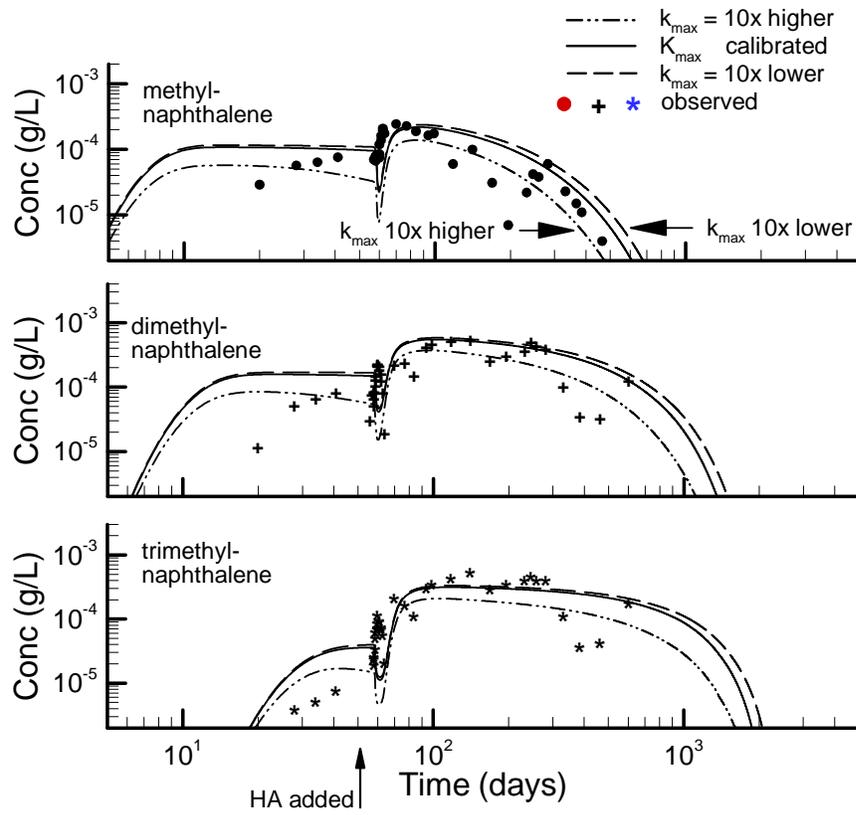


Figure 3.24: Breakthrough curves at T7C4 (1.5 m downgradient) showing effect of the maximum biodegradation rate for the naphthalenes.

3.6.3 Substrate-Carrier Sorption

The concentration of a reactive carrier will directly influence the rate of dissolution of a residual NAPL through the enhancement factor (equation 3.14). Although higher carrier concentrations will always increase the dissolution rate, sorption to aquifer solids at low carrier concentrations may, in fact, reduce the mobility of the dissolved phase organics. In this section, the sensitivity of the diesel fuel dissolution is tested with respect to the humic acid carrier concentration. The binding coefficients (K_m) remain the same as in the calibration simulation.

In the pilot scale experiment, humic acid was added to the tank at an effective concentration of 0.83 g/L, and was maintained at that level throughout the 5-year experiment. In field scale applications, however, maintaining constant carrier concentrations may be more difficult because of transient flow fields or aquifer heterogeneities. Conversely, one may also be interested in using even higher concentrations than 0.83 g/L.

In order to examine the influence of carrier concentrations, simulations of the pilot scale experiment were repeated with humic acid concentrations of 0.25 g/L and 10 g/L, and results compared with the experimental and calibrated results in Figure 3.25. The 0.25 g/L concentration was chosen as it lies at the breakpoint of the Langmuir isotherm (Figure 3.4), and Johnson & John (1999) use humic acid concentrations up to 12 g/l in their experiments. The results show a high sensitivity to the carrier concentration as would be expected from the corresponding enhancement factor ($E = 1 + K_m[HA]$). Decreasing the carrier concentration to 0.25 g/L, for example, increases the dissolution time for trimethylnaphthalene (to 10 $\mu\text{g/L}$) by 112%, while increasing the concentration to 10 g/L reduces the time by 71%. A summary of the relative impacts compared to the experimental conditions is provided in Table 3.7.

Table 3.7: Summary of naphthalene dissolution times (at T3B4, to 10 ppb) using different humic acid concentrations. Bracketed values represent percent differences in dissolution times relative to those from the experimental humic acid concentration of 0.83 g/L.

Diesel Component	Humic Acid Concentration		
	0.25 g/L	0.83 g/L	10.0 g/L
methylnaphthalene	700 days (+40%)	500 days (0%)	200 days (-60%)
dimethylnaphthalene	2000 days (+67%)	1200 days (0%)	400 days (-67%)
trimethylnaphthalene	3600 days (+112%)	1700 days (0%)	500 days (-71%)

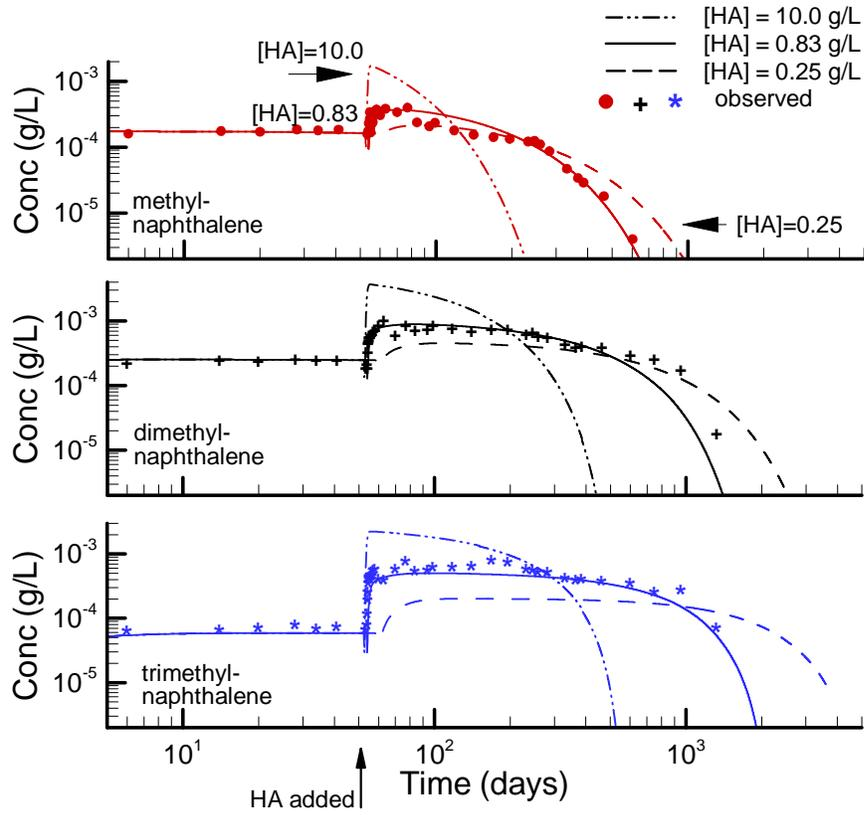


Figure 3.25: Breakthrough curves at T3B4 showing effect of humic acid concentration on enhanced dissolution of diesel fuel.

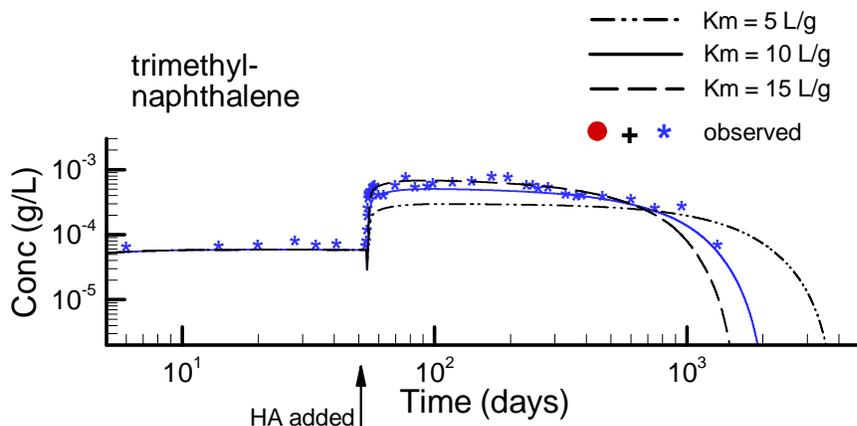


Figure 3.26: Breakthrough of trimethylnaphthalene at T3B4 showing sensitivity to the binding coefficient K_m .

3.6.4 Binding Coefficient: TMN - HA

The binding coefficient (K_m) describes the tendency for the organic components to bind to the mobile humic acid. For the base case (calibration) simulation, values of K_m were obtained from lab-derived data provided by Van Stempvoort et al. (2000), and listed here in Table 3.3. For the three naphthalene components, the most significant variation and uncertainty was observed for trimethylnaphthalene because of the greater number of isomers, of which only one was tested (2,3,5-TMN). Since trimethylnaphthalene is also the least soluble of the three naphthalenes, its binding coefficient would have the greatest effect on the bulk dissolution rate.

To determine the sensitivity of the diesel dissolution process to the binding coefficient of trimethylnaphthalene, the base simulation was repeated for 2 different values of K_m , and the results provided in Figure 3.26. The range of K_m was selected based on estimated uncertainty in the observed data. Reducing the coefficient from 10 L/g in the base simulation to 5 L/g clearly does not match the observed data and significantly increases the time for complete dissolution. Increasing the coefficient from 10 L/g to 15 L/g provides a somewhat improved match at early time (51-500 days), but slightly underestimates the dissolution time. The effect of changing the binding coefficient of TMN had a negligible effect on the behaviour of the other two naphthalenes.

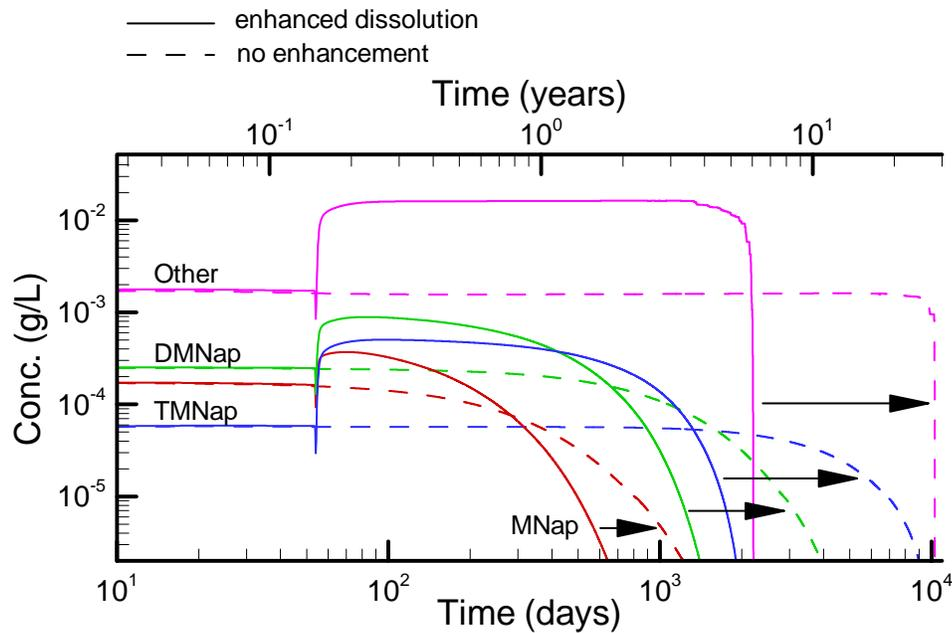


Figure 3.27: Long-term dissolution of the diesel fuel source: comparison between the calibrated, humic acid-enhanced model, and an equivalent simulation without a carrier. Arrows indicate shift in component dissolution curves from the carrier-enhanced simulation to the no-enhancement simulation.

3.6.5 Long-Term Dissolution

In the absence of a carrier, the diesel source will dissolve more slowly and the effective biodegradation rate will be reduced since the total aqueous phase organic concentrations are lower. This behaviour is shown in Figure 3.27 in which the base case (calibrated) dissolution profile is compared to an otherwise equivalent simulation assuming no carrier. The results show that the humic acid carrier has decreased the time required to reach drinking water limits by a factor of about 2 for methylnaphthalene, 2.5 for dimethylnaphthalene, 4 for trimethylnaphthalene, and 5 for the remaining components. Although the enhancement factors for the remaining components were unknown (assumed here constant at 10 L/g - see Table 3.3), both the observed and simulated sources were almost completely dissolved and degraded after 5 years hence we can be fairly confident of the simulated bulk dissolution behaviour for the unknown fraction.

3.7 Conclusions

The multiple nonlinear processes occurring during a humic acid-enhanced diesel fuel dissolution experiment have been accurately quantified using a 3D numerical model. The simulation approach considers multi-component NAPL dissolution, aqueous reactive transport and sorption kinetics in the presence of a mobile reactive carrier. Sorption parameters derived from complementary laboratory batch experiments provided excellent fits to the observed behaviour at the pilot scale, requiring the model to be calibrated only with respect to kinetic rates of sorption, dissolution and biodegradation. The simulations confirmed the observed 10-fold increase in apparent solubility of trimethylnaphthalene, with increases on the order of 2-5 for the methyl and dimethylnaphthalenes.

Simulated depletion plumes of dissolved oxygen followed the observed trends with almost complete oxygen depletion within the core of the organic plumes. Most biodegradation seemed to be maintained by the remaining, unmonitored fraction of the diesel components. Degradation of the methylnaphthalenes, at least near the source, appeared to be minimal. Simulated microbial growth patterns suggest that microbial pore clogging could explain some of the observed trends in the naphthalene concentrations that were not reproduced by the model. The decrease in relative permeability due to the residual diesel is not sufficient to cause significant flow bypassing.

A sensitivity analysis of the effective dissolution rate suggested that the naphthalenes within the diesel source were dissolving at or near equilibrium throughout most of the 5-year observation period. The influence of humic acid on the dissolution rate, however, could not be reproduced by simply assuming equilibrium dissolution and an instantaneous increase in the effective naphthalene solubilities. The observed behaviour is somewhat more complex and requires accounting for nonlinear and kinetic effects of the mobile carrier.

The solution appeared relatively less sensitive to the maximum biodegradation rate (k^m) for the naphthalenes. Changing the rates by a factor of $10\times$ gave generally poorer fits to the observed data, however the calibrated rates cannot be considered unique beyond a factor of about $2\times$. The low sensitivity is likely due to oxygen limitations.

The humic acid source concentration in the experiment was fixed at 0.83 g/L, which almost completely dissolved the source within 5 years. Increasing the HA concentration to 10 g/L reduced the simulated dissolution time by up to 71% for trimethylnaphthalene, while a decrease to 0.25 g/L more than doubled the required

dissolution time. Predictive simulations suggest that complete dissolution of the naphthalene components in the pilot-scale test would take up to 5 times longer in the absence of a humic acid carrier. The time required for complete remediation (to drinking water limits) of the complete diesel fuel source is limited, however, by the degree of solubilization of the remaining unknown diesel components.

The efficiency of using humic acid, both physical and economic, must be compared with that of surfactants and other remediation alternatives before a suitable remediation approach is chosen for a specific site. Full field-scale experiments and simulations would confirm remediation efficiency and help identify further limitations.

Chapter 4

Modelling the Impact of Ethanol on the Persistence of BTEX Compounds in Gasoline-Contaminated Groundwater

Abstract

The effect of ethanol on the persistence of BTEX in gasoline-contaminated aquifers is simulated using a multicomponent reactive transport model. The conceptual model includes a residual gasoline source which is dissolving at the water table into a 3D aquifer. Source dissolution, transport of the dissolved components and competitive aerobic biodegradation are solved using a Galerkin finite element scheme with Picard iteration. Comparisons are made between dissolved benzene plumes from a gasoline spill and those from an otherwise equivalent spill containing 10% ethanol. Simulations have shown that under some conditions, a 10% ethanol component in gasoline can extend the travel distance of a benzene plume by up to 150% relative to that from an equivalent ethanol-free gasoline spill. The increase occurs because ethanol preferentially consumes oxygen which reduces the biodegradation rate of benzene. The impact is limited, however, because oxygen rapidly disperses behind the ethanol plume into the slightly retarded benzene plume. A sensitivity analysis for two common spill scenarios showed that background oxygen concentrations, and benzene retardation had the most significant influence on ethanol-induced benzene persistence. A continuous gasohol spill over 10 years was found to increase the benzene travel distance by over 120% within 40 years and a pure ethanol spill into an existing gasoline plume increased travel distance by 150%. The results are highly relevant in light of the forthcoming ban of MTBE in California and its probable replacement by ethanol by the end of 2002.

4.1 Introduction

4.1.1 Background

The use of oxygenated gasoline has become a standard method of decreasing vehicular carbon monoxide and ozone precursor emissions into the atmosphere. The most commonly used gasoline oxygenate is methyl-tertiary-butyl-ether (MTBE) and although it has shown low toxicity, its low biodegradability in groundwater and strong taste and odor at $\mu\text{g}/\text{L}$ levels have resulted in its ban in California by the end of 2002. Ethanol is the second most common oxygenate in gasoline and it seems to be emerging as the preferred choice to replace MTBE.

Alcohols such as ethanol and methanol are easily degradable in groundwater environments and, due to their high solubility, are expected to readily dissolve from a spill or source zone (Malcolm Pirnie Inc., 1998; Reichhardt, 1999; de Oliveira, 1997). One potential problem in the spill of an ethanol-gasoline mixture, however,

is the preferential use of this alcohol as a substrate by the microbial community. This preferential use depletes the available electron acceptors and may increase the persistence of the remaining BTEX compounds (benzene, toluene, ethylbenzene and the xylenes) (Hunt et al., 1997; Corseuil et al., 1998). At sufficiently high concentrations, ethanol may also act as a cosolvent, increasing the concentration and mobility of the remaining BTEX components (Groves, 1988). The BTEX components of gasoline, and benzene in particular, are of primary concern because of their relatively high solubility and toxicity at low concentrations.

Manufacturers require a 3-year transition period to prepare for complete replacement of MTBE. Critical decisions must therefore be made soon, and must be based on a sound understanding of the influence of ethanol on a biodegrading dissolved gasoline plume. This understanding can be improved through advanced numerical tools, which can now provide decision-makers with important new insight into the behaviour of complex multi-component mixtures.

4.1.2 Review of Existing Modelling Approaches

Applications of models to predict the behaviour of benzene in ethanol-impacted groundwater are scarce and very limited in scope. Most references to ethanol in groundwater are with respect to its use as a cosolvent for enhanced remediation of NAPL-impacted groundwater (e.g. Lunn & Kueper, 1997). Interest in ethanol affecting BTEX in groundwater has only recently been increasing because of the potential use of ethanol as a replacement for MTBE. Furthermore, there is a lack of well-defined field spill sites on which models can be tested. On the other hand, model applications to gasoline contaminants (Poulsen et al., 1992; Munoz & Irarrazaval, 1998; Lu et al., 1999), or to MTBE-impacted contamination sites (Schirmer, 1998) have been well documented and much insight can be gained from these past efforts.

Existing model applications to study ethanol behaviour in groundwater systems include those by Heermann and Powers (1996, 1998), Malcolm Pirnie Inc. (1998), Ulrich (1999), and McNab et al. (1999). Rice et al. (1999) provide a detailed summary of the processes involved and review the current state-of-the-art in terms of modelling ethanol impacts in groundwater.

Although adding some insight, all previous approaches have been limited to some degree. Malcolm Pirnie Inc. (1998), for example, used a 2D analytical model and first-order degradation rates to compare benzene plume lengths under ethanol and ethanol-free conditions. The approach did not consider dynamic effects of co-transport and only activated benzene degradation once the ethanol concentrations

decreased below a given threshold. They predicted benzene plume length increases on the order of 17-34%.

Ulrich (1999) applied MODFLOW/MT3D to simulate ethanol impacts on benzene. Although a 3D approach was adopted, several simplifying assumptions limited the insights gained. First, the source was an existing dissolved plume of benzene and dissolution from a residual source was not considered. Second, since only a single component was transported for each simulation, dynamic interactions between benzene and ethanol were not considered. Instead, it was simply assumed that no degradation of BTEX occurred where ethanol was present from a separate simulation. Where degradation was active, first order rates were assumed. Grid elements also increased in size very rapidly from a respectable 0.3 m^2 near the injection well, to over 9 m^2 , throughout most of the plume area. Vertical definition of the plumes was unknown due to a lack of information provided. Application to a Borden-like flow system induced increases of 10% in the migration distance of the ethanol-impacted benzene plume. Including acetic acid as a more persistent by-product of ethanol degradation increased the length by a factor of about 1.8.

McNab et al. (1999) used a Monte Carlo approach to evaluate ethanol impacts using an analytical transport solution from Baetsle (1969), modified to include a finite source release area. By correlating benzene degradation rates with a variety of parameters, and by using superposition to quantify biological oxygen demand (BOD) from ethanol, they obtained probability distributions of benzene concentrations downgradient of the source area. The influence of retardation factors and competitive substrate utilization was neglected and first-order degradation rates were assumed. Their results suggested that ethanol would increase benzene plume lengths by less than a factor of 2.

Heermann & Powers (1996) simulated the transport of m-xylene and ethanol from a gasohol pool into a 2D aquifer system. The influence of ethanol was restricted to cosolvency alone and sorption and biodegradation were not considered. They found maximum ethanol-induced increases in benzene plume travel distances on the order of 10%. There was essentially no effect when lower interphase mass-transfer coefficients were assumed. A relatively high transverse vertical dispersivity of 0.1 m may have caused excess plume dispersion and contributed to the low predicted impact.

Heermann & Powers (1998) studied BTEX partitioning in gasoline-ethanol-water systems. Using batch experiments on a variety of gasoline/gasohol mixtures, they found that a dual linear/log-linear model describing BTEX partitioning at different ethanol volume fractions provided the best fit to observed data.

4.1.3 Objectives

The overall objective of this study is to provide new insight into the influence of ethanol on BTEX persistence in gasoline-contaminated groundwater. The focus will be on benzene. The objective is met by applying a 3D numerical model to simulate BTEX migration from three conceptual models of gasoline spills. The first conceptual model addresses the impact of a local spill of 10%-ethanol gasoline (hereafter termed gasohol) into a pristine aquifer. This type of spill is expected, for example, from leaking underground storage tanks (LUST's) (Rice et al., 1999).

In the second conceptual model, a pure ethanol spill is simulated within an existing residual gasoline source and dissolved plume. This model may represent, for example, a spill from an ethanol storage tank into a previous gasoline spill at a hydrocarbon fuel processing plant (Rice et al., 1999). Cosolvency is considered using the dissolution enhancement approach (Ji & Brusseau, 1998).

The third conceptual model is similar to the first, but differs in the approach for simulating the oxygen demand of ethanol. In the first conceptual model, ethanol represents the complete oxygen demand of ethanol itself, as well as its degradation products. In the third conceptual model, however, a somewhat more realistic system is assumed in which ethanol degrades rapidly to methane, which then exerts its own oxygen demand on the system.

In each conceptual model, comparisons are made between the ethanol-impacted benzene plume and the equivalent ethanol-free benzene plume, and various system parameters are adjusted to evaluate sensitivity and uncertainty. Simulations are compared to the continuing evolution of the previously-existing source and BTEX plumes, emphasizing differences in benzene plume concentrations and travel distance from the source.

The simulations are not meant to be interpreted as absolute predictions of BTEX and ethanol behaviour, but should be used to gain insight into the controlling factors where the focus is on relative effects between the gasoline and gasohol source plumes. The conceptual model is primarily based on a large-scale system and near-source processes have been somewhat simplified. All assumptions and limitations inherent in the modelling approach should be considered before relating the simulated results to field situations. Ideally, the conceptual model should be tested against a real field scale gasohol-impacted system.

4.2 Theoretical Development

4.2.1 Modelling Approach

In this study, we use BIONAPL/3D, a 3D finite element numerical model recently developed at the University of Waterloo (Frind et al., 1999; Molson, 2000). The relevant processes that are considered include multi-component dissolution from a residual gasoline or gasohol source, advective-dispersive transport within a 3D porous medium, and electron acceptor-limited competitive biodegradation and microbial growth. A full development is provided in Chapter 2.

The governing equation for mass transport of component m can be expressed as

$$\theta D_{i,j}^m \frac{\partial^2 C_w^m}{\partial x_i^2} - q_i \frac{\partial C_w^m}{\partial x_i} - \theta \lambda_{BIO}^m C_w^m + \theta \lambda_{DIS}^m (C_s^m - C_w^m) = \theta R_w \frac{\partial C_w^m}{\partial t} \quad (4.1)$$

where C_w^m (kg/m^3) is the aqueous (water) phase concentration of organic contaminant m , D_{ij}^m (m^2/day) is the hydrodynamic dispersion tensor, q_i (m/day) is the Darcy flux, λ_{BIO}^m (day^{-1}) is the biodegradation rate, λ_{DIS}^m (day^{-1}) is the gasoline dissolution rate coefficient, C_s^m is the effective solubility of the NAPL component (kg/m^3), R_w is the retardation, t is time ($days$) and x_i (m) represents the spatial dimensions ($x_i = x, y, z$).

Assuming linear equilibrium partitioning to the aquifer solids, the retardation term R_w can be expressed by $R_w = 1 + \rho_b K_d / \theta$ where ρ_b (kg/m^3) is the bulk density, K_d (m^3/kg) is the distribution coefficient and θ is the porosity.

The biodegradation rate λ_{BIO}^m for organic component m in equation 4.1 can be expressed as

$$\lambda_{BIO}^m = \sum_{n=1}^{N_A} k^m M \left(\frac{1}{K_C^m + C_w^m} \right) \left(\frac{A^n}{K_A^n + A^n} \right) \quad (4.2)$$

where M ($kg_{microbes}/m_w^3$) is the microbial concentration, k^m ($kg_{organic}/(kg_{mic}day)$) is the maximum utilization rate, A^n is the concentration of electron acceptor n , and K_C^m and K_A^n are the half-utilization rate concentrations for the organic and electron acceptor, respectively. Equation 4.2 represents the net organic biodegradation rate due to N_A electron acceptors.

The dissolution rate coefficient in equation 4.1 is expressed as (Frind et al., 1999)

$$\lambda_{DIS}^m = \frac{ShD^m}{(d_{50})^2} \left(\frac{f^m S_n}{S_{n_0}} \right)^{\beta^m} \quad (4.3)$$

where Sh is the Sherwood number, D^m (m^2/s) is the aqueous diffusion coefficient, d_{50} is the median grain diameter (m), S_n is the degree of NAPL saturation, with S_{n_0} the initial saturation, and f^m is the local volume fraction of component m .

The electron acceptor concentration (A^n) in equation 4.2 is assumed to be dissolved in the aqueous phase where transport is also governed by advection and dispersion according to

$$\theta D_{i,j} \frac{\partial^2 A^n}{\partial x_i^2} - q_i \frac{\partial A^n}{\partial x_i} - \theta \lambda_{BIO}^n \cdot A^n = \theta \frac{\partial A^n}{\partial t} \quad (4.4)$$

where the electron acceptor rate λ_{BIO}^n represents the net reaction (consumption) rate due to biodegradation of all N_m organic components according to

$$\lambda_{BIO}^n = \sum_{m=1}^{N_m} k^m M \mathbf{X}^m \left(\frac{C_w^m}{K_C^m + C_w^m} \right) \left(\frac{1}{K_A^n + A^n} \right) \quad (4.5)$$

where \mathbf{X}^m is the stoichiometric mass ratio of oxygen to organic substrate.

In this application, the aqueous organic phase concentrations (C_w) include benzene, two lumped pseudo-components and ethanol. The first pseudo-component is composed of toluene, ethylbenzene and the xylene isomers, while the second is composed of the remaining fraction of relatively less soluble gasoline components. Oxygen is assumed the dominant electron acceptor (A^n) together with a single microbial population (M).

Equations 4.1 and 4.4 are solved using a Galerkin finite element approach with deformable brick elements. The matrix equations are solved with a preconditioned conjugate gradient solver (Braess & König, 1995).

Gasoline Source Dissolution

The BIONAPL model can simulate kinetic (rate-limited) or equilibrium dissolution from a residual NAPL source. Kinetic dissolution is simulated using the source

term λ_{DIS}^m defined by equation 4.3 and by defining a nonlinear dissolution rate coefficient (Frind et al. 1999). Equilibrium dissolution can be simulated by choosing a sufficiently large value for the Sherwood number Sh , and by setting $\beta = 0$.

Alternatively, an equilibrium mixing cell algorithm based on Raoult's Law can be employed. Raoult's Law defines the concentration of a NAPL component in water that is in equilibrium with the NAPL (Mackay et al. 1991), and is given by

$$C_s^m = X^m C_o^m \quad (4.6)$$

where X^m is the mole fraction and C_o^m is the pure phase aqueous solubility of component m (Poulsen et al., 1992).

Equilibrium dissolution assumes ideal component behaviour and a large contact area between the residual NAPL and the groundwater. Cline et al. (1991) conclude that Raoult's law is valid for gasoline mixtures and there is evidence that at least some residual NAPL's (e.g. chlorinated solvents) can dissolve in the subsurface under essentially equilibrium conditions (Frind et al., 1999). Source heterogeneities and non-ideal component behaviour can, however, lead to apparent or real non-equilibrium dissolution at field contamination sites (Soerens et al., 1998).

Boundary Conditions

Boundary conditions for equation (4.1) can be either a fixed concentration (Dirichlet), a zero gradient (Neumann) or a mass flux (Cauchy) type. Dirichlet and Cauchy conditions are often used to represent sources while Neumann conditions are appropriate at exit or no-flow boundaries. The Cauchy boundary condition is ideal for the dissolving gasoline sources considered here, and is defined as

$$q_0 C_0 = \theta \left(vC - D \frac{\partial C}{\partial x} \right) \quad (4.7)$$

where $q_0(m/s)$ is the recharge rate, and $C_0(kg/m^3)$ is the source concentration. Equation 4.7 balances the mass flux on the outside of the boundary ($q_0 C_0$) with the mass flux on the inside. The source concentration C_0 can be either fixed or can vary in time depending on the source dissolution behaviour. Boundary and initial conditions must be specified for each of the organics and for each of the electron acceptors.

Cosolvency

This study is concerned with the influence of ethanol on BTEX behaviour in groundwater. When the aqueous volume fraction of ethanol becomes greater than about 0.1, however, the effective solubilities of the remaining gasoline components can increase significantly as they preferentially dissolve into the water-ethanol solution (Heermann & Powers, 1998). This cosolvency effect can be expressed as a dissolution enhancement factor E (Ji & Brusseau, 1998) defined for each organic component as:

$$E = \frac{S_m}{S_w} = 10^{\sigma f_c} \quad (4.8)$$

where S_m represents the solubility of the gasoline component in the water-cosolvent mixture, S_w is the solubility of the gasoline component in water, σ is the cosolvency factor, and f_c is the volume fraction of ethanol in the aqueous phase. A component enhancement factor of 10, for example, will increase the component solubility by $10\times$.

The cosolvency power can be expressed as $\sigma = \log(S_c/S_w)$ where S_c is the solubility of the component in pure cosolvent. Linear/log-linear functions have also been employed to predict cosolvency based on observed laboratory data (Heermann & Powers, 1998).

Assumptions

The following assumptions were made in this application of the BIONAPL model to the gasoline/gasohol system:

- The aquifer flow system is saturated, isotropic, homogeneous and at steady state.
- Contaminant concentrations are relatively dilute and density effects are not considered. In particular, the buoyancy effects of a high-concentration ethanol plume are neglected.
- The residual NAPL source is immobile, potential interfacial tension changes due to ethanol are assumed not significant.
- Sorption is assumed linear and reversible.

- NAPL dissolution occurs at equilibrium according to Raoult's Law.
- A single electron acceptor (oxygen) and a single microbial population are present.
- Substrate inhibition is neglected; the preferential degradation of ethanol is included by assuming $k_{ethanol} > k_{benzene}$ and by transporting all components simultaneously with oxygen.
- Biodegradation occurs only in the dissolved (aqueous) phase, not in the sorbed phase.
- The reaction stoichiometries assume complete organic degradation to CO_2 and H_2O .

4.3 Conceptual Model

4.3.1 Flow System

The conceptual flow model is provided in Figure 4.1 which represents a vertical slice through the 3D domain. The hydrogeological system is loosely based on the shallow, unconfined Borden aquifer, perhaps the best characterized sand aquifer in the world. Numerous natural gradient reactive tracer tests (Sudicky, 1986; Hubbard et al., 1994) and modelling studies (Frind and Hokkanen, 1987; Molson et al., 1992) provide an excellent data base of flow system parameters. The flow system properties assumed for this study are provided in Table 4.1.

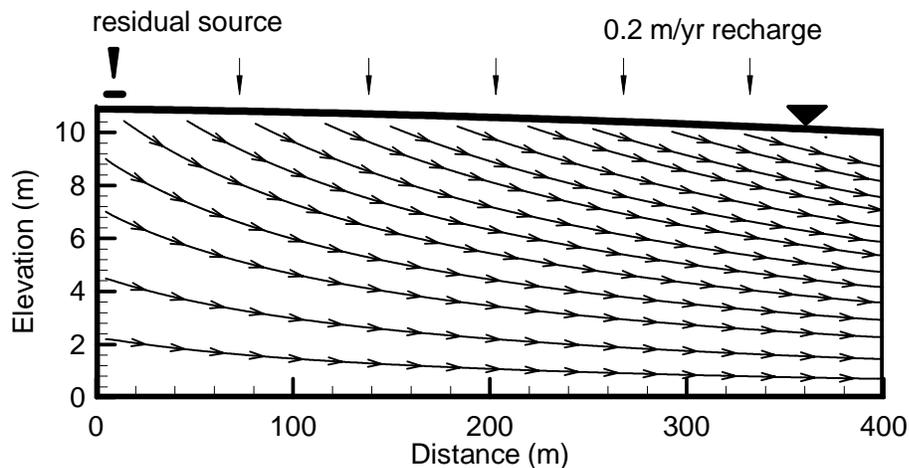


Figure 4.1: A vertical slice through the 3D steady state flow system assumed for the gasoline dissolution simulations. The residual source is located at the upper left.

The 3D aquifer system is 400 m long by 10 m thick by 12 m wide. The system is assumed symmetric about the vertical plane through the source centre therefore only a 6 m wide section is simulated. A flux of 2.5 m/yr is assigned along the left inflow boundary, and 0.20 m/yr is assigned as recharge along the top watertable boundary. The right exit boundary is assigned a head of 10.0 m and the lower boundary is considered impermeable. The flow system is assumed to be at steady state for all simulations. The model domain is resolved using a grid of 106×8

Table 4.1: Flow system properties for the gasoline/gasohol transport simulations.

Parameter	Value
Hydraulic conductivity	10^{-4} m/s
Porosity	0.35
Average hydraulic gradient	0.003
Groundwater velocity (variable along the flowpath)	0.03 - 0.1 m/day
Dispersivity:	
longitudinal	1.00 m
transverse horizontal	0.02 m
transverse vertical	0.01 m
Aquifer recharge	0.20 m/yr

$\times 30$ (= 25440) elements in the longitudinal, transverse horizontal and vertical directions, respectively and satisfies the grid Peclet and Courant constraints. A time step of 0.5 - 1.0 days was used for all transport simulations.

Dispersivities of 1.0 m, 0.02 m and 0.01 m in the longitudinal, transverse horizontal and vertical directions respectively, are consistent with estimates based on statistical analyses of Borden aquifer properties (Sudicky, 1986) and with previous model calibration to the large-scale Borden landfill plume (Molson and Frind, 1990; Frind and Hokkanen, 1987). These dispersivities will tend to minimize plume spreading and minimize mixing of substrates and electron acceptors. Field evidence tends to support this concept of low dispersion as long and thin BTEX and MTBE plumes have been well documented in the literature (Davis et al., 1999 (BTEX); Einarson et al., 1999 (MTBE)). Under such conditions of low transverse mixing, the biodegradation rate becomes limited by dispersion of the available electron acceptors (MacQuarrie et al., 1990).

The current approach assumes a fully 3D system, although references are made to several previous 2D simulation results with the same model (Molson et al., 2000a). In the two-dimensional model, hydrodynamic mixing is reduced since transverse horizontal dispersion is neglected. Electron acceptor-limited biodegradation rates were therefore somewhat underestimated relative to the current fully three-dimensional approach and, in this sense, the 2D results may represent a worst case scenario. Frind et al. (1989) and Schirmer et al. (1995), however, show by comparing 2D and 3D simulations of biodegrading organics, that 3D effects can become quite significant. The more realistic 3D approach is therefore considered here.

4.3.2 Transport System

This study considers two conceptual models representing different spill scenarios. A third conceptual model is similar to the first but differs in the approach for representing ethanol. In the first conceptual model, we consider a four-component gasoline mixture composed of benzene, TEX (toluene, ethylbenzene and xylenes), ethanol, and a relatively more inert remaining fraction which is treated as a single equivalent compound (this would include for example, alkanes and cycloalkanes). A single electron acceptor (oxygen) and a dynamic microbial population are also included. Anaerobic degradation is not considered because benzene biodegradation is not always observed under anaerobic conditions (e.g., Barker and Wilson, 1997). All simulation scenarios include a simple gasoline source, as well as a gasoline source mixed with a 10% volume fraction of ethanol to represent gasohol.

In the second conceptual model, the basic source geometry and chemistry are the same, however we consider a spill of pure ethanol into an existing BTEX source and plume generated from the first conceptual model. This spill scenario is one identified by Rice et al. (1999) as being of particular concern given the large number of hydrocarbon-handling sites with existing groundwater contamination.

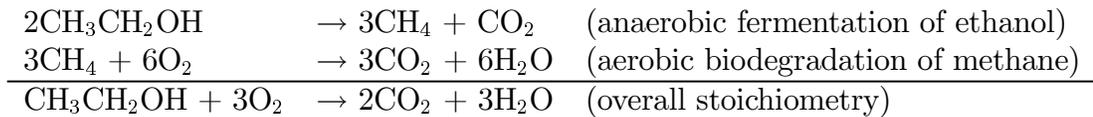
Ethanol has been shown to degrade under both aerobic and anaerobic conditions as long as ethanol concentrations are not toxic to the microbes, that is, as long as ethanol concentrations are less than perhaps 40,000 to 200,000 mg/L (summarized by Alvarez & Hunt, 1999). The model includes rapid aerobic degradation for ethanol, but does not directly include an anaerobic rate which should be rapid. Corseuil et al. (1998), for example, reported 80 to 100 mg/L of ethanol degraded within about 4 weeks under anaerobic conditions at 28 °C. At lower aquifer temperatures, anaerobic degradation would likely be slower. Hubbard et al. (1994) observed the persistence of methanol, a similar alcohol, in the Borden aquifer under aerobic and anaerobic conditions. Almost all of the 6000 mg/L methanol was degraded within 68 weeks. For most groundwater situations, 68 weeks is a relatively short time, and it is therefore reasonable to assume ethanol itself will not persist at significant concentrations in groundwater for more than a year or two.

The simulations emphasize the influence ethanol biodegradation has on the persistence of benzene. Corseuil et al. (1998) and Hubbard et al. (1994) demonstrated that ethanol (or methanol) is degraded much faster than BTEX when both are present and oxygen is available. The hypothesis is that most of the oxygen will be utilized by ethanol degraders and not by BTEX degraders, thus slowing the biodegradation of benzene when ethanol is present in the groundwater. The model captures this aspect by assigning biodegradation rate parameters for ethanol which

are higher than those for BTEX.

Even if ethanol is rapidly degraded, it may still have an impact on subsequent aerobic benzene biodegradation because its anaerobic biodegradation products (including organic acids and methane) will likely persist. These products will exert a demand for oxygen since they are readily degraded aerobically. As for ethanol, these products are assumed to be more readily degraded aerobically than BTEX. In this study, “ethanol” therefore represents the complete oxygen demand of the alcohol itself, as well as the oxygen-consuming by-products such as methane. This approach is meant to represent the worst-case scenario of a relatively persistent high oxygen demand.

The stoichiometry of the oxygen demand is based on the following reactions involving ethanol fermentation, followed by methane degradation:



The stoichiometry of 3 moles of oxygen required for each mole of either ethanol or methane is therefore maintained. Here, we assume a constant BOD (Biological Oxygen Demand) for ethanol and its by-products.

The residual source in both models occupies a volume 10 m long, 1 m wide and 0.50 m thick. The source is located at the watertable, starting 10 m from the left boundary and is assumed to dissolve at equilibrium into groundwater moving through the residual gasoline. Effluent concentrations from the dissolving source are entered into the domain as a Cauchy, or mass-flux boundary condition (equation 4.7) thus preserving complete mass balance from the dissolving source into the aquifer. Properties of the gasoline components and residual source are provided in Table 4.2 and Table 4.3 respectively. Kinetic biodegradation parameters for the base case are provided in Table 4.4.

The gasoline source is based on a PS-6 gasoline standard as defined by Brookman et al. (1985) which is often used as a source fuel for laboratory experiments (see, for example Poulsen et al., 1991; and Donaldson et al., 1994). The PS-6 source characteristics are first used to determine mole fractions for the gasoline components considered here. The mass of benzene is then fixed at 0.5 kg, and the mass of the TEX and remaining fraction determined by their mole fractions. The total source mass of 36.5 kg of gasoline yields an effective residual saturation (V_{NAPL}/V_{VOIDS}) of 0.023, sufficiently low to justify the assumption that the source remains immobile. With the addition of 3.5 kg (10% of gasohol by volume) of ethanol to the source,

only the mole fractions of the gasoline components change, the component masses do not. This means that for the gasohol case, the volume of gasohol is greater than the volume of gasoline, but the masses of BTEX are the same. This permits a comparison of benzene plumes based on the same initial mass of benzene for the gasoline and for the gasohol cases. Since we are considering a 3D symmetric system, the plumes actually correspond to field source masses of 71.2 and 80 kg for the gasoline and gasohol sources, respectively.

BTEX is assumed to migrate more slowly than groundwater with retardation factors increasing from ethanol (unretarded), through benzene, TEX, and the “other compounds”. The retardation factors (4.2) were thought to be more representative of California sand aquifers (not based on data, however) and are somewhat greater than those found in the Borden sand. A sensitivity analysis was also completed assuming different retardation factors.

Biodegradation rates and parameters for BTEX in Table 4.4 are based on a range of observed field data (Schirmer et al., 2000b). Published parameters based on local site conditions vary considerably, and defining a representative parameter set can be difficult (see for example, Bekins et al., 1998 and Alvarez et al., 1991); a sensitivity analysis is used to address this parameter uncertainty. The oxygen:substrate mass ratios in Table 4.5 assume complete organic degradation to CO_2 and H_2O . C8-isoalkane is used as a surrogate component to represent the oxygen demand of the remaining lumped components in gasoline. While the model tracks biomass change, it does not take the required carbon from the substrate. This biomass carbon is assumed to be a minor portion of the carbon degraded and this approach should not introduce significant bias.

The initial condition for Conceptual Model 1 is a clean aquifer, with a background oxygen concentration of 3.8 mg/L and an initial microbial concentration of 3.0 mg/L. An effective oxygen diffusion coefficient of $9.1 \times 10^{-10} \text{ m}^2/\text{s}$ was assumed based on a diffusion coefficient in water of $1.3 \times 10^{-9} \text{ m}^2/\text{s}$ (Luckner & Schestakow, 1991) and a tortuosity of 0.7. Oxygen is allowed to enter the domain at background levels along the left inflow and top watertable boundaries using the Cauchy boundary condition of equation 4.7.

Cosolvency is not considered in the first conceptual model because at and below the ethanol concentration in the source area of 2,000 mg/L, laboratory data suggest that cosolvency effects are not significant (Poulsen et al., 1992; Heermann and Powers, 1998). Similarly, no cosolvency modification of BTEX retardation was considered.

MTBE was not considered in this study, in part because MTBE biodegradation is not sufficiently understood to include as a process in this modelling. Also, MTBE

concentrations in groundwater are not likely to be significantly enhanced by ethanol cosolvency in Conceptual Model 2, because MTBE is already very soluble (50,000 mg/L) and most MTBE should already be moving away from the source area within a few years of its release. In general, ethanol is expected to have little impact on MTBE plumes unless MTBE biodegradation is affected.

Table 4.2: Physical properties of the gasoline components assumed in the model.

Compound	MW ⁽¹⁾ (<i>kg/mole</i>)	Pure Phase Solubility ⁽²⁾ (<i>kg/m³</i>)	Density ⁽³⁾ (<i>kg/m³</i>)	R ⁽⁴⁾	Diff. Coeff. ⁽⁵⁾ (<i>m²/s</i>)
Benzene	0.078	1.780	878.6	1.1	7.7e-10
TEX	0.104	0.288	870.0	2.0	6.2e-10
Other cpds.	0.100	0.02	900.0	2.8	6.2e-10
Ethanol	0.046	11.6*	789.0	1.0	11.5e-10

^{1,5} Wiedemeier et al. (1999), Appendix B, assuming a tortuosity of 0.7.

² Johnson et al. (1990), as referenced in Wiedemeier et al. (1999), p.88.

³ CRC Handbook of Chemistry and Physics (1980).

⁴ Retardation factors from Schirmer et al. (2000b).

* This solubility is the maximum possible which allows all the ethanol to dissolve in the initial source pore volume of groundwater. Note that Heermann and Powers (1998) concluded that > 99% of the ethanol in a gasohol source will partition into the aqueous phase. Similarly, Poulsen et al. (1992) found >99% of methanol dissolved into the initial pore volume of water.

Table 4.3: Assumed characteristics of the residual gasoline source.

Compound	Source Mass (<i>kg</i>)	Mole Fraction ⁽¹⁾	
		gasoline source	gasohol source
Benzene	0.5	0.018	0.015
TEX	6.0	0.158	0.131
Other cpds.	30.0	0.824	0.682
Ethanol	3.5	n/a	0.172

¹ PS-6 gasoline standard: Brookman et al. (1985); Poulsen et al. (1991)

Table 4.4: Assumed biodegradation parameters for the gasoline components, base case scenario.

Organic Component	Max. Rate k (mg_{org}/mg_{mic})/day	Organic Half Const. K_C (mg/L)	O ₂ Half Const. K_A (mg/L)	Microbial Yield Y mg_{mic}/mg_{org}
Benzene	1.0	2.0	2.0	0.5
TEX	1.0	2.0	2.0	0.5
Other cpds.	0.1	2.0	2.0	0.5
Ethanol	5.0	2.0	2.0	0.5

Source: Bekins et al. (1998), Schirmer (1998), Frind et al. (1989).

Table 4.5: Reaction stoichiometries for the simulated gasoline components.

Gasoline Component	Reaction Stoichiometry	O ₂ :Substrate mass ratio X
Benzene	$C_6H_6 + \frac{15}{2}O_2 \Rightarrow 6CO_2 + 3H_2O$	3.08
TEX	$C_7H_8 + 9O_2 \Rightarrow 7CO_2 + 4H_2O$	3.13
Others	$C_8H_{18} + \frac{25}{2}O_2 \Rightarrow 8CO_2 + 9H_2O$	3.5
Ethanol	$CH_3CH_2OH + 3O_2 \Rightarrow 2CO_2 + 3H_2O$	2.09

4.4 Simulation Results

4.4.1 Conceptual Model 1: A 10% ethanol gasoline spill into a pristine aquifer

Base Case (Scenario 1)

A base case simulation is first completed with both an ethanol-free gasoline source and a gasohol source containing 10% ethanol by volume. Parameters are chosen to represent nominal conditions that are later varied in a sensitivity analysis. All simulations are compared to the base case scenario.

Concentrations of the four gasoline components, in groundwater at equilibrium with the residual gasoline/gasohol source, are provided in Figure 4.2 for the base case simulation. In the ethanol-free gasoline source, the initial concentrations within the source for benzene, TEX and the remaining components are 31 mg/L, 46 mg/L and 16 mg/L respectively, corresponding to their initial effective solubilities. Under the assumed conditions with a recharge of 0.2 m/yr, an initial mass of 0.5 kg and an initial mole fraction of 0.018, benzene concentrations begin decreasing after approximately 2500 days, reaching a concentration of 10 $\mu\text{g/L}$ by 3600 days (about 10 years). The TEX and remaining fraction, which are relatively less soluble and have higher mole fractions, persist longer in the source.

The addition of 10% ethanol (by volume) to the gasoline source causes a small reduction in the mole fraction for the remaining compounds at early time. This reduces the effective solubilities as seen in the source concentrations (Figure 4.2) but does not significantly impact plume concentrations because of the rapid source depletion of ethanol. The ethanol concentration in the source reaches 2000 mg/L, which is sufficiently low to justify neglecting cosolubility effects. Because of ethanol's high solubility and limited mass in the gasohol source, ethanol is completely dissolved from the source within one pore volume, or approximately 320 days. Once the ethanol has completely dissolved, the effective solubilities of the remaining components return to the levels of the ethanol-free case. Although ethanol is rapidly depleted from the source, it persists immediately below the source (within the aquifer) for several hundred days longer because of dispersive mixing.

The one pore-volume flush time for ethanol is a consequence of its high solubility, its limited mass, and the volume of water within the available saturated pore space in the source area. This approach assumes no kinetic limitations or substrate interactions which may inhibit equilibrium dissolution. Donaldson et al.

(1994) provide evidence supporting this behaviour for methanol and concluded that methanol can dissolve quite rapidly, within a few pore volumes. Ethanol is expected to behave similarly.

The organic concentration profiles for the base case simulation at 10 and 20 years are shown in Figure 4.3 (for clarity, we only show the domain up to 200m). The organic plumes are long and thin, with high vertical concentration gradients resulting from a low transverse dispersivity and low numerical dispersion (note the vertical exaggeration).

The benzene plume, as defined by the $10 \mu\text{g}/L$ contour at 10 years, is approximately 100 m long and 3 m thick and has almost completely dissolved from the source. The plume length is similar to many BTEX plumes observed at the field scale (see for example Davis et al., 1999; Thierrin et al., 1995, Wiedemeier et al., 1999 - Table A2). By 20 years, biodegradation has removed most of the benzene mass, leaving only a small remnant of the plume from 100-140 m. In this ethanol-free benzene plume, degradation is therefore quite rapid; this plume will later be compared with those co-degrading with ethanol. Because of their relatively higher source mass and lower solubility, TEX and the remaining components continue to dissolve beyond 20 years and their plumes are therefore still connected to the source.

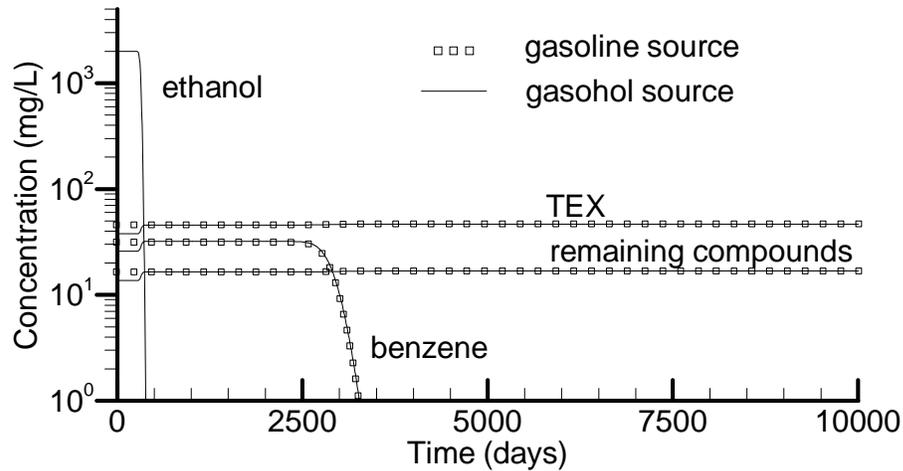


Figure 4.2: Simulated aqueous concentrations from the dissolving residual gasoline and gasohol sources: conceptual model 1, base case scenario.

The corresponding oxygen depletion plumes are provided in Figure 4.4 at 10 and 20 years. They can be correlated with the organic plumes although they are somewhat longer and wider because of a higher diffusion coefficient and unretarded oxygen transport. Oxygen concentrations vary from the initial background level of 3.8 mg/L at the far left and top right inflow boundaries, to 0 mg/L where biodegradation has consumed all the available oxygen.

As benzene dissolves from the source and enters the aquifer, the aqueous plume mass increases until it reaches a peak of about 0.14 kg after 2800 days (Figure 4.5). The mass lost to biodegradation continues to increase but increases at a slower rate once the benzene concentrations drop significantly below the half-utilization constant (K_C). A relatively minor fraction is sorbed to the solids. The sum of these mass components over the 25-year simulation time remains within 1.5% of the initial benzene source mass of 0.50 kg.

The maximum travel distance of the gasoline-source benzene plume is now compared to that from an equivalent gasohol source. In general, the time of maximum difference will depend on the parameter set and will generally occur before complete separation of the ethanol and benzene plumes. Once the ethanol plume begins to pull away from the benzene plume, benzene begins degrading at a more normal rate and the earlier effects of ethanol are reduced.

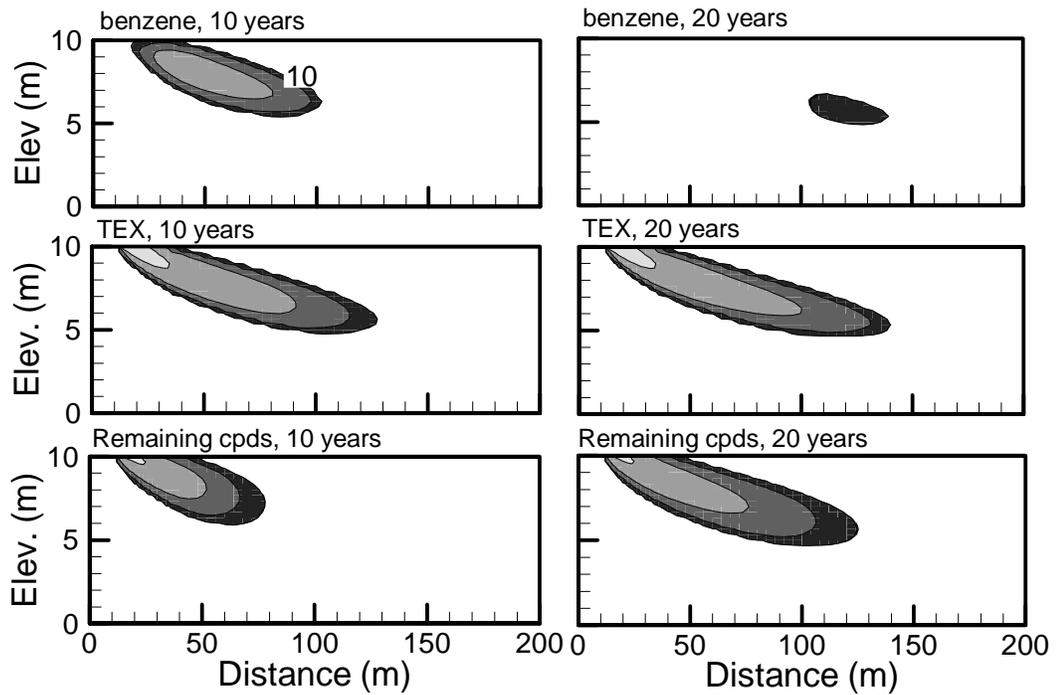


Figure 4.3: Simulated benzene, TEX and remaining component plumes from the base case gasoline source at 10 years (left) and 20 years (right). Contour intervals are 10, 100, 1000 and 10,000 ppb.

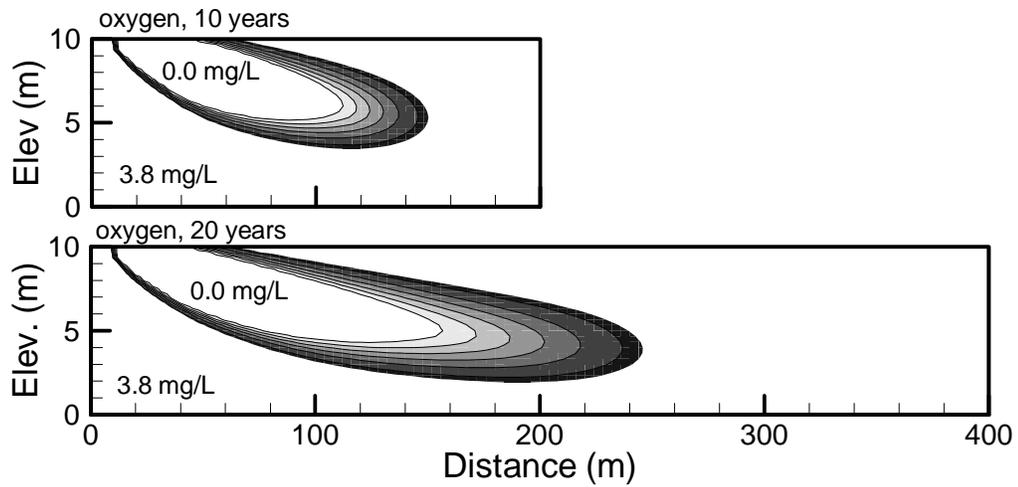


Figure 4.4: Simulated oxygen depletion plumes at 10 and 20 years.

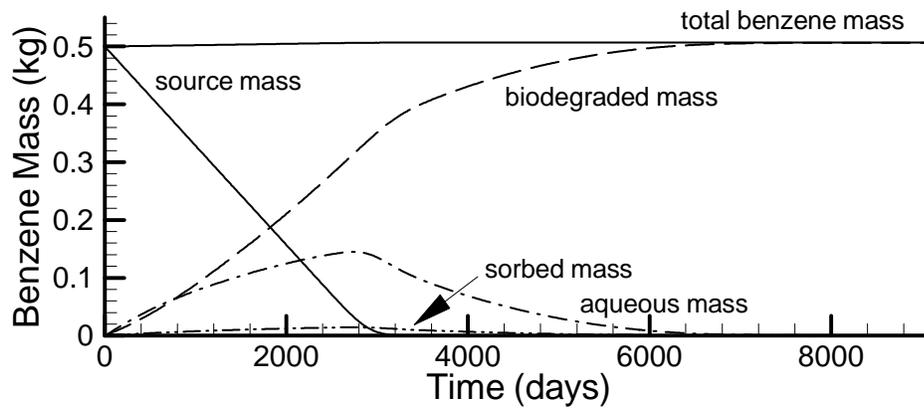


Figure 4.5: Simulated benzene mass distribution showing source mass depletion, mass lost to biodegradation and sorption, and aqueous plume mass.

The influence of ethanol in the base case (Scenario 1) simulation is shown in Figure 4.6 which shows the concentration profiles for benzene, originating from the gasohol source, at 10, 15 and 20 years. The addition of ethanol has extended the benzene plume migration distance by approximately 135% at 20 years, as defined by the 10 $\mu\text{g}/\text{L}$ contour, relative to the travel distance of the ethanol-free benzene plume. The difference increases to 150% at 21.5 years. Because benzene is now competing with ethanol for the available oxygen, and because ethanol reacts at a faster rate ($k_{ethanol} > k_{benzene}$), the rate of benzene mass loss is reduced and the plume migrates further relative to the ethanol-free (gasoline source) benzene plume. The presence of ethanol has effectively stretched and split the benzene plume into two lobes. The trailing lobe is relatively unaffected by the presence of ethanol since ethanol had long since dissolved from the source before this part of the benzene plume entered the aquifer. The advanced lobe, however, is carried along within the ethanol plume since ethanol is preferentially degraded. Although the advanced benzene lobe at 20 years ($> 10 \mu\text{g}/\text{L}$, Figure 4.6) does not contain much mass, it remains significant because the concentrations still exceed typical drinking water standards. The non-retarded ethanol plume is continually advancing relative to the benzene plume and will eventually completely degrade.

In Figure 4.6, an oxygen depletion zone surrounds the ethanol (including its anaerobic degradation products) plume at 20 years, and somewhat overlapping it to the rear, a second oxygen depletion zone surrounds the plumes of benzene, TEX and the remaining compounds. There appears to be only a limited, long-term residual oxygen shadow caused by the ethanol since oxygen eventually disperses back into the groundwater following the ethanol plume. This is only partially developed in Figure 4.6 since the oxygen-consuming hydrocarbon plumes are close behind. The trailing benzene plume, lagging behind the ethanol plume because of its higher retardation, is eventually exposed to nominal oxygen concentrations and can degrade at a rate similar to that of the ethanol-free benzene plume. Furthermore, because of the rapid source depletion of ethanol, most of the benzene still remains in the source after the ethanol has been completely dissolved. Hydrodynamic dispersion does provide some mixing near the source at later times, however a significant fraction of the benzene plume mass never comes in contact with the ethanol plume.

The plumes of TEX and remaining components remain relatively unaffected by the presence of ethanol (not shown). Because of their even slower dissolution rate and higher retardation ($R=2.0$, and 2.8 respectively) relative to benzene, these components lag even further behind the ethanol plume and are exposed to the same oxygen levels as in the ethanol-free case.

Although the benzene plume is significantly extended in the presence of ethanol, the impact on the mass of benzene in the plume and on the mass degraded is minimal (Figure 4.7). The maximum reduction in mass loss due to ethanol, for example, is only about 13% of the initial benzene source mass. The mass loss is not significantly affected because ethanol dissolves rapidly into only the leading edge of the benzene plume, and oxygen has sufficient time to disperse back behind the ethanol plume and replenish the zone of oxygen depletion. The effect is maximum shortly after benzene has completely dissolved from the source (at about 3600 days), and does not significantly affect the time required for complete mass removal.

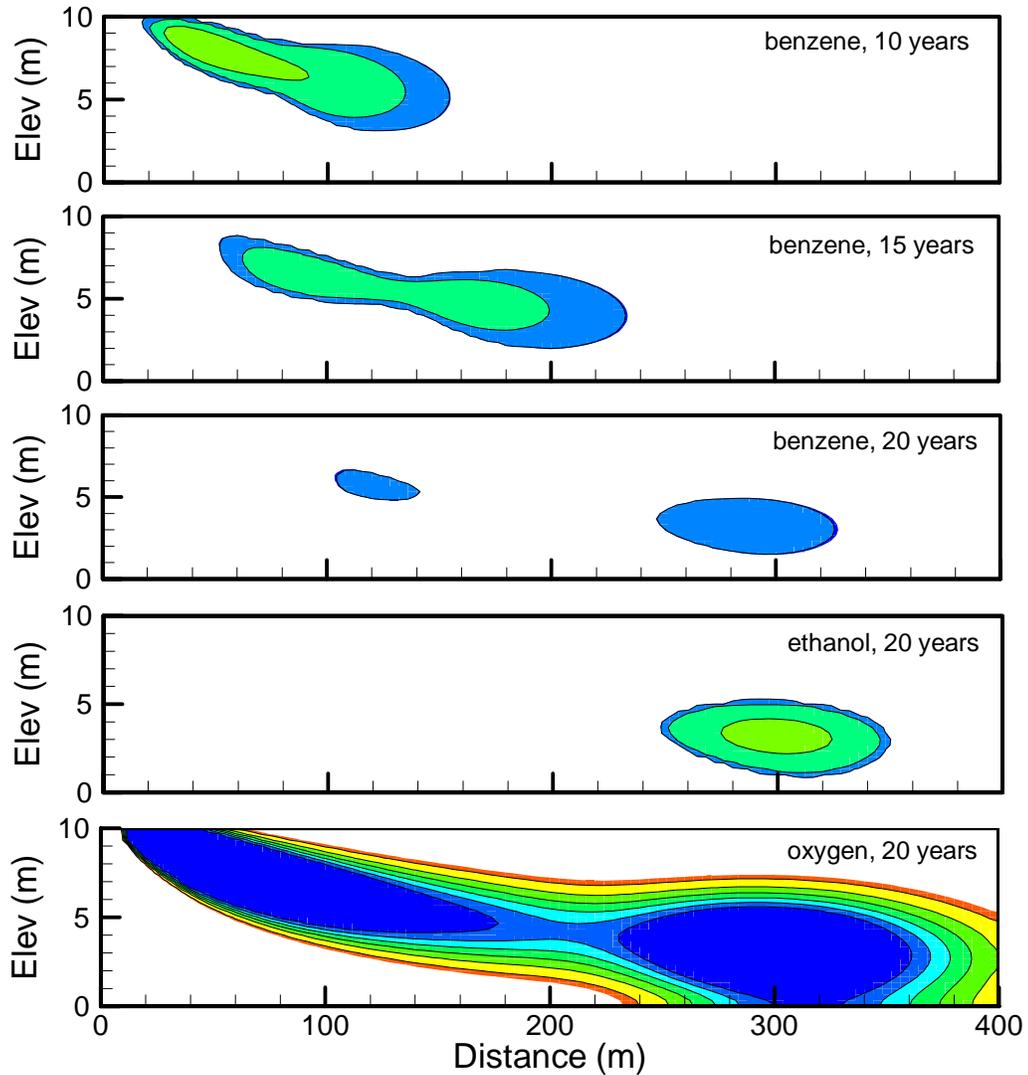


Figure 4.6: Simulated benzene plumes from the gasohol source at 10, 15 and 20 years. Also shown is the ethanol plume and dissolved oxygen depletion plume at 20 years. Benzene and ethanol concentration contours are 10, 100, 1000 ppb. Oxygen contours vary from a background of 3.8 mg/L to 0.0 mg/L within the gasoline and ethanol plumes.

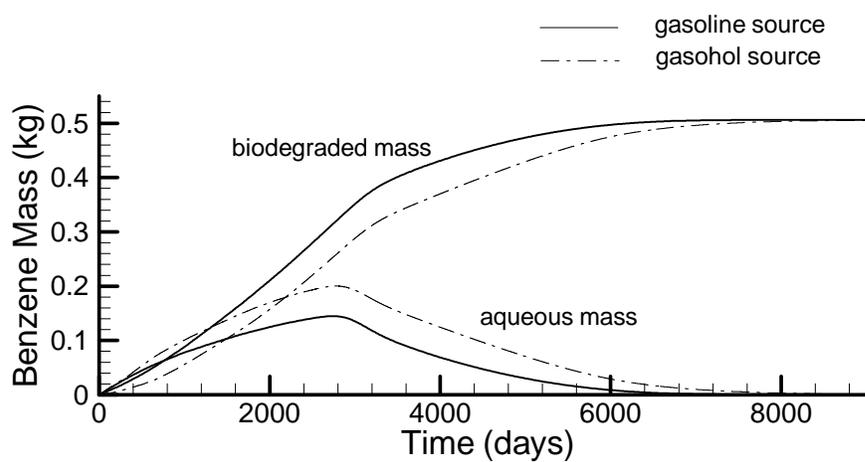


Figure 4.7: Comparison of mass profiles showing the effect of ethanol on benzene persistence.

4.4.2 Sensitivity Analysis

The base case scenario represents only a single set of system parameters, many of which show considerable variation and uncertainty in published laboratory and field data (see for example, Bekins et al., 1998). Molson and Frind (1990) for example, show that parameter uncertainty can lead to non-unique predictive simulations of biodegrading organics. A sensitivity analysis was therefore performed on the base case scenario to determine the influence of several of these parameters on system behaviour. To isolate the effects of ethanol alone, each new simulation was completed with and without ethanol, and results expressed as a percent change in benzene travel distance relative to the ethanol-free benzene plume. A more complete analysis was performed in a 2D system by Molson et al. (2000a). Those scenarios showing the greatest effects were repeated here in 3D and presented in Table 4.6.

Scenario 2 considers a higher benzene retardation which would represent an aquifer material with a higher organic carbon fraction. In Scenario 3, the background oxygen concentration was reduced to 2.0 mg/L, much lower than the oxygen saturation of 12.8 mg/L (at 5 °C, Appelo & Postma; 1993). Higher concentrations were not simulated since the 2D results suggested that oxygen concentrations higher than the 3.8 mg/L (used in the base case) induced only minor changes in travel distance (between the gasoline and gasohol source plumes). There was relatively low impact under higher oxygen concentrations because both the benzene and ethanol plumes were more rapidly degraded. Scenario 4 addresses the impact of a multiple release of 4 kg of gasohol each year over a 10-year period; a total source mass equivalent to the other scenarios.

In the previous 2D simulations of the same conceptual model (Molson et al., 2000a), additional parameters were varied including the time required to flush ethanol from the source. Ethanol flush times, or source persistence, may vary in field situations for example, due to diffusion limitations or preferential flow. Increasing the ethanol flush time from a single pore volume to 5 pore volumes had a relatively minor effect since these times are still much shorter than the time required to flush benzene from the source. The same behaviour would be expected in the 3D approach and was not repeated here.

Table 4.6: Overview of simulation scenarios and influence of ethanol on the extent of the benzene plume, Conceptual Model 1.

Scenario	Parameters	% change ¹
Scenario 1 (base case)	See Tables 4.2, 4.3 & 4.4	+150 (21.5yrs)
Scenario 2	$R_{benzene}$ increased from 1.1 to 1.5	+50 (17 yrs)
Scenario 3	O_2 decreased from 3.8 to 2.0 mg/L	+100 (25 yrs) ²
Scenario 4	Multiple spill: 4 kg/yr \times 10 years	+120 (40 years) ²

¹ maximum % change in the distance traveled from the source center to the down-gradient edge of the benzene plume at 10 $\mu g/L$.

² maximum not reached, % change may grow in time.

Scenario 2: Higher Benzene Retardation

In this scenario, the retardation factor for benzene is increased from the base case value of $R=1.1$ to $R=1.5$. This represents a common range of field-measured retardation factors reported in the literature. The retardation factors for TEX and the remaining components are not changed because this would have little impact on the fate of benzene. Ethanol is again assumed nonretarded. The corresponding evolution of the benzene plume from both the gasoline source and gasohol source is provided in Figure 4.8.

In a bioreactive system, increasing the retardation factor slows the plume advance and decreases the plume extent. A higher retardation factor, however, also reduces the effective biodegradation rate since the sorbed phase is assumed non-biodegradable. These processes have opposite effects on the apparent travel distance of the benzene plume. In the ethanol-free scenarios, the latter process dominates which results in a somewhat longer plume with higher concentrations relative to the plumes with lower retardation. At 20 years, for example, the higher retardation factor has increased the benzene plume length from about 50 m ($R_{ben}=1.1$: Figure 4.3) to about 80 m ($R_{ben}=1.5$: Figure 4.8). The corresponding peak concentrations increase from about 10 $\mu g/L$ to 100 $\mu g/L$.

The effect of adding ethanol to the source in this high retardation scenario is again an increase in the benzene plume travel distance relative to the ethanol-free benzene plume (Figure 4.8). The increase, however, is not as pronounced as in the base case ($R=1.1$) because the ethanol and benzene plumes are now travelling at significantly different rates and the plume overlap time is reduced. Nevertheless, by

15 years, an extended frontal lobe of the benzene plume has formed due to reduced biodegradation in the presence of the advancing ethanol. After 15 years, the plumes separate further which allows more oxygen into the benzene plume and allows the frontal lobe to rapidly degrade. By 20 years, the effect of ethanol has vanished and the two benzene plumes appear nearly identical.

The dynamic interaction between the ethanol and benzene plumes is clear from Figure 4.9 which shows the maximum extent of the $10 \mu\text{g}/\text{L}$ benzene concentration level over time, for both retardation scenarios. Note that these are apparent rates of advance, which depend on the retardation and effective biodegradation rates. The curves are somewhat irregular because of the grid discretization. In the base case scenario ($R=1.1$), the maximum extent of the benzene plume from the gasoline source advances at a relatively uniform rate until about 16 years. Beyond 16 years, the benzene plume reaches a steady-state maximum limit and is completely degraded at 21.5 years. In the high retardation ($R=1.5$) gasoline-source scenario, the apparent advance of the plume is retarded, but only slightly, because the slower travel velocity is offset by the lower effective biodegradation rate (the sorbed phase is not degrading) which increases plume persistence. The benzene plume in this case persists through to 25 years.

The benzene plumes from the gasohol source, however, (Figure 4.9), advance more rapidly relative to those from the gasoline plume because the leading lobe is co-transported within the oxygen-consuming ethanol plume. The difference in travel distance for the base case scenario ($R=1.1$), for example, reaches a maximum of about 150% at 21.5 years. Because of the higher effective biodegradation rate with lower benzene retardation, the benzene plume in this case is completely degraded by about 23.5 years. With a higher benzene retardation, however, the relative increase in travel distance due to the presence of ethanol is much less - reaching a maximum of only 50% at 17 years, after which the advanced lobe of the benzene plume is completely biodegraded. The furthest advance of the benzene then immediately returns to the leading edge of the upgradient lobe, hence the rapid drop in travel distance in Figure 4.9. While still potentially significant, the relative increase is less than in the base case with a lower retardation.

Where the mobility of benzene and ethanol is significantly different (i.e. with higher benzene retardation), the potential for extension of the benzene plume front in a gasohol spill is therefore reduced relative to that from a lower retardation scenario. Aquifers rich in organic matter are therefore more likely to be protected with respect to the influence of ethanol on benzene plume travel distances. Conversely, the base case scenario, which assumes an aquifer relatively low in organic carbon, appears to represent a worst-case scenario which is relatively more susceptible to

ethanol-induced benzene persistence.

These findings contradict the assumptions made by McNab et al. (1999) who suggest that effects of sorption could be neglected for assessing ethanol-impacts. This assumption was necessary for their solution approach to be valid. Furthermore, Malcolm Pirnie Inc. (1998) predicted *increasing* benzene plume lengths with higher retardation, using a simplified 2D analytical approach and assuming continuous source functions for both ethanol and benzene. These previous studies, however, were based upon relatively simplified conceptual models which did not consider limited source persistence and the full 3D system dynamics. In the Malcolm Pirnie model, for example, the retarded benzene plume remains within the continuous ethanol plume for a longer time, hence the relative persistence increases. By incorporating a more realistic source dissolution function in BIONAPL/3D, however, the ethanol plume rapidly dissolves and detaches from the source. This allows the more retarded benzene plume to degrade behind it and the relative persistence decreases.

Scenario 3: Low background O₂

In this scenario, the background oxygen concentration is reduced from 3.8 mg/L to 2.0 mg/L, which is well within the observed range for unconfined aquifers. Oxygen is still allowed to enter from the upper watertable boundary through recharge.

Reducing the initial background oxygen concentration from 3.8 mg/L to 2.0 mg/L reduces the degree of benzene degradation and produces a larger ethanol-free benzene plume relative to the base case (Figure 4.10). In the gasohol plume, the aerobic degradation rate of ethanol (and its products) is also reduced which increases the duration of overlap between the ethanol and benzene plumes. The result is an increase in the benzene plume length of approximately 64% at 20 years, relative to the gasoline-source benzene plume. The difference increases further at later times (not shown), reaching approximately 100% at 25 years. Proximity of the model boundary prevented estimates beyond 25 years, although the ethanol plume will eventually separate completely from the benzene plume and the difference will vanish.

Aquifers relatively low in dissolved oxygen are therefore potentially more susceptible to benzene persistence due to the addition of ethanol to gasoline. Since higher oxygen concentrations promote rapid biodegradation and therefore shorter plume overlap time, aquifers rich in oxygen should be relatively safe from increased benzene persistence (Molson et al., 2000a).

Scenario 4: Multiple Spill

In Scenario 4, we consider a multiple spill of the same total mass of gasoline and gasohol, but distributed with ten separate spills over a 10-year period. Each spill has one-tenth of the total initial mass of the base case scenario. Results are shown in Figure 4.11 at 10, 15 and 20 years. Although the spills are one year apart, the plumes appear continuous because of the short 2-year dissolution time and because of dispersive mixing. Furthermore, the high concentrations from each of the spills become attenuated due to degradation. In this multiple spill scenario, ethanol is distributed into the source over a longer time and is repeatedly flushed through each of the benzene plumes. The primary effects are an increase in the peak benzene concentrations, particularly near the source, and an elongation of the benzene plume as defined by the 10 and 100 $\mu\text{g}/\text{L}$ contours.

After 20 years, the benzene plume from the repeated gasohol spill has migrated about 66% further than that from the repeated gasoline spill. After 40 years, the benzene plume has migrated about 120% further (not shown). These increases are somewhat less than those of the base case of a single spill, where ethanol was flushed rapidly through only a small part of the benzene plume. In this multiple spill scenario, the relatively lower mass flux of ethanol into the aquifer consumes less oxygen, leaving more available to benzene. The impact is therefore less since both the gasoline and gasohol benzene plumes are degrading at similar rates, although both are somewhat longer due to the longer source duration. The simulations therefore suggest that continuing ethanol dissolution from a multiple gasohol spill will also lead to increased benzene travel distances, however the impact may be less, at least at early time (<20 years) than with a single, catastrophic spill. Relative impacts in this scenario likely increase further with time (>40 years), however the proximity of the model boundary prevented estimates to be made.

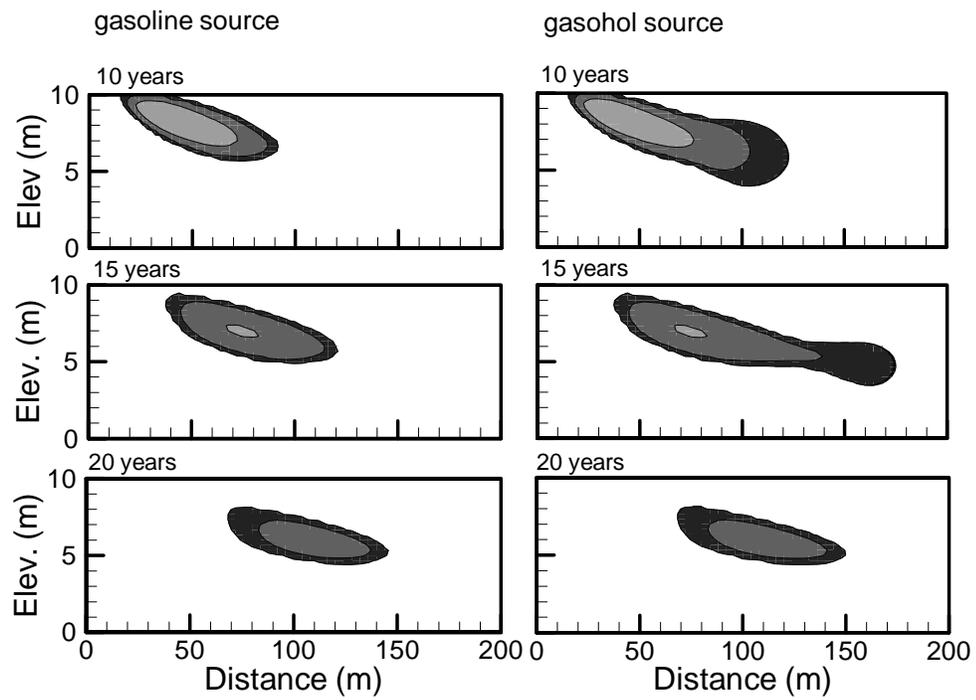


Figure 4.8: Simulated evolution of the benzene plume from a gasoline (left) and gasohol (right) source, assuming a relatively higher benzene retardation of 1.5.

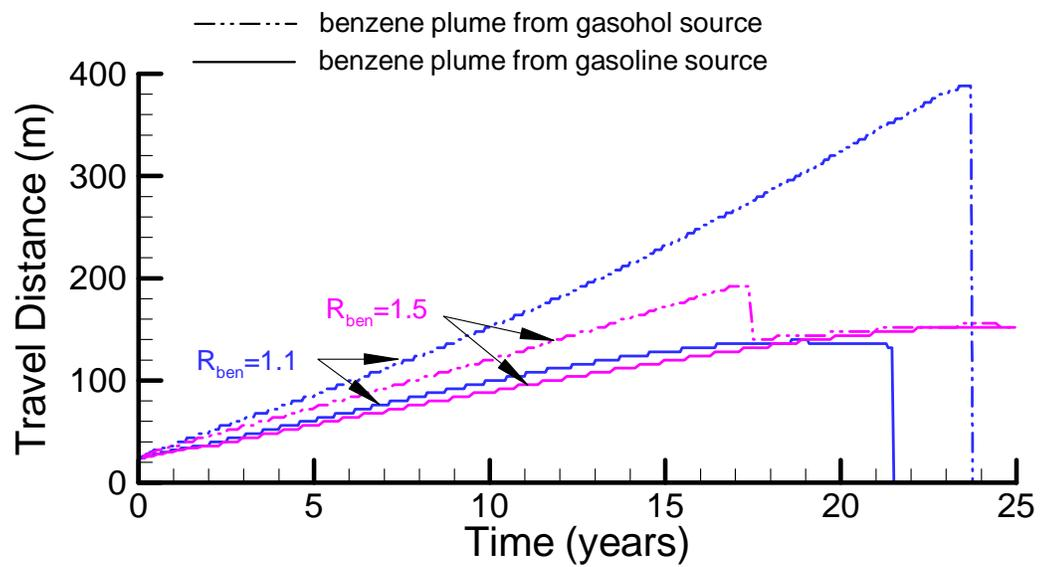


Figure 4.9: Simulated advance of the 10 ppb benzene contour from the gasoline and gasohol sources, comparing the effect of benzene retardation: base case ($R=1.1$) and high-retardation scenario ($R=1.5$).

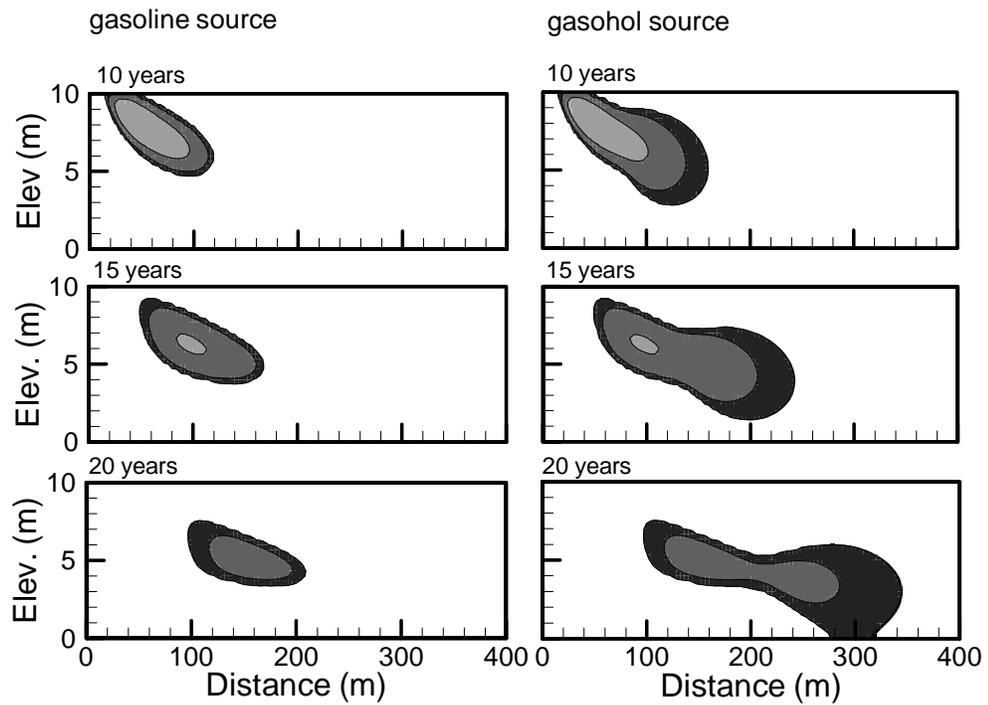


Figure 4.10: Simulated benzene plumes assuming a relatively lower background oxygen concentration of 2.0 mg/L.

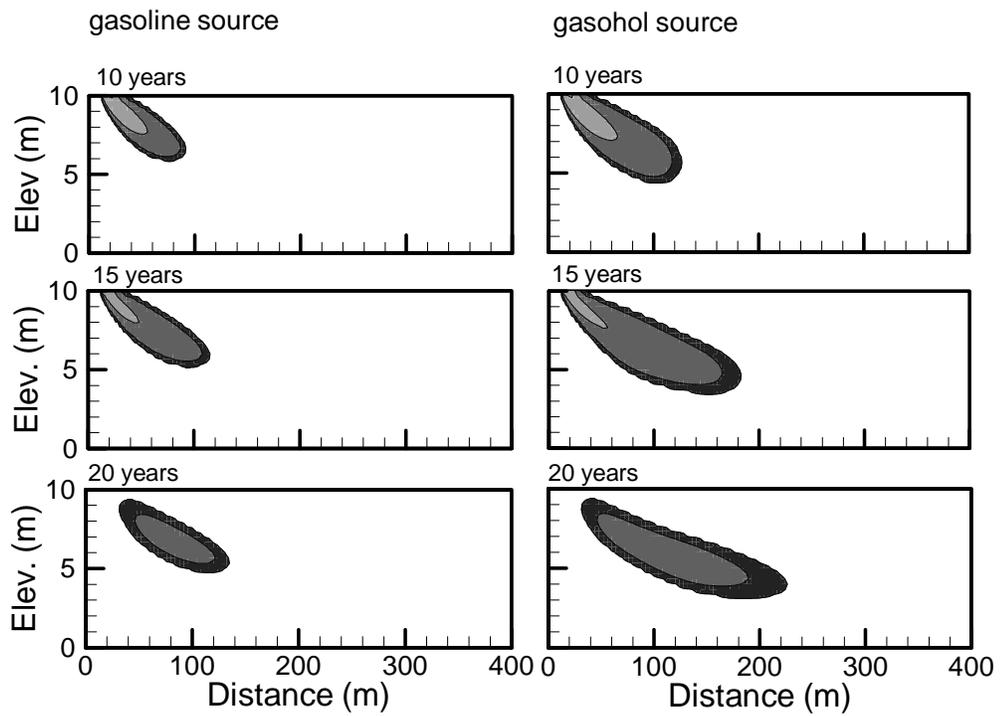


Figure 4.11: Multi-spill scenario: benzene plume evolution from gasoline (left) and gasohol (right) sources.

4.4.3 Conceptual Model 2: A Pure Ethanol Spill into an Existing Gasoline Plume

In this conceptual model, pure ethanol is spilled into the remaining source mass and the existing 5-year ethanol-free gasoline plume from the base case scenario of Conceptual Model 1. Targeting an initial aqueous phase source concentration of 500,000 mg/L, 437.5 kg of ethanol is spilled into a 2.5 m³ source volume, producing an initial aqueous volume fraction for ethanol of 0.63. At these high ethanol concentrations, cosolvency effects become important and must therefore be considered by the model.

The aqueous ethanol concentration at a real spill would depend on a number of factors, including the proportion of gasoline and water in the source area before the ethanol spill and the volume of this source area that would be impacted by spilled ethanol. The objective was to mimic a spill in which very high ethanol concentrations were generated in the source groundwater so as to enhance the impact of ethanol cosolvency.

Cosolvency is here represented as an increase in solubility using the enhancement factor approach given in equation 4.8 as $E = 10^{\sigma fc}$ where σ is the cosolvency factor, and fc is the volume fraction of ethanol in the aqueous phase. In the base case for Conceptual Model 2, we assign $\sigma = 2.0$ which produces a maximum enhancement factor at early time of approximately 18. The objective was to produce a maximum enhancement factor for benzene that is consistent with observed laboratory data. Heermann and Powers (1998), for example, suggest maximum enhancement factors for the BTEX components, in an ethanol-gasoline-water mix with $fc = 0.6$, on the order of 10-50. The aqueous volume fraction of ethanol (fc) is updated during the simulation as ethanol disperses and migrates away from the source area.

We here assume identical cosolvency factors for all gasoline compounds whereas they are likely somewhat higher for the less soluble compounds. Because the less soluble compounds would remain persistent regardless of a brief cosolvency effect, any differences in their cosolvency factors are expected to have minimal effect on the simulated outcome. The effect of cosolvency on the retardation of the various gasoline components is not considered. Ethanol concentrations are not likely to stay high enough to induce a lower retardation of benzene for very long or for much distance downgradient, given dispersive dilution of ethanol and subsequent ethanol biotransformation, both aerobically and anaerobically. For example, Hubbard et al. (1994) found an apparent half life of only about 200 days for methanol when its initial concentration was about 6,000 mg/L in Borden groundwater.

The simulated source concentrations of benzene, TEX, the remaining gasoline

components and ethanol for Conceptual Model 2 are shown in Figure 4.12. From 0-1860 days (5 years), the source concentrations follow those from the base case (ethanol-free) scenario of Conceptual Model 1. After 5 years, ethanol is introduced into the source which causes a sharp increase in the effective solubilities and source concentrations of the gasoline components. Source concentrations for benzene, for example, increase from 32 mg/L to 285 mg/L while TEX increases from 46 mg/L to 814 mg/L. As ethanol disperses from the source area and concentrations decline, the cosolvency effect is reduced and the effective solubilities for TEX and the remaining components return to normal levels. Benzene source concentrations continue to drop following the addition of ethanol because the source becomes depleted of benzene and the mole fraction declines. The apparent longer source persistence of ethanol relative to benzene is due to the location at which the concentrations are shown: benzene concentrations are located within the dissolving source whereas ethanol concentrations are located just within the domain where benzene would also persist somewhat longer. The ethanol-enhanced dissolution of benzene depletes the source of this component approximately 650 days earlier than with the ethanol-free source.

The simulated benzene plumes for Conceptual Model 2 are shown in Figure 4.13 at 10, 15 and 20 years. The ethanol spill begins at 5 years when the benzene plume is approximately 64 m long and about 37 % of the original benzene mass remains in the source. Ethanol is assumed to immediately partition into the aqueous (water) phase and begins to disperse within the oxygen depletion shadow of the BTEX compounds. Because of its low retardation ($R=1$) and higher diffusion coefficient, ethanol rapidly disperses and begins consuming oxygen ahead of the BTEX plumes. The benzene plume is more extended in the vertical direction in this scenario because of the more rapid source dissolution and because of significantly lower biodegradation within the larger ethanol plume.

In this cosolvency scenario, the ethanol spill has increased the benzene plume travel distance by about 112% at 20 years (Figure 4.13), relative to the ethanol-free benzene plume from Conceptual Model 1 (Figure 4.3). The increase is a result of two counteracting processes affecting benzene plume concentrations. First, the 5-year delay in the ethanol release has allowed the benzene plume to degrade at relatively higher rates at early time, thereby reducing benzene concentrations at the leading edge. The 5-year delay, however, also increases the degree of overlap between the ethanol and benzene plumes which tends to keep benzene concentrations higher because ethanol is preferentially consumed. The cosolvency effect further increases the extent of overlap by inducing a high concentration pulse of dissolved benzene into the aquifer at the same time as ethanol is released. Because of its short duration

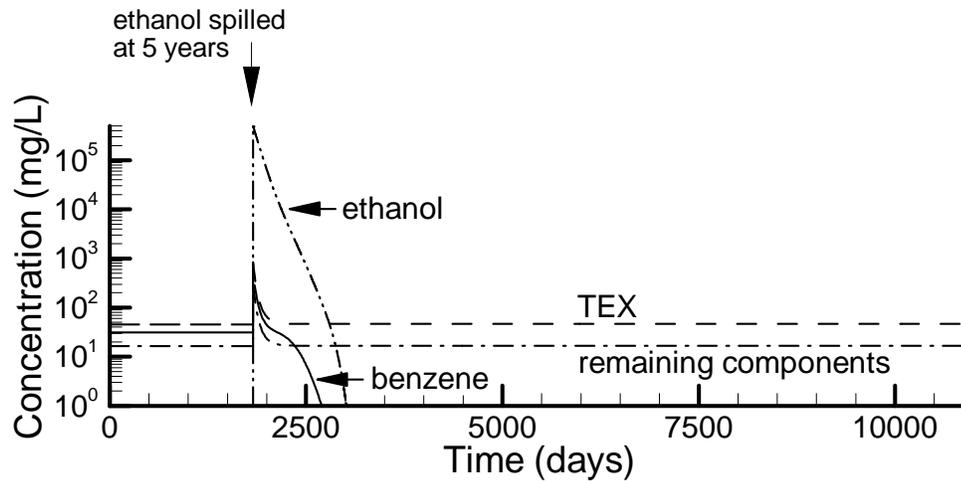


Figure 4.12: Simulated source concentrations for Conceptual Model 2: a pure ethanol spill at 5 years into an existing gasoline spill.

however, the cosolvency effect appears relatively less important.

As the ethanol plume disperses in this scenario, the effect of ethanol increases to at least 150% at 40 years (not shown), relative to the base case gasoline spill of Conceptual Model 1. Beyond 40 years, the plumes extend beyond the right outflow boundary and the full influence of the ethanol cannot be determined. A further increase on the order of 10-20% is possible. The maximum influence of ethanol is delayed because of the 5-year spill delay, but more importantly, because the larger ethanol plume overlaps the benzene plume for a longer time.

These results suggest that a later release of a pure ethanol spill, combined with the enhanced solubility of benzene, can lead to even longer benzene travel distances compared to gasohol spills in which the ethanol is more rapidly released from a gasohol source.

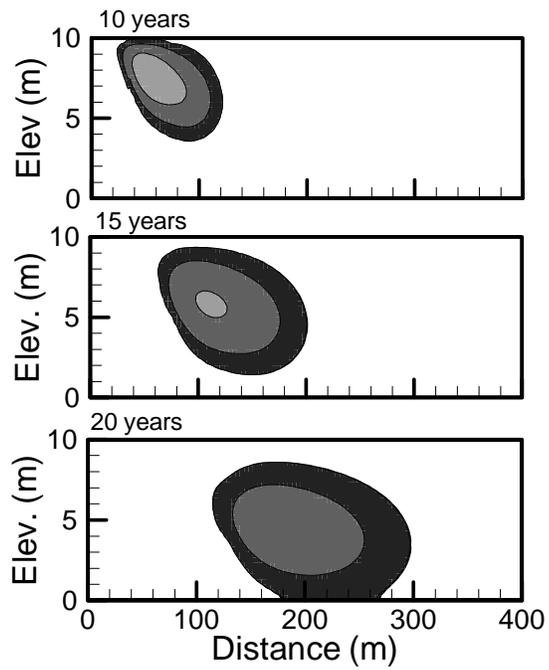


Figure 4.13: Benzene plumes from Conceptual Model 2: A pure ethanol spill into a 5-year gasoline plume. In this scenario, cosolvency effects are included.

4.4.4 Conceptual Model 3: A Gasohol Spill Simulation with Ethanol Conversion to Methane

In Conceptual Models 1 & 2, "ethanol" was assumed to represent the oxygen demand of ethanol itself, as well as its by-products. This approach can be justified on the basis of stoichiometry and total oxygen demand, however it is simplified because it neglects the different reaction rates along the degradation sequence. In this Conceptual Model 3, ethanol is allowed to degrade at a relatively rapid first-order (anaerobic) rate to methane, which is produced as a daughter-product, and exerts its own oxygen demand based on Monod kinetics. The system is still somewhat simplified but serves to illustrate the sensitivity of the rate parameters.

A first-order ethanol degradation rate of 0.007 day^{-1} ($t_{1/2} = 100 \text{ days}$) is assumed based on observed *methanol* degradation rates from Hubbard et al. (1994). A test simulation was first completed assuming a maximum aerobic degradation rate (k) for methane of $5.0 \text{ mg}_{\text{methane}}/\text{mg}_{\text{mic.}}/\text{day}$, equal to that for "ethanol" in Conceptual Model 1. The results (not shown) were essentially identical to those of Figure 4.6, validating the numerical approach of daughter-product generation and subsequent oxygen depletion.

This new conceptual model is now used as a basis for evaluating the influence of the biodegradation rate (k) of methane on the persistence of benzene from a gasohol spill. The simulation was repeated assuming $k_{\text{methane}} = 0.5 \text{ mg}_{\text{methane}}/\text{mg}_{\text{mic.}}/\text{day}$, which is a factor of 10 less than that assumed for "ethanol" in Conceptual Model 1. All other parameters remain identical to the base case (Table 4.4). In previous 2D simulations, under otherwise similar conditions, Molson et al. (2000a) showed a relatively low influence of higher degradation rates because of oxygen limitations.

The ethanol, methane, oxygen and benzene plumes from Conceptual Model 3 with a lower methane reaction rate are provided at various times in Figure 4.14. In this simulation, ethanol dissolves from the source at the same rate as in Conceptual Model 1, but on entering the aquifer, it is rapidly degraded to methane. Although the methane plume persists, as did the "ethanol" plume in Conceptual Model 1, in this case methane is consuming oxygen at a lower rate, leaving more available for benzene. The extension of the benzene plume has now essentially disappeared. The results confirm that lower degradation rates for methane (or for "ethanol" + products) would reduce benzene persistence due to the presence of ethanol. This same conceptual and numerical approach could be used to simulate gasohol contamination with multiple electron acceptors and more complex degradation pathways.

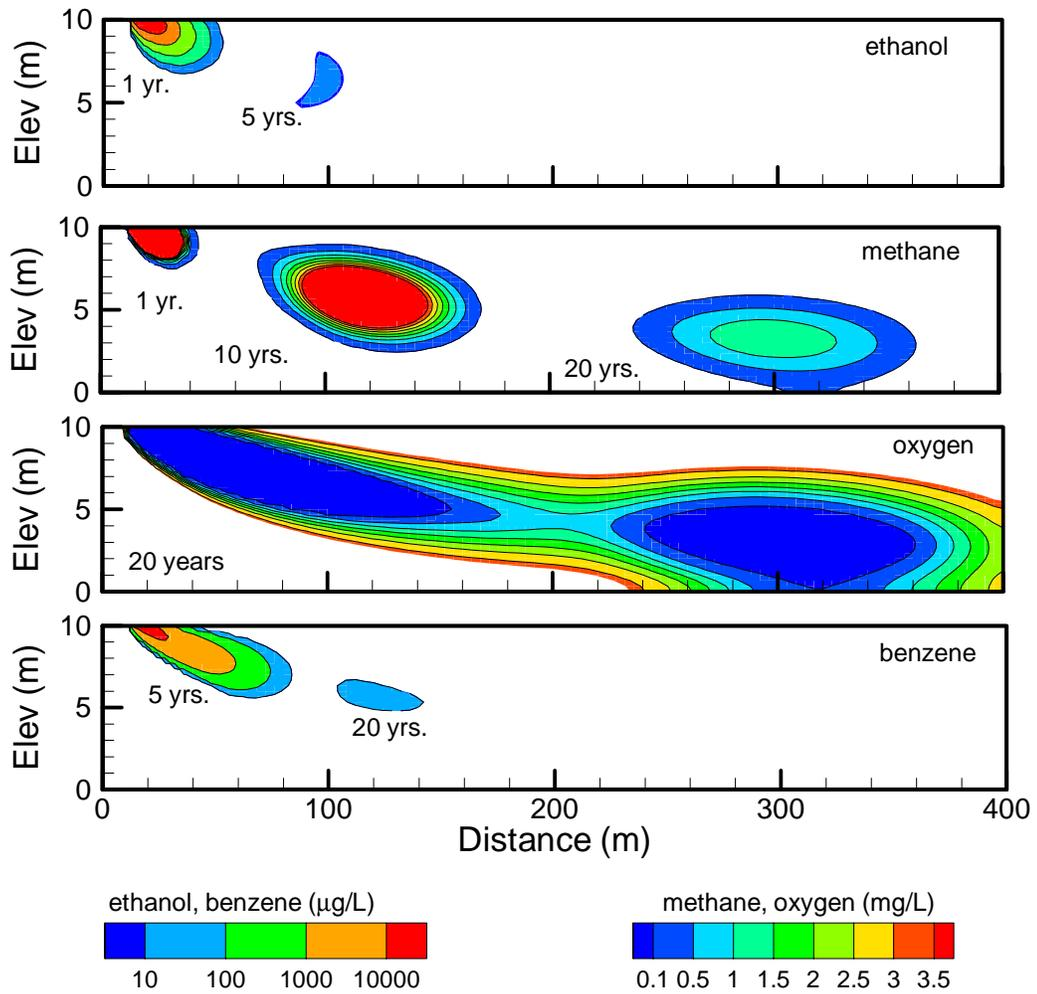


Figure 4.14: Simulated ethanol, methane, oxygen and benzene plumes: Conceptual Model 3.

4.5 Summary

The effect of ethanol on the persistence of BTEX gasoline components has been simulated for three conceptual models involving a spill of 10% ethanol gasoline (gasohol) into a pristine aquifer, and a pure ethanol spill into an existing BTEX plume. The conceptual models involve long and thin plumes with low transverse mixing under oxygen-limiting conditions. Several key parameters were adjusted in a sensitivity analysis to determine the response of the system, which was measured using the downgradient extent of the benzene plume.

The general effect of the use of gasohol in place of gasoline, for all scenarios tested, was to increase benzene plume travel distances by at least 50% relative to the ethanol-free benzene plumes as defined by the 10 $\mu\text{g/L}$ contour. The increase was most pronounced with low background oxygen, low retardation and with a multiple gasohol spill. Maximum increases on the order of 150% were simulated for both Conceptual Model 1 (gasohol spill) and Conceptual Model 2 (pure ethanol spill). The influence is likely even higher in some cases since the plumes reached the model boundary before the full effect could be realized. The predicted impacts are somewhat higher than previous estimates using more simplified approaches, which reached a maximum of 100%, or at most a doubling of plume lengths. The increase in travel distance is only evident, however, at the low concentration range of 10- 100 $\mu\text{g/L}$; degradation of the plume mass, contained mostly within the higher concentrations, remains relatively unaffected by the presence of ethanol.

The influence of ethanol on benzene persistence depends primarily on the degree of overlap between the benzene and ethanol plumes. Under most scenarios with a gasohol source, the rapid dissolution of ethanol combined with the slow dissolution and higher retardation of benzene created limited overlap between the two plumes. Oxygen has time to replenish the aquifer behind the ethanol plume and becomes available in sufficient quantity to the trailing organics. Lower benzene retardation, and low background oxygen concentrations increased the degree of plume overlap and reduced the relative degree of benzene biodegradation. Field situations that would show the greatest susceptibility would therefore involve gasohol source dissolution into aquifers with low retardation capacity (i.e., having low organic carbon content) and low dissolved oxygen.

Ethanol also enhances the persistence of benzene under Conceptual Model 2 in which pure ethanol is spilled into an existing BTEX plume. Although not yet simulated, repeated or continuous pure ethanol spillage could also have an impact on benzene plume extent. Enhanced solubility of benzene due to ethanol cosolvency is considered to have only a minor effect because of its short duration. The

dominant factor which increases the migration distance of the benzene plumes is the diminished aerobic biodegradation of benzene due to preferred biodegradation of ethanol, and its anaerobic degradation products, in the oxygen-limited plumes.

The results shown here suggest a relatively low influence of ethanol on benzene mass loss and are quite different than results from lab batch or microcosm studies which tend to show pronounced reduction of benzene degradation in the presence of ethanol (e.g. Corseuil, 1998). These small-scale static experiments do not consider flow system dynamics, effects of source dissolution rates and the potential for oxygen replenishment. The effect of these field-scale processes appears significant. The modelling results, however, are only based on simplified conceptual models, and this behaviour should be validated against field scale observations in aquifers.

This study uses perhaps one of the most sophisticated modelling approaches to date, although the conceptual model is still somewhat simplified. The first two conceptual models assumed that rapid anaerobic ethanol degradation does not significantly reduce its impact on benzene persistence, since the biodegradation products continue to exert an oxygen demand, which reduces the oxygen available for benzene biodegradation. This assumption was somewhat relaxed in Conceptual Model 3 in which methane was produced as a by-product of ethanol degradation, however the system remained simplified relative to a real field site. The process of NAPL dissolution in the source zone is also idealized. Oxygen was the only electron acceptor considered and Borden aquifer properties were assumed, leading to low dispersion and minimal electron-acceptor-supported mass loss rates. These approaches also lend greater persistence to biodegradable organics. Although these assumptions are reasonable, the simulation results may not be appropriate for other purposes, especially for inferring outcomes at actual field sites.

The simulations presented here provide a reasonable basis for developing expectations of the impacts in groundwater of blending ethanol into gasoline. While further laboratory experiments and numerical modelling can advance the understanding of the processes controlling the impact of ethanol in groundwater, the critical need is for high quality, field-scale studies in aquifers, including studies where actual ethanol-bearing spills occur.

Chapter 5

Summary and Conclusions

This research has provided new insights into the behaviour of hydrocarbon fuel contamination in groundwater through development and application of an advanced 3D numerical simulation model (BIONAPL/3D). The model simulates non-linear groundwater flow, multi-component carrier-enhanced NAPL dissolution, advective-dispersive transport, biodegradation with multiple electron acceptors and daughter-product generation.

The effectiveness of humic acid as a natural carrier for diesel fuel dissolution was quantitatively verified by reproducing conditions of a pilot-scale experiment, and the influence of ethanol on the persistence of benzene in gasoline-contaminated aquifers was evaluated for several conceptual spill scenarios.

Results from the humic acid-enhanced diesel dissolution simulations showed that:

1. Humic acid sorption to aquifer solids, as observed in batch experiments and in pilot scale breakthrough curves, can be accurately simulated using a two-site equilibrium/kinetic sorption model.
2. Laboratory-derived sorption and binding parameters appear suitable for application at the pilot scale, however the pilot scale kinetic sorption rate appears an order of magnitude higher than the laboratory-derived rate.
3. Transporting the free + HA-bound dissolved organics as an equivalent pseudo-phase is a successful approach which saves computational effort.

4. Dissolution of the diesel fuel components, in the presence of humic acid, was occurring at near-equilibrium conditions, even down to drinking water limits.
5. A shifting flow field due to microbial pore clogging is a likely cause of the observed naphthalene concentration anomalies. Relative permeability changes due to the residual diesel are not sufficient to explain the observed trends.
6. Flushing of humic acid decreased the dissolution time of the complete diesel source by a factor of about 5.

Results from the simulations of gasoline-contaminated aquifers, under the scenarios considered in this exercise, showed that:

1. A 10% ethanol fraction in gasoline can increase the persistence of benzene by up to 150% after 20 years, where persistence is defined by the travel distance of the 10 $\mu\text{g}/\text{L}$ benzene concentration.
2. Ethanol impacts are reduced with higher sorption capacity and higher background oxygen concentrations.
3. Cosolvency of benzene in ethanol has a relatively low influence on benzene persistence.
4. The increased benzene persistence in the presence of ethanol is due to competitive biodegradation and electron acceptor limitations.
5. Enhanced benzene persistence appears limited because of relatively rapid oxygen replenishment into the ethanol "shadow" and because of differences in retardation between ethanol and benzene which gradually separate the plumes.

In each model application, the importance of a fully three-dimensional simulation approach was critical, particularly under the given conditions of relatively localized NAPL sources, low dispersion and multiple reactive processes. Although the computational effort was significant, the model performed very well and simulation times were manageable. The 3D humic acid model, for example, consisted of nonlinear flow coupled with 11 reactive species on a grid of 19,488 nodes. A 5-year simulation included on the order of 10,000 time steps and required approximately 20 hours of CPU time on a Pentium III/400. The computational effort is primarily dependent on the number of reactive species and electron acceptors, and could have

been reduced in the humic acid model by lumping the four BTEX components into the remaining “lumped” pseudocomponent.

The humic acid experiment provided an excellent database for testing model accuracy and versatility, for quantifying the relevant reactive processes and assessing remediation efficiency. While the simulated processes appeared to closely match those of the experiment, much work remains for assessing efficiency at field scales. The benefits of using humic acid, for example, must be compared to those of surfactants and cosolvents.

With respect to the influence of ethanol on benzene persistence, the simulations here were based solely on conceptual models of hypothetical generic spills. Although model parameters were based on real field sites and published data, to “validate” these conceptual models and corresponding simulations, detailed field data on existing sites must be considered.

Bibliography

- Abdul, A. S., T. L. Gibson, and D. N. Rai, Use of humic acid solution to remove organic contaminants from hydrogeologic systems, *Environ. Sci. Technol.*, *24*, 328–333, 1990.
- Acton, D. W., and J. F. Barker, In situ biodegradation potential of aromatic hydrocarbons in anaerobic groundwaters, *J. Contam. Hydrol.*, *9*, 325–352, 1992.
- Alvarez, P. J. J., P. J. Anid, and T. M. Vogel, Kinetics of aerobic biodegradation of benzene and toluene in sandy aquifer material, *Biodegradation*, *2*, 43–51, 1991.
- Alvarez, P. J. J., and C. S. Hunt, The effect of ethanol on BTEX biodegradation and natural attenuation, Volume 4, Chapter 3, LLNL Draft Report UCRL-AR-135949 - Report to the Governor of the State of California, 1999.
- Appelo, C. A. J., and D. Postma, *Geochemistry, Groundwater and Pollution*, A.A. Balkema, Rotterdam, Netherlands, 1993.
- Baetsle, L. H., Migration of radionuclides in porous media, in Progress in Nuclear Energy Series XII, Health Physics, edited by A. M. F. Duhamel, 707–730. Elmsford, NY, Pergamon Press, 1969.
- Ball, H. A., and M. Reinhard, Monoaromatic hydrocarbon degradation under anaerobic conditions at Seal Beach, California: laboratory studies, *Environ. Toxicol. Chem.*, *15*(2), 114–122, 1996.
- Barker, J. F., and J. T. Wilson, Natural biological attenuation of aromatic hydrocarbons under anaerobic conditions, in Subsurface Restoration, edited by C. H. Ward, J. A. Cherry, and M. R. Scaif, Chapter 18. Michigan, Ann Arbor Press Inc., 1997.
- Bekins, B., E. Warren, and E. M. Godsy, A comparison of zero-order, first-order and Monod biotransformation models, *Groundwater*, *36*(2), 261–268, 1998.

- Bouwer, E. J., and P. L. McCarty, Modeling of trace organics biotransformation in the subsurface, *22*(4), 433–440, 1984.
- Boving, T. B., and M. L. Brusseau, Solubilization and removal of residual trichloroethene from porous media: comparison of several solubilizing agents, *J. Contam. Hydrol.*, *42*(1), 51–67, 2000.
- Braess, D., and C. König. A fast conjugate gradient algorithm for three-dimensional groundwater flow problems. Ruhr-Universität Bochum, 1995.
- Brookman, G. T., M. Flanagan, and J. O. Kebe, Laboratory investigation of petroleum hydrocarbons in groundwater, Technical report, American Petroleum Institute, Washington, DC, API publication number 4395, 1985.
- Brun, A., P. Engesgaard, and E. O. Frind, A coupled microbiology-geochemistry transport model for saturated groundwater flow, in Proceedings, Transport and Reactive Processes in Aquifers, IAHR Symposium (T.H. Dracos F. Stauffer, Eds.), 457–462, Zuerich, Switzerland, 1994.
- Brusseau, M. L., D. A. Sabatini, J. S. Gierke, and M. D. Annable, *Innovative Subsurface Remediation: Field Testing of Physical, Chemical and Characterization Techniques*, Am. Chem. Soc., 1999.
- Bryan, N. D., V. J. Robinson, F. R. Livens, N. Hesketh, M. N. Jones, and J. R. Lead, Metal-humic interactions: a random structural modelling approach, *Geochimica et Cosmochimica Acta*, *61*(4), 805–820, 1997.
- Burnett, R., and E. Frind, Simulation of contaminant transport in three dimensions: 2. Dimensionality effects, *Water Resour. Res.*, *23*, 695–705, 1987.
- Burris, D. R., and W. G. MacIntyre, Water solubility behaviour of hydrocarbon mixtures - implications for petroleum dissolution, in Oil in Freshwater: Chemistry, Biology, Countermeasures Technology, edited by H. Vandermeulin, and S. Hrudey, 85–94. Symposium of Oil Pollution in Freshwater, Edmonton, Canada, 1987.
- Carter, M. C., and W. J. Weber, Modeling adsorption of TCE by activated carbon preloaded by background organic matter, *Environ. Sci. Technol.*, *28*(4), 614–623, 1994.
- Chapelle, F. H., Bioremediation of petroleum hydrocarbon-contaminated groundwater: The perspectives of history and hydrology, *Groundwater*, *37*(1), 122–132, 1998.
- Chiou, C. T., D. E. Kile, T. I. Brinton, R. L. Malcolm, J. A. Leenheer, and P. MacCarthy, A comparison of water solubility enhancements of organic

- solutes by aquatic humic materials and commercial humic acids, *Environ. Sci. Technol.*, *21*(12), 1231–1234, 1986a.
- Chiou, C. T., R. L. Malcolm, T. I. Brinton, and D. E. Kile, Water solubility enhancement of some organic pollutants and pesticides by dissolved humic and fulvic acids, *Environ. Sci. Technol.*, *20*(5), 502–508, 1986b.
- Chrysikopoulos, C. V., and K. Y. Lee, Contaminant transport resulting from multicomponent nonaqueous phase liquid pool dissolution in three-dimensional subsurface formations, *J. Contam. Hydrol.*, *31*, 1–21, 1998.
- Cline, P., J. J. Delfino, and C. R. Suresh, Partitioning of aromatic constituents into water from gasoline and other complex solvent mixtures, *Environ. Sci. Technol.*, *25*, 914–920, 1991.
- Corapcioglu, M. Y., and S. Jiang, Colloid-facilitated groundwater contaminant transport, *Water Resour. Res.*, *29*(7), 2215–2226, 1993.
- Corapcioglu, M. Y., and S. Kim, Modeling facilitated contaminant transport by mobile bacteria, *Water Resour. Res.*, *31*(11), 2639–2647, 1995.
- Corey, A. T. Mechanics of immiscible fluids in porous media. Water Resour. Publ. Fort Collins, Colorado, 1986.
- Corseuil, H. X. C., C. Hunt, R. C. dos Santos Ferreira, and J. J. Alvarez, The influence of the gasoline oxygenate ethanol on aerobic and anaerobic BTX biodegradation, *Water Research*, *32*(7), 2065–2072, 1998.
- Cozzarelli, I. M., J. S. Herman, M. J. Baedeker, and J. M. Fischer, Geochemical heterogeneity of a gasoline-contaminated aquifer, *J. Contam. Hydrol.*, *40*, 261–284, 2000.
- CRC Handbook, *CRC Handbook of Chemistry and Physics*, CRC Press, 1980.
- Danzer, J., and P. Grathwohl, Coupled transport of PAH and surfactants in natural aquifer material, *Phys. Chem. Earth*, *23*(2), 237–243, 1998.
- Daus, A. D., E. O. Frind, and E. A. Sudicky, Comparative error analysis in finite element formulations of the advection-dispersion equation, *Adv. Water Resour.*, *8*, 86–95, 1985.
- Davis, G. B., C. Barber, T. R. Power, J. Thierrin, B. M. Patterson, J. L. Rayner, and Q. Wo, Variability and intrinsic remediation of a BTEX plume in anaerobic sulphate-rich groundwater, *Jour. Contam. Hydrol.*, *36*, 265–290, 1999.
- de Oliveira, E. Ethanol flushing of gasoline residuals - microscale and field scale experiments. Ph.D. thesis, University of Waterloo, 1997.

- Donaldson, C. R., J. Barker, and I. Chatzis, Subsurface fate and transport of a methanol/gasoline blend (M85): A Laboratory investigation, Technical report, American Petroleum Institute, Washington, DC, API publication number 4569, 1994.
- Dunnivant, F. M., P. M. Jardine, D. L. Taylor, and J. F. McCarthy, Transport of naturally occurring dissolved organic carbon in laboratory columns, *Soil Sci. Soc. Am. J.*, 56, 437–444, 1992.
- Durrant, G. Modelling of the Migration and Natural Fate of a Coal Tar Creosote Plume. M.Sc. Project, Dept. of Earth Sciences, University of Waterloo, 2000.
- Einarson, M. D., M. Schirmer, P. Pezeshkpour, D. M. Mackay, and R. D. Wilson, Comparison of eight innovative site characterization tools used to investigate an MTBE plume at Site 60, Vandenberg Air Force Base, California, in 1999 Petroleum Hydrocarbons and Organic Chemicals in Ground Water Conf., Houston, TX.
- EPA, *In Situ Remediation Technology Status Report: Surfactant Enhancements*, USEPA Solid Waste and Emergency Response. EPA 542-K-94-003. 22 pp., 1995.
- Essaid, H. I., and B. Bekins. *BIOMOC, A Multispecies Solute-Transport Model with Biodegradation*. U.S. Geological Survey, Water-Resources Investigations Report 97-4022, Menlo Park, CA, 1997.
- Essaid, H. I., B. A. Bekins, E. M. Godsy, E. Warren, M. J. Baedecker, and I. M. Cozzarelli, Simulation of aerobic and anaerobic biodegradation processes at a crude oil spill site, *Water Resour. Res.*, 31(12), 3309–3327, 1995.
- Forsy, S. In situ chemical oxidation of coal tar/creosote. Ph.D. thesis, Dept. of Chemistry, University of Waterloo, 2000.
- Frind, E. O., Simulation of long-term transient density-dependent transport in groundwater, *Adv. Water Resour.*, 5, 73–88, 1982.
- Frind, E. O., W. H. M. Duynisveld, O. Strelbel, and J. Boettcher, Modeling of multicomponent transport with microbial transformation in groundwater: the Fuhrberg case, *Water Resour. Res.*, 26(8), 1707–1719, 1990.
- Frind, E. O., and G. E. Hokkanen, Simulation of the Borden plume using the alternating direction Galerkin technique, *Water Resour. Res.*, 23(5), 918–930, 1987.
- Frind, E. O., J. W. Molson, M. Schirmer, and N. Guiguer, Dissolution and mass transfer of multiple organics under field conditions: The Borden source, *Water Resour. Res.*, 35(3), 683–694, 1999.

- Frind, E. O., E. A. Sudicky, and J. W. Molson, Three-dimensional simulation of organic transport with aerobic biodegradation, in *Groundwater Contamination*, edited by L. Abriola, 89–96. IAHS Publication No. 185, 1989.
- Gauthier, T. D., W. R. Seltz, and C. L. Grant, Effects of structural and compositional variations of dissolved humic materials on pyrene Koc values, *Environ. Sci. Technol.*, *21*(3), 243–248, 1987.
- Ghassemi, F., J. W. Molson, A. Falkland, and K. Alam, Three-dimensional simulation of the Home Island freshwater lense: preliminary results, *Environmental Modelling Software*, *14*, 181–190, 1999.
- Grathwohl, P., C. Eberhardt, I. Klenk, H. Ruegner, and U. Maier, Transverse vertical dispersivity in aquifer materials: Implications on mass transfer across the capillary fringe and the length of steady state plumes, in *Proceedings, GW2000, International Conference on Groundwater Research* (P.L. Bjerg, P. Engesgaard, Th.D. Krom, Eds.), 19–20, Copenhagen, Denmark, 2000.
- Grimberg, S. J., W. T. Stringfellow, and M. D. Aitken, Quantifying the biodegradation of phenanthrene by *Pseudomonas stutzeri* P16 in the presence of a non-ionic surfactant, *Applied and Environmental Microbiology*, *62*(7), 2387–2392, 1996.
- Gron, C., L. K. Hansen, and J. Heinemeier, Origin of aquifer humic substances identified by advanced chemical characterization, in *Proceedings, GW2000, International Conference on Groundwater Research* (P.L. Bjerg, P. Engesgaard, Th.D. Krom, Eds.), Copenhagen, Denmark, 2000.
- Groves, F. R., Effect of cosolvents on the solubility of hydrocarbons in water, *Environ. Sci. Technol.*, *22*(3), 282–286, 1988.
- Grubb, D., and N. Sitar, Mobilization of trichloroethene (TCE) during ethanol flooding in uniform and layered sand packs, *Water Resour. Res.*, *35*(11), 3274–3283, 1999.
- Gu, B., J. Schmitt, Z. Chen, L. Liang, and J. F. McCarthy, Adsorption and desorption of natural organic matter on iron oxide: Mechanisms and models, *Environ. Sci. Technol.*, *28*, 38–46, 1994.
- Guetzloff, T. F., and J. A. Rice, Does humic acid form a micelle?, *Sci Tot. Environ.*, *152*, 31–35, 1994.
- Guha, S., and P. R. Jaffe, Biodegradation kinetics of phenanthrene partitioned into the micellar phase of nonionic surfactants, *Environ. Sci. Technol.*, *30*(2), 605–611, 1996.

- Haggerty, R., and S. M. Gorelick, Multiple-rate mass transfer for modeling diffusion and surface reactions in media with pore-scale heterogeneity, *Water Resour. Res.*, *31*(10), 2383–2400, 1995.
- Heermann, S. E., and S. E. Powers, The dissolution of BTEX compounds from oxygenated gasoline, in ACS Symposium: Petroleum Contamination in the Environment: Assessment and Remediation, New Orleans, LA, 1996.
- Heermann, S. E., and S. E. Powers, Modeling the partitioning of BTEX in water-reformulated gasoline systems containing ethanol, *J. Contam. Hydrol.*, *34*, 315–341, 1998.
- Hubbard, C. E., J. F. Barker, S. F. O’Hannesin, M. Vandegriendt, and R. W. Gillham, Transport and fate of dissolved methanol, methyl-tertiary-butyl-ether, and monoaromatic hydrocarbons in a shallow sand aquifer, Technical report, Health and Environmental Science Department, API Publication Number 4601, API, Washington, D.C., 1994.
- Hunt, C. S., R. D. S. Ferreira, H. X. Corseuil, and P. J. J. Alvarez, Effect of ethanol on aerobic BTX degradation, in In situ and onsite bioremediation, 49–54.
- Hunter, K. S., Y. Wang, and P. V. Cappellan, Kinetic modelling of microbially-driven redox chemistry of subsurface environments: coupling transport, microbial metabolism and geochemistry, *Journal of Hydrology*, *209*, 53–80, 1998.
- Huyakorn, P., and G. Pinder, *Computational Methods in Subsurface Flow*, Academic Press Inc., London, 1983.
- Ibaraki, M., and E. A. Sudicky, Colloid-facilitated contaminant transport in discretely-fractured porous media 1: Numerical formulation and sensitivity analysis, *Water Resour. Res.*, *31*(12), 2945–2960, 1995.
- Jardine, P. M., F. M. Dunnivant, H. M. Selim, and J. F. McCarthy, Comparison of models describing the transport of dissolved organic carbon in aquifer columns, *Soil Sci. Soc. Am. J.*, *56*, 437–444, 1992.
- Ji, W., and M. L. Brusseau, A general mathematical model for chemical-enhanced flushing of soil contaminated by organic compounds, *Water Resour. Res.*, *34*(7), 1635–1648, 1998.
- Johnson, P. C., M. W. Kemblowski, and J. D. Colthart, Quantitative analysis of cleanup of hydrocarbon-contaminated soils by in-situ soil venting, *Groundwater*, *28*(3), 413–429, 1990.
- Johnson, W. P., Sediment control of facilitated transport and enhanced desorption, *Jour. Env. Engineer.*, *126*(1), 47–56, 2000.

- Johnson, W. P., and G. L. Amy, Facilitated transport and enhanced desorption of polycyclic aromatic hydrocarbons by dissolved natural organic matter in aquifer sediments, *Environ. Sci. Technol.*, *29*(3), 807–817, 1995.
- Johnson, W. P., G. L. Amy, and S. C. Chapra, Modelling of NOM-facilitated PAH transport through low-foc sediment, *J. Environ. Eng.*, *121*(6), 438–446, 1995.
- Johnson, W. P., and W. W. John, PCE solubilization and mobilization by commercial humic acid, *J. Contam. Hydrol.*, *35*, 343–362, 1999.
- King, M. W. G. Migration and Fate of a Coal Tar Creosote Plume. Ph.D. thesis, Dept. of Earth Sciences, University of Waterloo, 1997.
- Knabner, P., K. U. Totsche, and I. Koegel-Knabner, The modeling of reactive solute transport with sorption to mobile and immobile sorbents 1. Experimental evidence and model development, *Water Resour. Res.*, *32*(6), 1611–1622, 1996.
- Knaus, M. Modellsimulationen zur Freisetzung von Schadstoffen aus kohärenter Flüssigphase. Diplomarbeit, Eberhard-Karls-Universität Tübingen, 1999.
- Lacombe, S., E. A. Sudicky, S. K. Frappe, and A. J. A. Unger, Influence of leaky boreholes on cross-formational groundwater flow and contaminant transport, *Water Resour. Res.*, *31*(8), 1871–1882, 1995.
- Laha, S., and R. G. Luthy, Inhibition of phenanthrene mineralization by nonionic surfactants in soil-water systems, *Environ. Sci. Technol.*, *25*, 1920, 1991.
- Laha, S., and R. G. Luthy, Effects of nonionic surfactants on the solubilization and mineralization of phenanthrene in soil-water systems, *Biotechnol. Bioeng.*, *40*, 1367–1380, 1992.
- Lee, L. S., M. Hagwall, J. J. Delfino, and P. S. Rao, Partitioning of polycyclic aromatic hydrocarbons from diesel fuel into water, *Environ. Sci. Technol.*, *26*, 2104–2110, 1992.
- Lesage, S., H. Xu, K. S. Novakowski, and S. Brown, Use of humic acids to enhance the removal of aromatic hydrocarbons from contaminated aquifers, Report to GASReP, Groundwater Remediation Project, National Water Research Institute, Environment Canada, 1997.
- Lewis, M. A., Chronic and sublethal toxicities of surfactants to aquatic animals, a review and risk assessment, *Water Research*, *25*, 101–113, 1991.
- Liu, H., and G. L. Amy, Modeling partitioning and transport interactions between natural organic matter and polynuclear aromatic hydrocarbons on groundwater, *Environ. Sci. Technol.*, *27*(8), 1553–1562, 1993.

- Lu, G., T. P. Clement, C. Zheng, and T. Wiedemeier, Natural attenuation of BTEX compounds: Model development and field-scale application, *Groundwater*, 37(5), 707–717, 1999.
- Luckner, L., and W. Schestakow, *Migration Processes in the Soil and Groundwater Zone*, Lewis Publishers, U.S., 1991.
- Ludvigsen, L., H.-J. Albrechtsen, G. Heron, P.L. Bjerg and T.H. Christensen, Anaerobic microbial redox processes in a landfill leachate contaminated aquifer, *J. Contam. Hydrol.*, 33, 273–291, 1998.
- Lunn, S. R. D., and B. Kueper, Removal of pooled dense, nonaqueous phase liquid from saturated porous media using upward gradient alcohol floods, *Water Resour. Res.*, 33(10), 2207–2219, 1997.
- Lyngkilde, J., and T. H. Christensen, Redox zones of a landfill leachate pollution plume (Vejen, Denmark), *J. Contam. Hydrol.*, 10, 273–289, 1992.
- Mackay, D. M., W. Y. Shiu, A. Maijanen, and S. Feenstra, Dissolution of non-aqueous phase liquids in groundwater, *J. Contam. Hydrol.*, 8, 1991.
- MacQuarrie, K. T. B., E. A. Sudicky, and E. O. Frind, Simulation of biodegradable organic contaminants in groundwater: 2. Plume behaviour in uniform and random flow fields, *Water Resour. Res.*, 26(2), 207–222, 1990.
- Magee, B. R., L. W. Lion, and A. T. Lemley, Transport of dissolved organic macromolecules and their effect on the transport of phenanthrene in porous media, *Environ. Sci. Technol.*, 25(2), 323–331, 1991.
- Malcolm Pirnie Inc., Evaluation of the fate and transport of ethanol in the environment, Report prepared for the American Methanol Institute, Nov. 1998.
- Martel, R., P. K. Gelinis, and J. Desnoyers, Aquifer washing by micellar solutions: 1. Optimization of alcohol-surfactant-solvent solutions, *J. Contam. Hydrol.*, 29, 319–346, 1998.
- Mayer, U. A numerical model for multicomponent reactive transport in variably saturated porous media. Ph.D. thesis, Dept. of Earth Sciences, University of Waterloo, 1999.
- McCarthy, J. F., K. R. Czerwinsky, W. E. Sanford, P. M. Jardine, and J. D. Marsh, Mobilization of transuranic radionuclides from disposal trenches by natural organic matter, *J. Contam. Hydrol.*, 30, 49–77, 1998.
- McCarthy, J. F., and B. D. Jiminez, Interactions between polycyclic aromatic hydrocarbons and dissolved humic material: binding and dissociation, *Environ. Sci. Technol.*, 19, 1072–1076, 1985.

- McCarthy, J. F., T. M. Williams, L. Liang, P. M. Jardine, A. V. Palumbo, L. W. Jolley, L. W. Cooper, and D. L. Taylor, Mobility of natural organic matter in a sandy aquifer, *Environ. Sci. Technol.*, *27*, 667–676, 1993.
- McCarthy, J. F., and J. M. Zachara, Subsurface transport of contaminants, *Environ. Sci. Technol.*, *23*(5), 496–502, 1989.
- McCarthy, J.F., B. Gu, L. Liang, J. Mas-Pla, T.M. Williams and T-C. J. Yeh, Field tracer tests on the mobility of natural organic matter in a sandy aquifer, *Water Resour. Res.*, *32*(5), 1223–1238, 1996.
- McNab, W., S. E. Heermann, and B. Dooher, Screening model evaluation of the effects of ethanol on benzene plume lengths, Volume 4, Chapter 4, LLNL Draft Report UCRL-AR-135949 - Report to the Governor of the State of California, 1999.
- Molson, J., E. O. Frind, and C. D. Palmer, Thermal energy storage in an unconfined aquifer, 2. Model development, validation and application, *Water Resour. Res.*, *28*(10), 2857–2867, 1992.
- Molson, J. W. *BIONAPL/3D User Guide: A 3D Groundwater Flow, Multi-component NAPL Dissolution and Reactive Transport Model*. University of Waterloo, Waterloo, 2000.
- Molson, J. W., J. Barker, and M. Schirmer, Modeling the impact of ethanol on the persistence of BTEX compounds in gasoline-contaminated groundwater, Technical report, The California MTBE Research Partnership, Gina Melin (Ed.), NWRI-00-01, 2000a.
- Molson, J. W., and E. O. Frind. *SALTFLOW User Guide: A 3D Density Dependent Groundwater Flow and Mass Transport Model*. University of Waterloo, Waterloo, 1994.
- Molson, J. W., and E. O. Frind, Enhanced NAPL dissolution and biodegradation: Modelling the effect of organic carriers, in Proceedings, GW2000, International Conference on Groundwater Research (P.L. Bjerg, P. Engesgaard, Th.D. Krom, Eds.), Copenhagen, Denmark, 2000.
- Molson, J. W., and E. O. Frind, Perspectives on non-uniqueness in three-dimensional transport simulations of biodegrading organic contaminants, in IAHS International Conference on Calibration and Reliability in Groundwater Modelling, The Hague, Sept. 1990.
- Molson, J. W., E. O. Frind, D. W. Blowes, and C. J. Ptacek, Predicting the behaviour of thermal energy and temperature-dependent reactive mass trans-

- port in shallow aquifers, in Proceedings, CALORSTOCK '94, 6th International Conference on Thermal Energy Storage, Espoo, Finland, 1994.
- Molson, J. W., E. O. Frind, D. R. V. Stempvoort, and S. Lesage, The Use of Humic Acids to Enhance Dissolution and Mobilization of PAH's in Groundwater Remediation 2. Numerical Model Development and Application, *J. Contam. Hydrol.*, in preparation, 2000b.
- Molson, J. W., E. O. Frind, D. V. Stempvoort, and S. Lesage, Numerical Simulation of enhanced diesel fuel dissolution and biodegradation in groundwater, in Proceedings, 53rd Canadian Geotechnical Conference (Joint CGS-IAH), Montreal, 2000c.
- Munoz, J. F., and M. J. Irarrazaval, A numerical model for simulation of bioremediation of hydrocarbons in aquifers, *Groundwater*, 36(2), 215–224, 1998.
- Oswald, S., Dichteströmungen in porösen Medien: Dreidimensionale Experimente und Modellierung, ISBN 3-906445-01-1, Institut für Hydromechanik und Wasserwirtschaft, ETH Höggerberg, Zürich, 1999.
- Poulsen, M., L. Lemon, and J. Barker, Chemical fate and impact of oxygenates in groundwater: solubility of BTEX from gasoline-oxygenate compounds, Technical report, American Petroleum Institute, Washington, DC, API publication number 4531, 1991.
- Poulsen, M., L. Lemon, and J. Barker, Dissolution of monoaromatic hydrocarbons into groundwater from gasoline-oxygenate mixtures, *Environ. Sci. Technol.*, 26, 2483–2489, 1992.
- Powers, S. E., L. M. Abriola, J. S. Dunkin, and W. J. Weber, Phenomenological models for transient NAPL-water mass transfer processes, *J. Contam. Hydrol.*, 16, 1–33, 1994a.
- Powers, S. E., L. M. Abriola, and W. J. Weber, An experimental investigation of nonaqueous phase liquid dissolution in saturated subsurface systems: Transient mass transfer rates, *Water Resour. Res.*, 30(2), 321–332, 1994b.
- Ramaswami, A., and R. G. Luthy, Mass transfer and bioavailability of PAH compounds in coal tar NAPL-slurry systems 1. Model development, *Environ. Sci. Technol.*, 31, 2260–2267, 1997.
- Rebhun, M., F. D. Smedt, and J. Rwetabula, Dissolved humic substances for remediation of sites contaminated by organic pollutants. Binding-desorption model predictions, *Water Resour. Res.*, 30(9), 2027–2038, 1996.
- Reichhardt, T., Fuel additives put under scrutiny - again, *Nature*, 397, 96, 1999.

- Rice, D. W., S. E. Powers, and P. J. J. Alvarez, Health and environmental assessment of the use of ethanol as a fuel oxygenate, Volume 4: Potential ground and surface water impacts, Chapter 1, In: LLNL Draft Report UCRL-AR-135949 - Report to the Governor of the State of California, 1999.
- Rifai, H. S., C. J. Newell, J. R. Gonzales, S. Dendrou, L. Kennedy, and J. Wilson. *BIOPLUME III Natural Attenuation Decision Support System Version 1.0, User's Manual*. prepared for the U.S. Air Force Centre for Environmental Excellence, Brooks Air Force Base, San Antonio, TX, 1997.
- Rivett, M. O., S. Feenstra, and J. A. Cherry, Groundwater zone transport of chlorinated solvents: A field experiment, in *Modern Trends in Hydrogeology, Canadian Chapter*, International Association of Hydrogeologists, Hamilton, Ontario, 1992.
- Rouse, J. D., D. A. Sabatini, J. M. Suffita, and J. H. Harwell, Influence of surfactants on microbial degradation of organic compounds, *Critical Reviews on Microbial Degradation of Organic Compounds*, 24, 325–370, 1994.
- Roy, S. B., and D. A. Dzombak, Sorption nonequilibrium effects on colloid-enhanced transport of hydrophobic organic compounds in porous media, *J. Contam. Hydrol.*, 30, 177–198, 1998.
- Sabatini, D. A., R. C. Knox, and J. H. Harwell, *Surfactant-Enhanced Subsurface Remediation: Emerging Technologies*, American Chemical Society, Washington, DC, 1995.
- Schäfer, D., W. Schäfer, and W. Kinzelbach, Simulation of reactive processes related to biodegradation in aquifers 1. Structure of the three-dimensional reactive transport model, *J. Contam. Hydrol.*, 31, 167–186, 1998.
- Schirmer, M., E. O. Frind, and J. W. Molson, Transport and biodegradation of hydrocarbons in shallow aquifers: 3D modeling, in *API Workshop: Comparative Evaluation of Groundwater Biodegradation Models*, Fort Worth, Texas, 1995.
- Schirmer, M., J. W. Molson, and E. O. Frind, Influence of transient flow on contaminant biodegradation, *Groundwater*, (in submission), 2000a.
- Schirmer, M., J. W. Molson, E. O. Frind, and J. F. Barker, Biodegradation modelling of a dissolved gasoline plume applying independent lab and field parameters, *J. Contam. Hydrol.*, in press, 2000b.
- Schirmer, M. S. Investigation of Multiscale Biodegradation Processes: A Modelling Approach. Ph.D. thesis, Dept. of Earth Sciences, University of Waterloo, 1998.

- Schmid, G., and D. Braess, Comparison of fast equation solvers for groundwater flow problems, in *Groundwater Flow and Quality Modelling*, (Custodio et al. Ed.) NATO ASI Series C, Vol. 224, D. Reidel Co., Dordrecht Holland, 173–188, 1988.
- Sleep, B. E., and J. F. Sykes, Modeling the transport of volatile organics in variably saturated media, *Water Resour. Res.*, *25*(1), 81–92, 1989.
- Soerens, T. S., D. A. Sabatini, and J. H. Harwell, Effects of flow bypassing and nonuniform NAPL distribution on the mass transfer characteristics of NAPL dissolution, *Water Resour. Res.*, *34*(7), 1657–1673, 1998.
- Stevenson, F. J., and K. M. Goh, Infrared spectra of humic acids and related substances, *Geochim. Cosmochim. Acta*, *35*, 417–483, 1971.
- Sudicky, E. A., A natural gradient experiment on solute transport in a sand aquifer: spatial variance of hydraulic conductivity and its role in the dispersion process, *Water Resour. Res.*, *22*(13), 2069–2082, 1986.
- Sudicky, E. A., A. J. A. Unger, and S. Lacombe, A noniterative technique for the direct implementation of well bore boundary conditions in three-dimensional heterogeneous formations, *Water Resour. Res.*, *31*(2), 411–415, 1995.
- Thierrin, J., G. B. Davis, and C. Barber, A ground-water tracer test with deuterated compounds for monitoring in situ biodegradation and retardation of aromatic hydrocarbons, *Ground Water*, *33*(2), 469–475, 1995.
- Thierrin, J., G. B. Davis, C. Barber, B. M. Patterson, F. Pribac, T. R. Power, and M. Lambert, Natural degradation rates of BTEX compounds and naphthalene in a sulphate reducing groundwater environment, *Hydrol. Sci. J.*, *38*(4), 309–322, 1993.
- Tiehm, A., Degradation of polycyclic aromatic hydrocarbons in the presence of synthetic surfactants, *Appl. Environ. Microbiol.*, *60*, 258–263, 1994.
- Totsche, K. U., J. Danzer, and I. Koegel-Knabner, Dissolved organic matter-enhanced retention of polycyclic aromatic hydrocarbons in soil miscible displacement experiments, *J. Environ. Quality*, *26*, 1090–1100, 1997.
- Ulrich, G. The fate and transport of ethanol-blended gasoline in the environment. Report by SURBEC-ART Environmental LLC., submitted to the Governor's Ethanol Coalition, Lincoln Nebraska, 1999.
- Van Stempvoort, D.R., Binding of methylnaphthalenes to aqueous humic acid, in submission to *Jour. of Contam. Hydrol.*, 2000.

- Van Stempvoort, D.R. and S. Lesage, Sorption of methylnaphthalenes by winter sand, a model aquifer material, in submission to *Jour. of Contam. Hydrol.*, 2000.
- Van Stempvoort, D.R., S. Lesage and S. Brown, The use of humic acids to enhance dissolution and mobilization of PAHs in groundwater remediation 1. A pilot scale test, in submission to *Jour. of Contam. Hydrol.*, 2000.
- Visser, S. A., Oxidation-reduction potentials and capillary activities of humic acids, *Nature*, *November 11*, 4958, 1964.
- Warwick, P. W., A. Hall, V. Pashley, N. D. Bryan, and D. Griffin, Modelling the effect of humic substances on the transport of europium through porous media, *J. Contam. Hydrol.*, *42*(1), 19–34, 2000.
- Widdowson, M. A., F. J. Molz, and L. D. Benefield, A numerical transport model for oxygen and nitrate based respiration linked to substrate and nutrient availability in porous media, *Water Resour. Res.*, *24*, 1553–1565, 1988.
- Wiedemeier, T. H., H. S. Rifai, C. J. Newell, and J. T. Wilson, *Natural Attenuation of Fuels and Chlorinated Solvents in the Subsurface*, John Wiley and Sons Inc., New York, 1999.
- Zhang, Y., W. J. Maier, and R. M. Miller, Effect of rhamnolipids on the dissolution, bioavailability and biodegradation of phenanthrene, *Environ. Sci. Technol.*, *31*(8), 2211–2217, 1997.